A Physical Investigation of Air/Water Interactions Leading to Geyser Events in Rapid Filling Pipelines

by

James William Lewis

A dissertation submitted in partial fulfillment
of the requirements for the degree of
Doctor of Philosophy
(Civil Engineering)
in the University of Michigan
2011

Doctoral Committee:

Professor Steven J. Wright, Chair
Professor Steven L. Ceccio
Professor Nikolaos D. Katopodes
Professor Scott A. Yost, University of Kentucky

Table of Contents

List of Tables

List of Figures

List of Symbols

A, A_p	area of pipe (full cross-section of tunnel)
a	constant parameter used in determining air migration (Little, et al. 2008)
A_1, A_2, etc.	area of pipe in the control volume specified by the subscript
A_{fs}	area of water cross-section within the free-surface portion of the tunnel
C	ratio of air intrusion velocity to $\sqrt{(gd)}$
c_1	velocity of air intrusion in an emptying pipeline
d	diameter of tunnel
D_1, D_2, etc.	diameter of pipe in the control volume specified by the subscript
D_{ris}	diameter of vertical riser
DS	abbreviation for downstream
$\vec{F}$	external forces acting on control volume
$\boldsymbol{F}$	Froude number: $v / \sqrt{(gd)}$
f, f_1, f_2, etc.	friction factor
g	gravitational acceleration
h	water depth downstream of air intrusion
H	height of air phase downstream of intrusion front
H_{base}	pressure head at the base of the vertical riser in the center of the tunnel
H_R	reservoir pressure head at the upstream end of the tunnel
H_{Res}	height of reservoir surface
H_{rise}	water height of rise
$H_{s,1}$	pressure head at the intersection between control volumes 1 and 2
$H_{s,2}$	pressure head at the intersection between control volumes 2 and 3
H_w	pressure head at the downstream weir
K	local energy loss coefficient
L	length of the tunnel; also used as length of a control volume
L_1, L_2, *etc.*	length of the control volume specified by the subscript
n	time index
p	absolute air pressure
P	gage water pressure

Q, Q_1, Q_2	water flow rate
Re	Reynolds number of water flow: v / (νD)
t	time
U_B	upward air velocity of a bubble according to Davies and Taylor (1950)
US	abbreviation for upstream
v	water velocity
V	water velocity behind an advancing bore
v_1, v_2, etc.	water velocity in the control volume specified by the subscript
Vol_{air}	volume of air
V_s	velocity of pipe-filling bore
$\vec{v}$	water velocity vector
$\forall$	volume of the control volume
$\forall_D$	dimensionless volume of the air pocket
$\bar{y}_{fs}$	centroid depth of water within the free-surface portion of the tunnel
Z	pressure head behind an advancing hydraulic bore
α	half of the angle subtended from the center of the pipe to the free surface
ε, ε_1, ε_2, etc.	material roughness of pipe walls
Δ	energy dissipation caused by air intrusion front
δ	liquid film flow thickness around rising air pocket
γ	ratio of specific heats
Δt	time step
μ, μ_w	dynamic viscosity of water
ρ, ρ_w	density of water
ρ_a, ρ_{air}	density of air
θ	pipe slope relative to horizontal

Chapter 1

Introduction

Combined sewer collection systems can fill rapidly during large precipitation events exceeding the hydraulic capacity and leading to problems such as basement flooding. In order to avoid sewer backups, overflows have been constructed to release the low quality water to surface waters resulting in declines in surface water quality requiring beach closings and other schemes to protect public health. One strategy for preventing combined sewer overflows (CSOs) is to construct underground storage tunnels to handle the extra runoff. Water is diverted into the tunnel once the capacity of the sewer system is exceeded. These CSO tunnels typically have a large diameter in order to handle the capacity of a major storm event and can be very expensive to construct.

There are several issues which are relevant to the design of these large CSO storage tunnels. Various reports in the literature (e.g. Zhou, et al. 2002; Hamam and McCorquodale 1982) mention structural damage to sewer systems during rainfall events, presumably due to the occurrence of transient pressures associated with the filling process. As in other pipelines, hydraulic surges can occur which cause pressure fluctuations to oscillate throughout the entire system. Usually a pipeline is very susceptible to extreme surge events just as the pipeline undergoes a transition from free

surface to pressurized flow. Although the pressure surges that occur after the pipeline is completely filled are relatively well understood and predicted, it is less certain what processes influence the pressure variation as the tunnel transitions to a surcharged state.

A less understood dynamic condition that occurs in these large underground storage tunnels is referred to as "geysering" due to the resemblance of the above ground manifestation to thermal geysers. Geyser events have been observed in several systems in which an intense upward movement of an air (presumably) and liquid mixture rises through a manhole or other vertical shaft beyond the grade elevation. In some instances, the untreated liquid mixture jets tens of meters above the ground surface posing safety risks and flooding hazards. Geyser events are a relatively new subject of research within the civil engineering community. It is unclear that current understanding of the conditions leading to geyser formation is adequate to allow for system design to avoid their occurrence. Further investigation is needed to fully understand the geyser phenomenon.

There are several examples of geyser events that have occurred in large underground storage tunnels around the United States. One such event occurred from the storm of October 3, 1986 in the Tunnel and Reservoir Plan (TARP) system of Chicago, Illinois (similar events also occurred during the summer of 2010). The exact height of the geyser event was not recorded, but researchers were prompted to initiate a study of the phenomenon (Guo and Song 1990; Guo and Song 1991). The provided explanation for the Chicago geyser event is that a bore front due to the rapid filling of the system reached the upstream end of the tunnel and initiated an inertia-induced high pressure surge.

On the issue of air interactions, Guo and Song (1991) state, "It has been ascertained that if the drop shaft is ventilated, as most are, the cover could not be blown off by air pressure alone. That is, most blowoffs are caused by the impact force of the rising water. Therefore, it is sufficient to study the hydrodynamics alone." Although the basis for the above statement that air pressure cannot dislodge a manhole is perhaps questionable, the assumption that neither air entrapment nor pressurized air pockets are associated with geyser events is common throughout the existing literature. The reasons for this are not clear, except perhaps for the desire to hypothesize a simplified framework more amenable to numerical modeling.

The presence of air in large systems has been recognized as a potential concern, primarily associated with air entrainment at drop shafts (for example Anderson and Dahlin 1975) where special designs have been implemented to reduce or eliminate the air entering into systems that are flowing in a surcharged state. An important question is whether there are other mechanisms by which large volumes of air can be present in a filling system. If so, then alternate design procedures may be required to mitigate potential problems.

To date, most discussions of the rapid filling of stormwater systems present analyses of inertia-induced surges in the system. Even studies such as that by Zhou, et al. (2002) which considers pressure rises due to the inadequate ventilation of air from a filling system, consider the inertia of the inflowing water as the source of the air compression. The next chapter presents data collected in a stormwater system that casts doubt on the assumption that analysis of the inertia of the filling water is sufficient to understand and predict the geysering phenomenon in at least some situations.

This dissertation aims to clarify the physical processes that may occur in rapidly filling pipeline systems to cause geyser events. Various experiments to investigate the air interactions in a rapidly filling, nearly horizontal pipeline were performed in order to develop an understanding of some of the key processes associated with air release through vertical shafts connected to the pipeline. The order of this dissertation is based on the following processes which may be linked to create a geyser event:

- **Air pocket formation**: Some scenarios of how air may become entrapped in a pipeline are investigated in Chapter 4.
- **Air pocket migration**: The movement of discrete air pockets is studied in Chapter 5.
- **Initial air release**: The two-phase flow behavior which occurs as the nose of the air pocket rises within a liquid column is examined in Chapter 6.
- **Annular acceleration of air release**: Once the air pocket breaks through the free surface of the surrounding liquid, an annular two-phase flow may develop which accelerates the air velocity. This accelerated air may entrain or project liquid upward beyond the free surface and is studied in Chapter 7.
- **Inertial surge**: This term is used for the phenomenon of accelerating or decelerating a large mass of liquid. The analogy of starting or stopping a heavy train is helpful for visualizing the physical mechanism of bringing the liquid up to a certain speed or to rest. Large pressures or forces may result as a flowing system is slowed down, for example as the storage tunnel approaches its capacity. Inertial surge has been the traditional explanation for geyser events due to the flow up through a vertical shaft connected to a tunnel associated with locally high

pressures as a large amount of flowing liquid is brought to rest. Although a goal of this study is to separate the inertial surge mechanism from the process of air release creating a geyser event, the investigations reported in Chapter 8 suggest that the release of trapped air through a vertical shaft may induce significant surges in the pipeline. Since this phenomenon cannot be analyzed without describing the air interactions, a different modeling framework will be required.

Chapter 2

Motivation

2.1 Geyser Event in Minneapolis, MN

This dissertation study is largely motivated by the occurrences of dangerous geyser events in sewer collection systems around the world. In general, a geyser event which occurs in a larger system is more problematic than in a smaller system. The continued increase in size of designed CSO storage tunnels may partially explain the recent increase in attention paid to these types of events. Practicing engineers typically use single phase flow models to simulate the transients associated with the filling process. Although commercially available numerical models such as the Stormwater Management Model (SWMM) (James, 1992) can be used to simulate the dynamics of filling systems, the majority of these are not capable of resolving dynamic events such as hydraulic bores that may propagate through a filling system. Specialized models such as the MXTRAN model based on earlier work by Cardle and Song (1988) have been developed to simulate these extreme transient events. Even these more sophisticated models are based on the presumption that only the water phase needs to be modeled. It is important to know whether there are other important physical processes which can lead to geyser formation so that the design can be properly developed. In this chapter, observations from a location in Minneapolis, Minnesota subject to recurring geysers during large rainfall

events are shown to "break the mold" of the traditional inertia explanation for geyser events, implying that air plays an important role. A hypothesis for the physical behavior of the geyser event is presented below and future chapters of this dissertation will use the Minnesota geyser example for comparison with physical model results.

The city of Minneapolis, Minnesota is known to have experienced geyser events through a large diameter manhole of its stormwater collection system. Figure 2.1 shows images of two different geyser events occurring at a manhole of the I-35W tunnel system at the 35th Street location. The left image is from an event that occurred on July 13, 1997 and the right image is from an event that occurred on July 3, 1999. The explanation provided in these papers is that rapid filling of these large systems can create an inertial surge great enough to lift the water through a vertical riser connected to a nearly horizontal pipeline. In order for this process to generate the event depicted in Figure 2.1, the piezometric head in the pipeline would need to extend well above ground level. As discussed below, since a geyser event may consist of several discrete geysers separated by relatively short periods of time, this requires inertial oscillations within the system in order that this explanation can be valid.

The images appear to indicate a mixture of air and water, raising the possibility that interactions with air in the stormwater tunnel may be relevant to the geyser event. Geysers have also been reported in hydropower systems and were attributed to air entrained in a hydraulic jump within a portion of the piping system (Nielsen and Davis, 2009). However, no instrumentation was installed in that system to record system behavior during geyser occurrence.

Figure 2.1: Geyser events in the I-35W storm sewer tunnel of Minneapolis, Minnesota

Extensive laboratory studies on transients associated with the rapid filling of nearly horizontal pipelines have occurred in recent years at the University of Michigan (e.g. Vasconcelos and Wright, 2005; and Wright, et al., 2008), many of which the author has participated. Observations suggest that geysers form as a result of the expulsion of large pockets of entrapped air through vertical ventilation shafts. Vasconcelos (2005) presents the results of additional investigations on the interactions of trapped air pockets with surcharged vertical ventilation shafts. However, the jet exiting a vertical riser does not resemble that indicated in Figure 2.1, almost certainly due to scale effects in the much smaller laboratory experiments. While these experiments suggest the importance of air/water interactions, the limitations due to the relatively small scale laboratory experiments limit the ability to draw firm conclusions regarding field events.

2.2 Field Observations

The Minnesota Department of Transportation contracted with the St. Anthony Falls Hydraulics Laboratory at the University of Minnesota to install video equipment and pressure transducers to record geyser events such as those shown in Figure 2.1 above

at the 35th street location of the I-35W tunnel and another nearby location. 13 geyser events were recorded in this section of the tunnel between 1999 and 2005, with multiple geysers occurring in at least some events. Various versions of some of the video records collected at the two locations where data was recorded are available on the Internet, although it is not commonly known that pressure and velocity measurements were collected at the same locations. The Minnesota Department of Transportation agreed to the release of this additional data for a geyser event that occurred on July 11, 2004; additional data from other events exist. A video record of a portion of the July 11 event was posted for a period of time on the website for the Minneapolis Star Tribune. Modifications to the two manholes that experienced geyser formation were made in 2009 in an attempt to eliminate the phenomenon. The system is a stormwater tunnel constructed with an egg-shaped cross-section roughly 3.7 m in diameter and the manhole has a diameter of 2.4 m. The tunnel invert is 28.6 m below grade at the 35th Street manhole location. Complete geometrical details of the tunnel have not been provided, but it is understood that the manholes at which the geysers were observed are located in a section of the tunnel with a relatively flat slope with steeper slopes both upstream and downstream of this section as depicted in Figure 2.2.

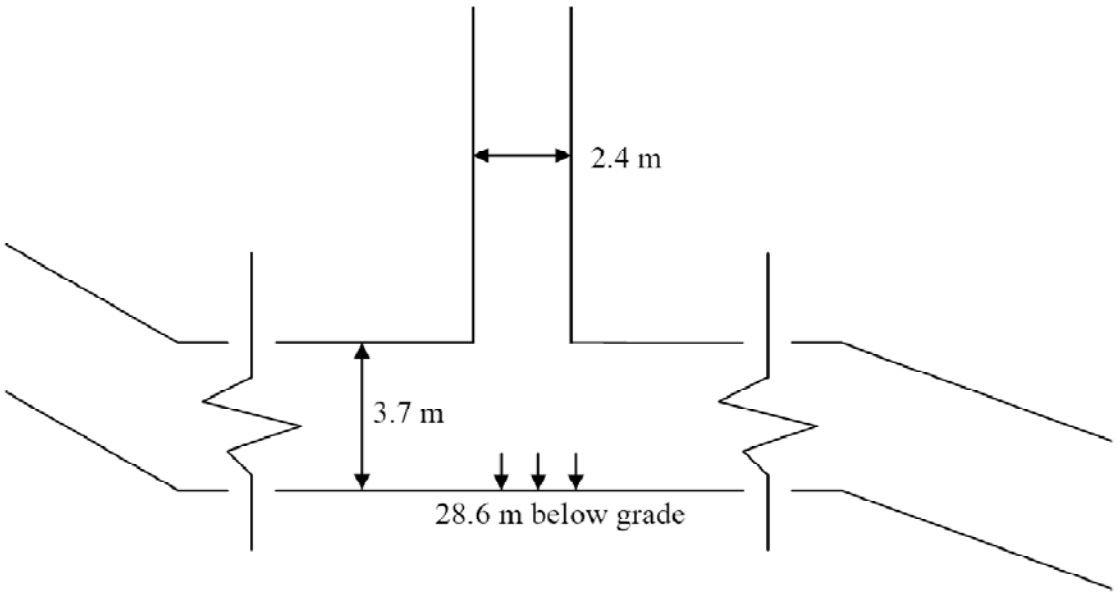

Figure 2.2. Simplified diagram of Minneapolis, MN stormwater tunnel system at the 35th Street manhole location.

Two pressure transducers were installed in the tunnel as well as a velocity probe (Sigma velocity-area flow meter). The pressure transducers were located 0.47 and 2.88 m above the tunnel invert. Velocities and pressures were recorded at five minute intervals until the water level began to rise in the tunnel. Automatic controls on sample frequency resulted in the collection of pressure data once every five seconds if the water level in the tunnel was between 0.47 and 2.88 m and once per second for higher water levels. The particular data set that was provided was collected on July 11, 2004 at approximately 5:30 AM. Nine independent geysers were observed in the video record of the event; although there is some variability, each geyser lasted for about 10-25 seconds with about 75-90 seconds separating the onset of each one. The velocity record shown in Figure 2.3 indicates that the tunnel velocity was relatively constant at about 1 m/s between about 5:30 and 8:50 AM with no indication of fluctuations that would indicate inertial oscillations in the pipeline. The absence of inertial oscillations cannot be

confirmed from the velocity records since velocity measurements are only recorded at five minute intervals.

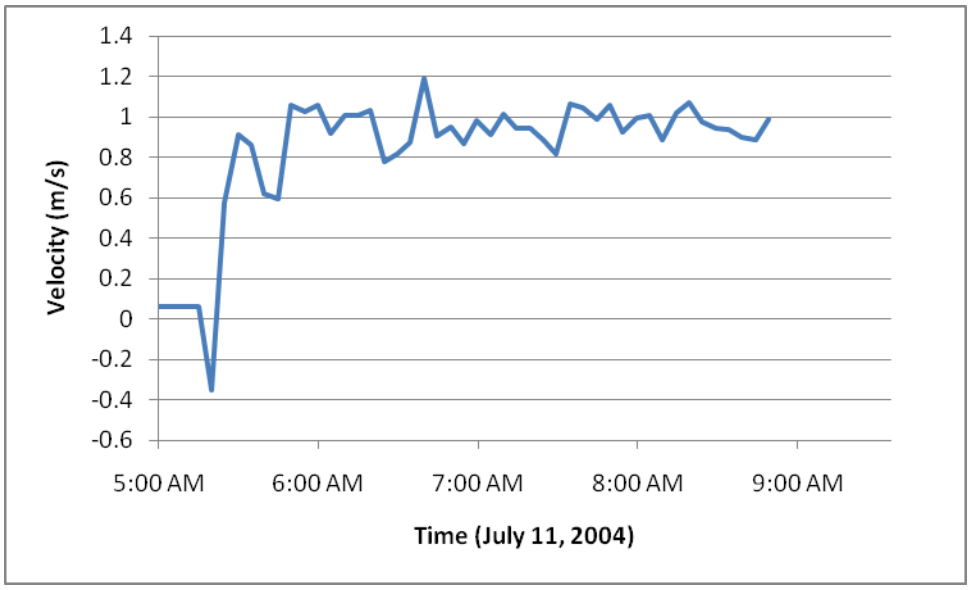

Fig. 2.3 Recorded velocity during geyser event of July 11, 2004

The upper pressure transducer provided questionably higher pressure measurements than would be expected relative to the lower transducer. If the tunnel is surcharged with no air present, then the two pressure readings should be shifted by 2.88 - 0.47 m from each other. This is not the case in this measurement and in fact the difference is less. This could be interpreted to imply that air is present in the system but it is hard to understand how if the upper portion of the tunnel (more than the difference between 3.7 and 2.88 m) is filled with pressurized air, water can escape up the manhole. It is understood that in other geyser events, for which data was not provided, the measured pressure difference was consistent with the elevation difference between the two transducers. In the absence of more knowledge of the system, it is chosen to ignore the upper pressure transducer readings; although it is acknowledged that this may result

in a loss of important information. Nevertheless, the upper transducer only registers higher pressures relative to the tunnel invert and does not contradict any conclusions made below.

The pressure history (lower pressure transducer) spanning the entire sequence of geysers is presented in Figure 2.4. The measured pressure has been increased by 0.47 m so that the pressure head is relative to the tunnel invert. Superimposed on the pressure trace are the timing of the visual observations of individual geysers and the elevation of the tunnel crown. The tunnel is indicated to be in a surcharged state between about 5:29 and 5:46 AM spanning the duration of the geyser event (approximately 5:35 to 5:44 AM). The maximum pressure head never rises above 6.0 m which is far below a value of 28.6 m that would be required to lift the water to grade under hydrostatic conditions. There is also no indication of inertial oscillations in the pressure record. Figure 2.5 presents the lower pressure transducer measurements (referenced to the tunnel invert) of about five minutes of the record during the middle of the geyser event. In general, the pressure is seen to follow an overall trend with a gradual rise and fall of pressure associated with the rainfall event as seen more clearly in Figure 2.4. The onset of an individual geyser is followed by a pressure drop that lasts until about the end of the geyser event after which the pressure tends to recover to follow the gradual trend.

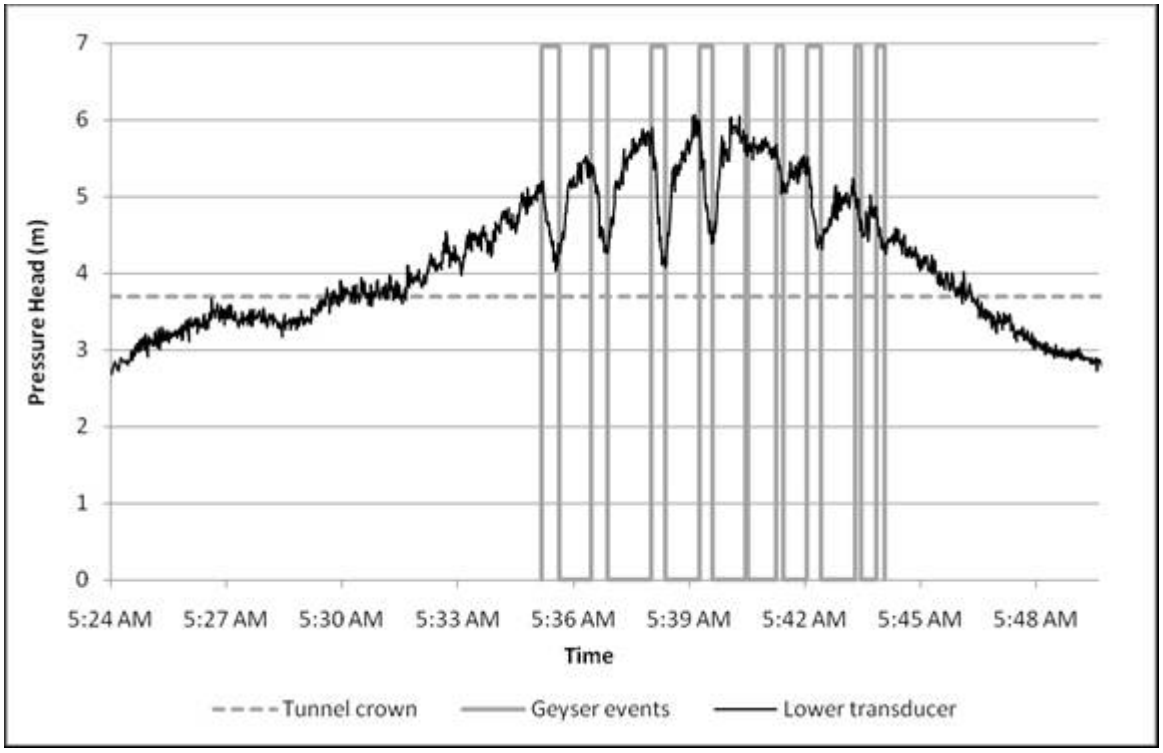

Fig. 2.4 Recorded pressure in lower transducer during the geyser event of July 11, 2004

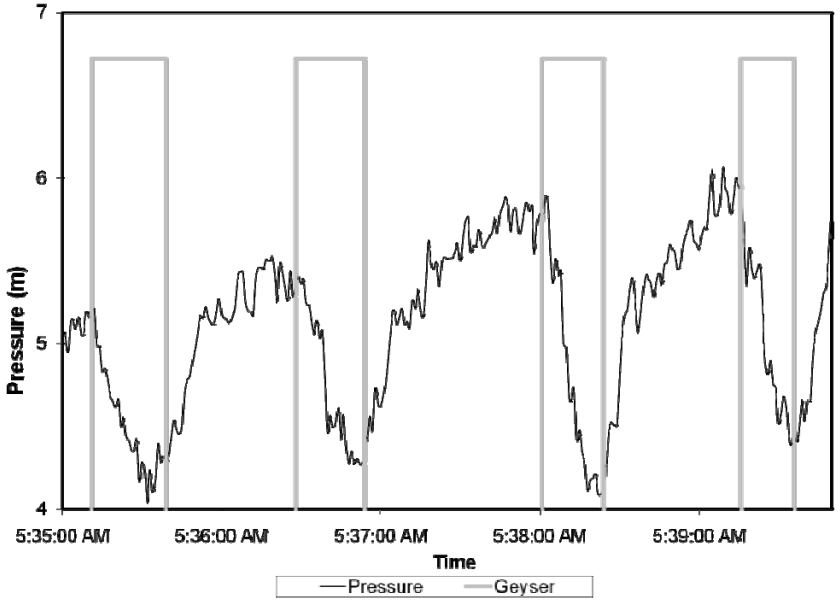

Figure 2.5 Higher resolution of lower transducer pressure record

2.3 Discussion

The extremely high rise of liquid in the video observations cannot be explained by an inertia-induced surge in the system. Using the light poles for scale in the video images from the July 11 event, it is conservative to assume that the rise of water is well over 15 m in height. If we assume that the rise is solely due to the inertia of the water at the manhole, we can write a simplified energy equation between the manhole outlet and the peak of rise, as shown in Equation 2.1:

$$H_{rise} = \frac{v^2}{2g} \qquad [2.1]$$

where H_{rise} is the height of rise, g is the gravitational acceleration, and v is the velocity of the liquid at the manhole outlet. Solving for v when H_{rise} = 15 m gives v = 17.2 m/s. This velocity in the manhole would require a flow rate of $Q = v*A$ = 77.6 m^3/s (2740 cfs or 1.23 million gpm) where Q = discharge and A = area of the manhole. This is a very large flow which would be clearly visible as ground flooding and while the videos show evidence of standing water on the ground surface, it is not consistent with a discharge of this magnitude. Also, the velocity record in the tunnel is roughly 1 m/s, indicating a flow of about 10.8 m^3/s in fully surcharged conditions which is significantly smaller than 77.6 m^3/s. It is doubtful that this geyser event could be explained by an inertia-induced surge and seems better explained by the release of a large air volume or series of discrete volumes from the system.

It seems unlikely that a water discharge even approaching the tunnel discharge could be supported up through the manhole, indicating that the jet of water must contain only a small percentage of water by volume and is comprised mostly of air. This possibility allows the development of the estimated large discharge velocity with

relatively low tunnel pressures. Consider that a pressure difference can drive an air-water mixture according to the approximation $\Delta P \sim \rho_m V^2$ with the air/water mixture at a density $\rho_m \ll \rho_w$ with ρ_w the water density. Using this relation, a maximum observed pressure head (relative to the tunnel crown) from Figure 2.4 of about 2.3 m (maximum observed pressure = 6.0 m; tunnel crown = 3.7 m) and the previously estimated jet velocity of 17.2 m/s, the required ρ_m would be about 60 kg/m^3 implying a water content of the jet on the order of 6% which seems plausible.

Another observation is that air compression does not seem to be an important part of these geyser events although it is possible to visualize that air expansion associated with decreasing pressures could enhance the geyser strength. An approximation can be made for the change in volume of the air pocket caused by the 2.3 m pressure drop. Assuming polytropic conditions, the term $p(Vol_{air})^{\gamma}$ is constant for expansion or compression, allowing the determination of either the pressure or volume change if the other is given. Here, p is the absolute pressure of the air pocket, Vol_{air} is the volume of the air pocket, and γ is the ratio of specific heats (1.2 for air in a pseudo-adiabatic process). Specifically, $p_1\left(Vol_{air,1}\right)^{\gamma} = p_2\left(Vol_{air,2}\right)^{\gamma}$, or rearranged: $\frac{Vol_{air,2}}{Vol_{air,1}} = \left[\frac{p_1}{p_2}\right]^{1/\gamma}$.

Using p_1 = 2.3 m of water pressure head beyond atmospheric pressure and p_2 = atmospheric pressure (10.3 m), the ratio of $Vol_{air,2} / Vol_{air,1}$ = 1.18. In other words, the maximum increase in volume of the air pocket is 18% using the observed pressure data. It is unlikely that the entire air pocket would increase in volume by 18% but rather only the portion of volume which is rising through the liquid in the vertical shaft. In

general, expansion of the air volume is unable to explain the geyser event, since the grade elevation is so high (24.9 m above the tunnel crown).

A question arises as to whether the air originates from upstream or downstream of this section of tunnel. The limited measurements and lack of detailed information about the system prevent a complete delineation of the air source. The mild slope in this section makes it likely that free surface flow conditions exist in the steeper portions of the tunnel upstream and downstream as this flatter section experiences a slight surcharge. Depending on the influences of gravity and hydrodynamic forces, near-horizontal systems could experience air migration in either direction, as observed in Vasconcelos and Wright (2005). Chapter 3 will discuss in more detail that the liquid velocity required to prevent upstream migration of air is proportional to the square root of diameter, as shown in Equations 2.2 and 2.3:

$$\frac{v}{\sqrt{gD}} = 0.54 \qquad \textit{Benjamin (1968)} \qquad [2.2]$$

$$\frac{v}{\sqrt{gD}} = a + 0.56(\sin\theta)^{0.5} \qquad \textit{Little, et al. (2008)} \qquad [2.3]$$

where v is the water velocity, D is the tunnel diameter, θ is the pipe slope relative to horizontal, and a equals 0.45 for $\forall_D < 0.06$, 0.50 for $0.06 \le \forall_D < 0.12$, 0.57 for $0.12 \le \forall_D < 0.30$, and 0.61 for $0.30 \le \forall_D$ where $\forall_D$ represents the dimensionless volume of the air pocket divided by ($\pi D^3/4$). Since the diameter of the tunnel in this situation is 3.7 m, the liquid velocity required to prevent upstream migration of an air pocket is roughly 3.5 m/s according to the Benjamin relation in Equation 2.2. This required velocity is greater than the measured 1 m/s in the tunnel. Therefore, the air

pockets most likely migrate upstream, originating from the downstream section that is likely to be flowing with free surface conditions.

The hypothesis of how a geyser could occur due to the release of large air pockets is indicated in the conceptual sketch of Figure 2.6. A related discussion is presented in Wright, et al. (2007). A large air pocket reaches a surcharged vertical shaft and accelerates upward due to buoyancy effects. As the air flows upward, momentum is transferred to the liquid above it as reported by Vasconcelos (2005), causing the liquid to begin accelerating upward as well, with a downward leakage of liquid around the perimeter of the vertical shaft. The recorded pressures from the field observations indicate that the liquid surcharge volume is relatively small. Therefore, it is likely that the air pocket breaks through the free surface of the liquid before the liquid reaches the top of the manhole. In the conceptual sketch of Figure 2.6, this transition would occur between images (b) and (c). The corresponding drop in system pressure is noticed in Figures 2.4 and 2.5 as this break-through occurs.

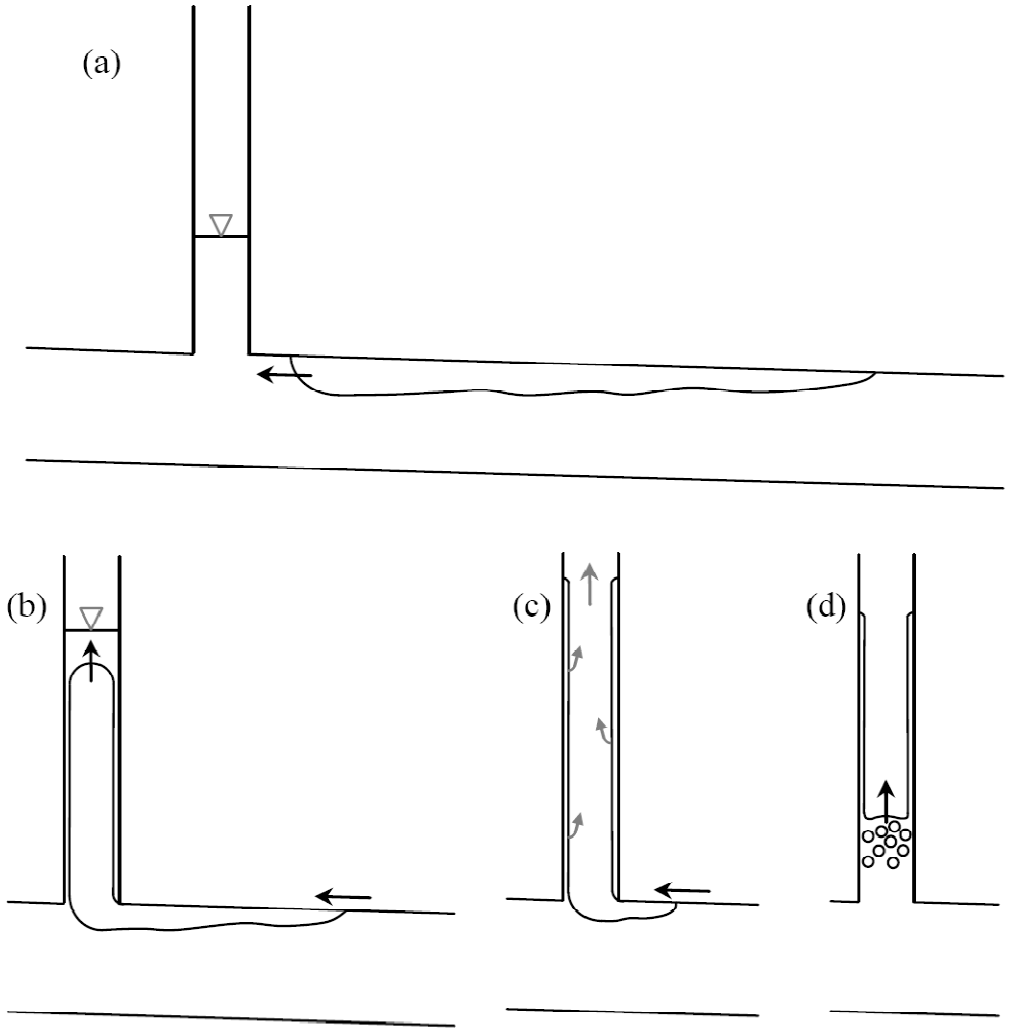

Figure 2.6. A conceptual sketch of geysering due to the release of a large air pocket: (a) The large air pocket migrates towards the vertical shaft. (b) The acceleration of the air pocket into the vertical shaft due to buoyancy causes the water level to rise. (c) The geyser is observed as the high velocity air flow entrains liquid due to flooding instability; (d) The arrival of the tail of the air pocket potentially causes the pressure to increase.

The rise height of the water jet indicates that the air velocity is great enough to trigger flooding instability at the vertical interfaces between the air and liquid. The high shear between the rising air and falling water creates interfacial instabilities as described, for example, by Guedes de Carvalho, et al. (2000). Experimental results by Guedes de Carvalho, et al. revealed that air velocities greater than 3-7 m/s in small diameter pipes

near atmospheric pressure are capable of generating disturbances on the vertical interface. Air velocities beyond this threshold can generate liquid entrainment into the upward air flow. The phenomenon of flooding instability is not observed in the small scale experiments of Vasconcelos (2005) and others because the rising air velocity does not reach a sufficient magnitude to produce flooding instability. Instead, the air-liquid interface remains relatively smooth while the air is released.

The practical example in this chapter provides a framework for the importance of considering the effect of air in filling systems. It is certainly possible that other mechanisms could create conditions associated with a strong flow of air and water from a filling system; Chapter 4 describes another alternative. However, even the results presented in this chapter indicate the importance of considering air interactions. Although it would be valuable to have more field data, the available evidence strongly suggests the importance of air to the process of geyser formation. There seems to be no mechanism of single phase water flow capable of producing the observed geyser events. This dissertation physically investigates relevant air release processes that can lead to geyser events.

Chapter 3

Background

To provide additional context beyond the results presented in Chapter 2, information that motivated various aspects of the present study are described. This discussion is followed by a discussion of the research literature relevant to processes that are deemed to be pertinent to some aspect of the present study.

3.1 Air Pocket Formation within Pipelines

An initial important consideration is simply the definition of the term "geyser" or "geysering" in the context of the current application. Because of an apparent lack of understanding of the mechanisms involved in the example from Chapter 2, and due to the apparent lack of dynamic similarity between that situation and smaller scale laboratory studies, a number of unrelated definitions of geysering have been advanced. For example, the quote by Guo and Song (1991) presented in Chapter 1 implies that they would consider any rise of water through a vertical shaft that results in water spilling at the ground surface constitutes a geyser. This is perhaps too general a definition that can lead to confusion as to the level of concern that should be attached to geysers. A problem at the laboratory scale, as discussed in Chapter 2, is that jets of air-water mixtures such as depicted in Figure 2.1 are not generally observed. One approach is to suggest that any

explosive release of air and water through a vertical shaft constitutes a geyser, regardless of whether there is any connection to the events described in Chapter 2. Because there is currently no complete understanding of the process and therefore no consensus on a definition, this study simply follows a convention that a release of air and water through a vertical riser to levels greater than hydrostatic pressure head constitutes a geyser.

During the course of experimentation that is described in Vasconcelos and Wright (2005), a short video was recorded of an experiment. The overall setup involved a horizontal pipe with a head box to admit inflow through at one end and a large diameter riser serving in the role of a surge tank at the opposite end. Near the center of the pipe, a small diameter short vertical riser was installed which also had an orifice plate installed at the top of the riser. Inflow was initiated into a stagnant, partially full pipe and the air at the top of the pipe was forced towards the surge riser at the downstream end by a pipe-filling bore. Air was not free to escape at that location and was trapped in the pipeline once the bore passed the location of the vertical riser. Following the reflection of the inflow surge at the far end of the pipe, a large air pocket returned to the riser. A strong ejection of water was observed from the top of the riser at both the arrival of the air pocket at the riser and upon the arrival of the tail end of the pocket at the riser; visually, the water ejections appear to be of about equal strength with perhaps the second process resulting in the higher ejection of water. This observation drove the planning of initial experiments. The findings from this study will be used to interpret that video.

During the course of this study, others in the research team were involved in a preliminary design analysis for a proposed combined sewer overflow storage tunnel for the City of Washington, DC. Numerical simulations were performed with a version of

the two-component pressure approach numerical framework proposed by Vasconcelos, et al (2006). The results of the numerical modeling were used as a rationale for conducting some of the experiments described in this dissertation, notably the results presented in Chapter 4. In addition, the Washington DC Water and Sewer Authority (DCWASA) was willing to provide support for some of the experiments related to dynamics of air interaction in vertical ventilation shafts. Some of the particular experimental conditions tested related to preliminary design configurations that were under consideration at the time. This has led to some variations among various sets of experiments, making it somewhat difficult to make direct comparisons.

The specific concern of this research involves the interactions of discrete air pockets, i.e. that are completely surrounded by water and their interaction with vertical ventilation shafts, manholes, etc. There are several processes by which the existence of air in this state can occur. One of the most commonly recognized ones is due to the entrainment of air in drop shafts through which water is admitted into a storage tunnel for example. The falling water in the drop shaft entrains air, and if de-aeration is not allowed to happen, the air gets carried along the crown of the storage tunnel as a more or less continuous input. There has long been a recognition of this issue and specific design modifications have been made to drop shafts (for example Ettema, et al., 1982) or de-aeration chambers have been added to allow the escape of air (Kennedy, et al. 1988) from the water prior to entry into the tunnel. Physical hydraulic models are often constructed to study this process, with substantial air fluxes into the tunnel of more than 15% reported for a proposed system in Portland, Oregon (Roberts 2004) to less than 0.5% reported for the proposed DCWASA system (Lyons 2010). Another apparently less recognized

process for entrapment of air in storage tunnels involves various transient flow features as the tunnel undergoes a transition between a free surface and a pressurized flow state. Vasconcelos and Wright (2006) report on a number of different ways in which air can become trapped during such a process; a common feature is the interaction of a hydraulic bore with system boundaries. Additional mechanisms have since been identified and some of these are discussed later in this dissertation. One fundamental difference between these two situations is that air entrainment within drop shafts may be distributed in smaller air pockets compared to larger air volumes that might occur due to hydraulic bore interactions such as discussed in Chapter 4. One question is whether the air entrained in each of the processes discussed above behaves in a similar fashion with respect to potential for geysering.

Once air becomes entrapped within a pipeline, it can be expected to escape vertically at locations where that possibility has been created. This could occur at access shafts (manholes) or it could be at ventilation shafts that have been expressly included in the design in order to vent air from the system. It is expected that air will escape due to the relative buoyancy of the air at these points in systems when the vertical shafts are attached to the tunnel at or near the crown. If the tunnel exists in a surcharged state as the air arrives at the location, water will be standing in the vertical shaft at a level reflecting the piezometric head in the tunnel at that location. It is considered that the interaction between the water occupying the space above the entering air and the rising air will play an important role in defining the potential for a geyser event to occur. A related question is what happens at the end of the air venting process when the shaft returns to a state totally occupied by liquid.

Reflecting the chronological order of the processes presumed to occur in the formation of a geyser event, the next subsections of this chapter discuss an overview of the available literature related to this study.

3.2 Horizontal Air Pocket Movement

A question arises about the general direction of discrete air pocket migration through a sloped pipeline filled with liquid. In general, an air pocket is less dense than the surrounding liquid and the buoyancy of the air will cause it to rise up the slope. If the liquid is flowing through an upward inclined pipe the air and liquid will both flow in the same direction, up the slope of the pipe. However, air migration could be in either direction when water is flowing in a downward inclined pipe. If the slope is relatively small and the liquid is flowing at a high enough velocity, the liquid is capable of preventing the air migration up the slope and will push the air in the downstream direction.

The study of Benjamin 1968 provided a broad theoretical exploration of the movement of air cavities within full pipes. The study considered the intrusion of an air front and its assumed analogue, the intrusion of a gravity current, or a density current such as salt water flowing into a body of fresh water. Figure 3.1 shows the typical scenario where a long, horizontal, rectangular system is initially filled with liquid and then one end is opened to create a free outflow due to gravity.

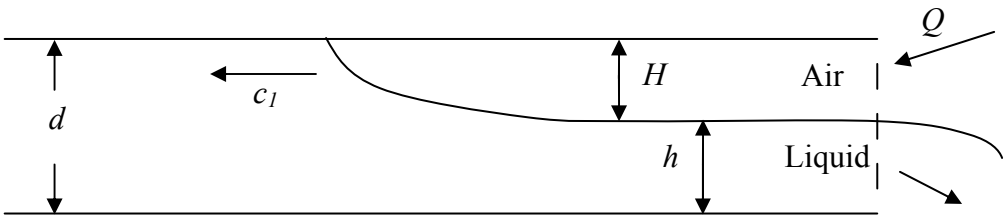

Figure 3.1: Illustration of Air Intrusion Motion

Benjamin assumes that provided there is enough length, the air intrusion will reach a certain steady state, relative to the frame of reference moving with the intrusion front, which balances the buoyant force with the drag force at the head of the intrusion. The depth downstream of the front, *h*, approaches a constant value. Using the conservation laws of mass, momentum, and energy (no dissipation) the ratio of *h* / *d* is found to be 0.5 for a two-dimensional intrusion, the value of $c_1 = 0.5\sqrt{gd}$, and the value of $Q = 0.25\sqrt{gd^3}$ per unit span. When energy dissipation is permitted, Benjamin showed that *h* / *d* must be greater than 0.5, therefore $0.5 < h/d < 1$. Various relationships were developed in the Benjamin study including the energy dissipation Δ and the dimensionless numbers $c_1/\sqrt{gd}$, Δ/d , and $Q/\sqrt{gd^3}$ which are functions of *h* / *d*. Wilkinson (1982) showed that one way to produce a smaller air intrusion thickness than predicted by the energy conserving solution was to restrict the water outflow by placing a weir at the outlet section, thus more limited air flow situations are likely to result in a smaller intrusion thickness and different propagation characteristics.

The study by Benjamin revealed many other interesting aspects of the air intrusion scenario. Without energy dissipation, the free-surface region of the downstream flow ($h = 0.5d$) is supercritical with a Froude number ($\boldsymbol{F} = v / \sqrt{(gh)}$ where *v* is the water velocity downstream from the air intrusion) of 1.414 and capable of forming a hydraulic

jump. Including energy dissipation, the maximum value of $c_1/\sqrt{gd}$ occurs at an h / d ratio of 0.6527 while $c_1/\sqrt{gd}$ = 0.5273, providing an estimate for the maximum air intrusion; air intrusions less than this limit are also permitted. The energy dissipation is also a maximum in this situation, with Δ/d = 0.0209. Following this argument leads to the general rules for two–dimensional rectangular flow:

$$1 < \boldsymbol{F} < \sqrt{2} \quad \text{for} \quad 0.5 < h/d < 0.6527$$

$$\boldsymbol{F} = 1 \text{ for } h/d = 0.6527 \text{ (when } c_1 \text{ is maximum)}$$

$$\boldsymbol{F} < 1 \quad \text{for} \quad h/d > 0.6527$$

Further study by Benjamin showed that the typical shape of a real air cavity intrusion in a "great depth" case is similar to Figure 3.2. There is a head shape at the intrusion front followed by a breaking wave similar to a hydraulic jump. Assuming a wake region at the top of the liquid region due to the breaking wave, Benjamin showed that the pressure inside of this air cavity is approximately equal to ρgH. In the case where the pressure of the cavity (p_c) is fixed and the rate of supply is unrestricted, the intrusion velocity is $c_1 = \sqrt{2gH}$. On the other hand, if the supply rate, Q=c_1H, is fixed then $c_1 = (2gQ)^{1/3}$ and the mean depth $H = \sqrt{Q^2/2g}$.

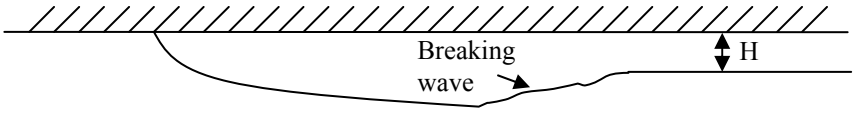

Figure 3.2: Illustration of Real Air Intrusion

Similar results were discussed by Benjamin for a circular cross section, a typical geometry for pipelines. In summary, the solution of the equations without energy dissipation shows that $c_1/\sqrt{gr} = 0.767$ and the angle α is 82.76 degrees, where *r* is the radius of the circular pipe as shown in Figure 3.3. Equation 3.1 will be referred to throughout this dissertation, which rewrites the above expression in terms of diameter:

$$c_1 = 0.54\sqrt{gD} \qquad [3.1]$$

where the constant 0.54 will be important for comparison purposes. The corresponding Froude number is 1.328 downstream, as compared with 1.414 for the 2-D rectangular case.

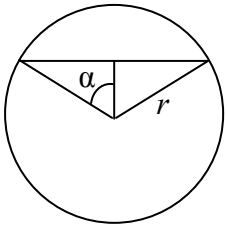

Figure 3.3: Circular cross section

Further research by Little, et al. (2008) confirmed the work of Benjamin with experiments in a 150 mm diameter pipe using finite air volumes. The experimental results were used to develop an empirically adjusted equation for the flow in a downward sloping pipe required to prevent upward air migration:

$$\frac{v}{\sqrt{gD}} = a + 0.56(\sin\theta)^{0.5}$$

where $\forall_D$ represents the volume of the air pocket normalized by ($\pi D^3/4$); and *a* equals: 0.45 for $\forall_D < 0.06$, 0.50 for $0.06 \le \forall_D < 0.12$, 0.57 for $0.12 \le \forall_D < 0.30$, and 0.61 for

$0.30 \leq \forall_D$; and θ equals the pipe slope relative to horizontal. It is suggested that this equation will apply to horizontal pipelines as well. Little, et al. (2008) also performed an investigation using computation fluid dynamics (CFD) software to confirm their experimental results. The air cavity size for these experiments was limited, with a $\forall_D$ value of 0.06. Based on their study, they suggest the above equation is applicable for diameters up to 2 m and perhaps beyond.

The experimental work of Vasconcelos and Wright (2008) studied the situation of a 95 mm diameter horizontal pipe emptying from a completely filled state by opening the downstream end. An equation for the air intrusion velocity in circular pipes based on the Benjamin analysis was given, as also indicated by Townson (1991):

$$\frac{c_{air}^2}{gD} = \left[\frac{\pi - \alpha - \sin\alpha\cos\alpha}{\pi}\right]^2 \times \left\{\frac{1 - \frac{1}{3\pi}\left[3\sin\alpha + 3(\pi-\alpha)\cos\alpha - \sin^3\alpha\right]}{\left(\frac{\pi - \alpha + \sin\alpha\cos\alpha}{\pi}\right)\left[2 - \left(\frac{\pi - \alpha + \sin\alpha\cos\alpha}{\pi}\right)\right]}\right\}$$

where c_{air} is the intrusion velocity of the air, and 2α is the angle subtended from the center of the pipe to the free surface. The experimental results showed that the above relations can only be applied to situations when air is actually intruding into the liquid region. In general, as the intrusion propagates upstream the intrusion thickness decreases. Free surface waves may reach the pipe crown behind the thin intruding front resulting in the disintegration of the intrusion. The loss of the head-like structure of the intrusion results in the rapid downstream migration of the air/water interface.

These studies of air migration focus mainly on air intrusions of emptying pipes and it is unclear how transferable these results are to the behavior of discrete air pockets. Theoretically, very long air pockets with a limit on the air volume could develop similar

shapes as seen above in Figure 3.2 and analytical relations such as Equation 3.1 near the front of the air pocket. The recent work of Wickenhauser and Kriewitz (2009) studied air migration in large downward inclined pipes with slopes between 0.004 and 0.087. Their investigation offers many helpful insights related to the physical behavior of discrete air pockets in a downward inclined pipeline. Their experiments measuring air migration as a function of water velocity and air flow rate observed that smaller air bubbles are carried with the water flow while larger bubbles migrated up the slope. For a specific slope and water velocity, a threshold can be observed for the maximum air flow that is transported in the direction of water flow. Any extra air added to the pipe beyond this threshold will migrate up the slope.

3.3 Vertical Air / Water Interactions

Vertical shafts are often designed as a means for air ventilation in pipelines. If the vertical shaft is in a surcharged state as air is ventilated, water stands within the shaft approximately to the level of the local piezometric head as discussed earlier in this chapter. As trapped air enters the shaft, the momentum of a rising air pocket may be capable of lifting the liquid a significant distance. In this scenario, a vertical two-phase flow of air and liquid, driven by the buoyancy of the air, is established as air is released through the liquid column. This physical process, although studied in some detail in other fields, has received relatively little attention among the civil engineering community. In most cases the air behavior is ignored entirely. Depending on the size of the system and the volume of air which is being ventilated, this vertical two phase flow situation may be capable of lifting water far beyond the system pressure.

Nicklin (1963) discusses many of the complexities of vertical air/water flow including the delineation of the different types of vertical flow regimes. For low air concentrations, the "bubble" flow regime contains a distribution of small bubbles. Increasing the air concentration leads to the "slug" flow regime with long round-nosed air bubbles. Further increase of air flow can lead to "annular" flow where a continuous air pocket exists through the center of the vertical tube. The focus of Nicklin's study is air-lift pump theory with slug flow as the primary regime and the time scale of interest is very different from potential geyser events created by air release in CSO storage tunnels. Operation of air-lift pumps considers function at longer time scales (i.e. much longer than the interaction time for a single air pocket) where it is desirable to focus on sustained air/water interactions. Concepts related to geyser events, however, deal with the short time scales associated with the motion of a single air pocket and extremes in behavior.

The interfacial profiles of upward air flows in a 25.8 mm diameter tube were studied by Sekoguchi, et al. 1996. For upward flow, the leading edge of upward moving air pockets formed a convex shape. Sekoguchi, et al. found that very small bubbles tend to gather near the tube wall. As the bubble size increases, the air phase generally tends to occupy the center of the vertical shaft while the liquid forms a thin film flow downward around the perimeter.

Experiments of Davies and Taylor (1950) measured the rise velocities of large air bubbles within an emptying cylinder which was closed at the top and air entry at the bottom. The removal of the container's bottom initiated the gravitational drainage of water downward around the air that was replacing it. Davies and Taylor developed an

analysis that showed that the rise velocity was proportional to the square root of the diameter:

$$u_s = 0.35\sqrt{gD\frac{\left(\rho - \rho_g\right)}{\rho}}$$

where u_s is the vertical velocity of the gas slug, ρ is the density of the liquid and ρ_g is the density of the gas. The primary difference between this experimental setup and most sewer collection systems is that the free surface level of the liquid is not confined as in the Davies and Taylor experiments. In real collection systems the upward momentum of the rising air may be transferred to the surrounding liquid, causing the liquid free surface to move upward. Nevertheless, the Davies and Taylor study is a starting point in the discussion of such two-phase flow situations although in systems with small discrete air pockets, the rising air may not exist in a continuous column.

Vasconcelos and Wright (2011) developed a numerical model for the release of a single air pocket through a liquid-surcharged vertical shaft. A simplified framework of a 1-D rigid column (or lumped mass) model is used for the column of liquid above the arriving air pocket. As the air is released some mass of the liquid leaves the column in the form of film flow around the perimeter. An assumption of the modeling framework is that the liquid film thickness, calculated using equations developed by Batchelor (1967), remains constant throughout the air pocket rise. The liquid momentum is also conserved and the air pressure below the liquid column is capable of accelerating the liquid upwards. The air pressure is calculated similar to the method developed by Li and McCorquodale (1999) for each time step. The key parameters which are updated with each time step are the interface position between the liquid column and the air pocket, the

velocity of the interface, the volume of the air pocket, the pressure of the air pocket, the position of the free surface of the liquid column, and the velocity of the free surface.

Vasconcelos and Wright (2011) showed that experimental results compared relatively well with the numerical model. The setup consisted of a single vertical shaft installed on a closed horizontal pipe. A butterfly valve separating the air pocket from the liquid within the pipe was opened rapidly to initiate the air migration toward the vertical shaft. The essential features of the experimental and numerical results are consistent, and in general, the movements of the air/water interfaces above and below the liquid match. The general trend of the air pressure is described well while some details are not entirely consistent. It is unknown whether the application of this numerical model to other system configurations is appropriate. Their apparatus involved a horizontal pipeline which was divided into a water-filled segment and a smaller air-filled one separated by a valve with a vertical riser mounted along the water-filled portion. When the valve was opened, the water level in the riser quickly adjusted to equalize system pressures. The difficulty with this arrangement is that the water level in the riser after valve opening controlled system pressures. In an actual system, it is presumed that flow conditions in the tunnel control the pressure in the riser, rather than the other way around.

The liquid film around the outside of an escaping air bubble may develop instabilities due to the counter-current shear between the air and liquid, as discovered by Hewitt and Wallis (1963). The study by Nakazatomi, et al. (1992) of the rising characteristics of gas slugs in a 19.2 mm diameter tube showed that the film thickness gradually decreased in the downward direction and reached a minimum at the start of the formation of waves. An increase to the flow of air increases the countercurrent shear

between the upward moving air and the downward flowing water. Surface waves may develop at this interface (Hewitt and Wallis 1963) and become unstable due to the increased shear. This physical process is very difficult to study at the laboratory scale because a large diameter shaft would be required to produce air velocities high enough to cause flooding instability with the experimental configuration of Vasconcelos and Wright (2011).

The work of Guedes de Carvalho, et al. 2000 studied the flooding instability of gas slugs rising in vertical tubes filled with water. The tubes used in their experiments were 21.0 and 32.8 mm in diameter. Guedes de Carvalho, et al. found that the onset of flooding instability was highly dependent on the upward velocity of the gas. The small diameter tubes at this scale generally make it difficult to achieve sufficiently large velocities to create flooding instabilities. This study accounted for this by increasing the pressure of the gas used which increased the gas density and decreased the required velocities for onset of flooding according to a scaling law that they proposed. Gas velocities beyond this flooding threshold were capable of entraining liquid into the upward gas flow.

The work of Vijayan, et al. (2001) visually observed the importance of shaft diameter to the phenomenon of flooding. The setup for this study was different than would be expected for a CSO tunnel, with the water being injected near the top of a vertical pipe with air flowing upward. The setup of Vijayan, et al. created high air velocities which aided the ability to visualize flooding. The results indicated a qualitatively different physical mechanism between a 25 mm diameter pipe and a 67 or 99 mm diameter pipe. The flooding in the smaller pipeline occurred by the upward

movement of large waves created near the liquid outlet, but these waves were absent from the larger diameters. Flooding in the 67 and 99 mm diameter pipes occurred by the rapid creation and breaking of waves which resulted in droplets being entrained in the air flow, giving the appearance of a turbulent churn-like flow within the liquid. A similar phenomenon is expected for vertical shafts of CSO tunnels where large diameters allow for the potential of much higher upward velocities. The implications are that large systems are more conducive to flooding instability which could result in liquid being entrained in the air release process.

Other studies have addressed the problem of air in pipelines, but the connection to the problem of geyser formation is unclear. Zhou, et al (2002) report on an experimental and numerical study of pressure rises due to compressibility of air in a rapidly filling pipeline with a restriction on the air escape. While this may be an important issue in the design of large sewers, it is not clear that there is any connection with geyser events. Li and McCorquodale (1999) discuss the motion of entrapped air pockets that are formed due to interfacial instabilities associated with the velocity shear at the air-water interface in the horizontal pipeline and present experimental data that show pressure spikes associated with air release through a vertical shaft. However, there is no discussion of geysers or any direct way to connect the small scale laboratory measurements to the event depicted in Figure 2.1. Wickenhäuser and Kriewitz (2009) report on experiments related to de-aeration and release of entrained air in a hydropower tunnel; these bear some resemblance to some of the experiments mentioned above but do not directly address geyser formation. Izquierdo, et al (1999) report on the release of small air pockets from a filling pipeline such as a water main, where the air pocket is compressed and acts like a

spring to increase the upward velocity of water in a riser. Again, this study did not discuss whether or not the physical process of air release is alone capable of producing a geyser event in a large scale system.

3.4 Knowledge Gaps

The aim of this dissertation is to fill some of the knowledge gaps that exist regarding air and water interactions within CSO storage tunnels during rapid filling which may be capable of producing geyser events. Listed below are some specific aspects that will be addressed in this study:

- The existing literature does not provide compelling evidence that geysering is only explained by inertia-induced surge. It is arguable whether surge can explain the magnitudes of these events in at least some circumstances. The data provided by the Minnesota Department of Transportation shows that the system pressures are not large enough to explain the geyser event recorded with a surge explanation. The literature does not provide a discussion of the physical mechanisms for how geysers could occur independent of inertial surges.
- The literature related to air-lift pumps shows that air is capable of lifting water, but it is unclear whether the physical process of air lift alone is capable of causing a geyser event such as the Minneapolis example discussed in Chapter 2.
- The literature does not provide a discussion for quantifying or estimating the amount of potential air trapped in a pipeline other than the air entrained at drop shafts. A comparison between the likelihood of drop-shaft entrainment versus entrapment during rapid filling as the source of air in geyser events is also absent.

- With a few exceptions (Trajkovic, et al. 1999 and Politano, et al. 2000, mentioned later in Chapter 4), most of the research related to flow regime transitions during rapid filling have focused on pipe filling bores while disregarding the possibility of gradual flow regime transitions. If the process of air release of large air volumes is considered to be particularly important, then the gradual flow regime transition is of importance.
- Geometric properties of a real storage tunnel system could result in multiple hydraulic bores propagating through the pipeline simultaneously. A specific scenario of two gradual flow regime transitions colliding together is of interest due to the potential for air entrapment. An investigation of possible geyser events resulting from this scenario has not been performed.
- It is unclear how the infinite air intrusion relations studied in the literature can be applied to the migration of discrete air pockets in a near-horizontal pipeline. Limited experimental data is available to compare the similarities between the two scenarios.
- There is a limited amount of experimental data related to the release of a discrete air pocket through a partially surcharged vertical shaft. A better understanding of air and water velocities associated with the initial rise of a large air pocket in a vertical shaft would be valuable. It is unclear whether the experimental setup of Vasconcelos and Wright (2011) appropriately estimates the potential for rapid air and water rise. A configuration that may approximate what happens in a real system more closely would be useful.
- In general, it is unknown what size and numbers of air pockets are the most problematic for geyser events.

- The arrival of the tail of an air pocket at a vertical shaft re-introduce water into the shaft and this inflow may result in intertial oscillations. Experimental work by Vasconcelos (2005) indicates that this situation may result in a geyser event. Important factors in determining the strength of this vertical oscillation are unclear. As mentioned in the introduction to this chapter, the observation of approximately an equal strength ejection of water when both the front and tail of the air pocket arrived at the vertical shaft was observed in a laboratory experiment of Vasconcelos (2005). It would be helpful to understand the air release process sufficiently to be able to suggest which one of the two processes is more relevant to geyser formation.
- Assuming that the geysering phenomenon is a result of the release of air pockets within CSO storage tunnels, it is a new area of research to approach the mitigation of such events. Disrupting the interaction of an upward accelerating air slug with a thin film of downward water flow around the outside could be useful. A way of breaking up this air/water interaction could hypothetically be to introduce a geometric adjustment to the vertical shaft. One specific mitigation idea is to install an expansion of the riser diameter.
- Preliminary numerical modeling efforts by Vasconcelos, et al. (2006) have attempted to follow the air phase pressurization during rapid filling of a pipeline in a one-dimensional framework. It is unclear whether modifications to this modeling framework can accurately predict the vertical two phase flow dynamics of a geyser event; for example, the upward velocity of the air pocket and the transfer of momentum to surrounding liquid. In addition, there may be feedback between the fluid dynamics within the main tunnel and that within the vertical shaft which may provide significant limits to the application of a 1-D single phase numerical model.

3.5 Expected Contribution

The following brief list represents the primary objectives of this dissertation research. The experiments described in the subsequent sections of this paper will aim to study these objectives in detail.

- Understand the role that inertial surge and air release play in flow behavior in vertical shafts connected to nearly horizontal conduits and how this may relate to geyser formation.
- Conduct experiments to develop an understanding of the formation of the observed Minnesota geyser event.
- Use experimental observations to identify some critical air release scenarios including the role that air pocket size has on the process.
- Measure the migration velocities of large discrete air pockets in comparison to infinite air intrusion velocities available in the literature.
- Compile a physical data set of the vertical air and water interactions during the air release process. Some experimental variables of interest are the riser diameter, equilibrium water level, and the method for air introduction to the main tunnel.
- Preliminary observations of various solution strategies intended to mitigate geyser events.
- Suggest requirements for numerical modeling techniques to account for the influence of trapped air in the development of a system design.

Chapter 4

Rapid Filling and Air Pocket Formation

4.1 Objective

Rapid filling of a combined sewer collection system occurs when inflows are very large during a precipitation event. In some cases, the inflow is large enough to create a filling front, otherwise known as a shock wave or hydraulic bore. As the liquid continues to fill the system, a transition from the free surface flow regime to a pressurized conduit flow regime may occur in two forms: a pipe-filling bore or a gradual flow regime transition. The study of these two types of bore scenarios has important implications for explaining the mechanisms of both pressurized surges and air-induced geyser events. Nearly all previous experimental investigations of flow regime transition have involved the study of pipe-filling bores; this seems to be a consequence of the experimental setup implemented as opposed to a necessarily common occurrence in prototype systems. Numerical computations using the TPA framework of Vasconcelos, et al. (2006) for the Washington, DC Water and Sewer Authority revealed that the flow regime transition commonly occurs as a gradual flow regime transition that involves a regular free surface bore followed by a gradually sloping free surface up to the pipe crown. A primary objective of the experiments in this chapter was to clearly distinguish these two types of flow regime transitions. It is hypothesized that the gradual flow regime transition could

be very conducive to air entrapment within the system. Therefore, a further objective is to observe the capability of air pockets which are trapped during the flow regime transition to produce geyser events.

4.2 Introduction

Large storage tunnels are a common way to retrofit combined sewer systems to reduce the number and volume of releases of poor quality water to the environment. Typically, storage tunnels are constructed well below the grade of the existing sewer system with drop-shafts providing the connection to divert water into storage when the capacity of the existing sewers is exceeded. Inflow thus enters the tunnel at a number of discrete locations. There are two major transient conditions that must be considered in the design of these systems; namely preventing large surges caused by pressurization and the avoidance of geyser events (discussed by Guo and Song 1990). Both phenomena apparently involve the transition of the tunnel from a free surface flow state to a pressurized one, especially under rapid filling conditions.

The flow regime transition will result in the formation of hydraulic bores under conditions of rapid filling. These bores may be one of two types; a regular free surface bore with free surface flow conditions on either side of the bore or a "pipe-filling bore" exhibiting pressurized conditions on the back side of the bore (see Figure 4.1). In the case of a free surface bore, there may be a gradual transition to a pressurized condition potentially well behind the bore, although the distance involved will depend on filling conditions, the frictional resistance, and the geometry of the pipeline. This situation is referred to as a "gradual flow regime transition". Previous experimental investigations

have mainly created conditions that result in the pipe-filling bore, although a notable exception is the study by Trajkovic, et al. (1999) in which the most common experimental result was a gradual flow regime transition. The differences between the laboratory observations and the prototype system expectations can be explained by two factors: 1.) The relatively shorter conduit length in the laboratory model prevents a gradual flow regime transition before a pipe-filling bore is created by reflections from one of the two pipe ends, and 2.) The laboratory models are typically tested by creating an essentially instantaneous inflow rather than the more gradual filling hydrographs created by the interaction of the rainfall/runoff process with the surface sewer system. Consequently, it is believed that many prototype systems will more typically experience gradual flow regime transitions as compared to pipe-filling bores. Numerical models used for design analysis must be capable of resolving both types of bores. One recent numerical model formulation that explicitly accounts for the gradual flow regime transition is Politano, et al. (2007).

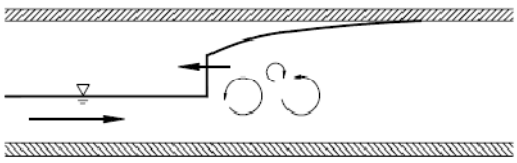

Figure 4.1a – Gradual Flow Regime Transition

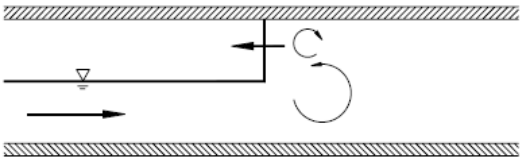

Figure 4.1b – Pipe Filling Bore

Storage tunnels are generally constructed with a small slope to facilitate de-watering and flushing after the storm event. A common scenario during filling involves the entering water flowing down the slope and the tunnel generally undergoes the flow regime transition between free surface and pressurized flow at or near the portion of the

tunnel with the lowest elevation. The flow regime transition then propagates relatively quickly to the opposite end of the system. Both surges and geysers are possible outcomes associated with the propagation of the filling front, especially following the reflection of the filling front off the upstream end of the tunnel system. Because there are a wide variety of geometric conditions associated with systems that have been constructed to date, it is stressed that the above comments are only a generalization and may not apply to all systems.

Under certain conditions, the flow regime transition may occur in ways that trap significant volumes of air at the pipe crown. Vasconcelos and Wright (2006) suggest a variety of ways that this air entrapment can occur, depending on the tunnel geometry and the mode of filling. Subsequently, additional ways that air entrapment occurs have been observed. Given the nature of the flow regime transition, it appears that an important way for air to become trapped in a tunnel system is for a gradual flow regime transition to propagate until it arrives at a location where it is partially or completely reflected, resulting in a pressurized condition at the reflection location. Depending on specifics of the geometry and the filling process, a potential exists to trap the large volume of air lying above the water surface between the location of the bore and the actual flow regime transition. Subsequent transport of this trapped air to a vertical shaft then produces the conditions for a geyser event to form. Proper placement of adequate ventilation is critical to eliminating the air from the tunnel while avoiding the occurrence of geysers. Discussion of this scenario appears to be absent from the previous literature on transients in rapidly filling tunnel systems.

4.3 Experimental setup and procedure

The purpose of the experimental investigation was to produce the two types of bores discussed above. These bores were formed by suddenly introducing flow at the upstream end of an initially empty pipe. An actual collection system would experience inflow hydrographs at a number of discrete locations. However, the essential behavior of a typical tunnel filling scenario (filling from the lower elevation end of the system) could be reproduced with the simpler experimental configuration and no attempts were made to reproduce complex filling scenarios that may occur in more complex systems. The reflection of the filling front off the closed downstream end of the pipe created a bore that subsequently propagated back towards the filling end. Depending on the inflow rate applied at the filling location, the resulting bore could be either of the free surface or pipe filling type. The laboratory setup for this experiment is shown in Figure 4.2. The system consists of 0.095 m-diameter clear acrylic pipe, with a total length of 14.14 m placed initially level inside of an adjustable slope flume. Once the system was constructed and leveled, a slope of 0.391% was obtained by adjusting the flume slope such that the upstream or filling end was at a higher elevation than the downstream end. The pipe was capped at the downstream end and a vertical inlet pipe was constructed at the upstream end. This inlet standpipe was connected to a directional valve that could either allow flow to enter the pipe system or it could discharge flow to a waste stream. The inflow dropped through a vertical pipe of the same diameter (.095 m) approximately 1 m in height under the influence of gravity before being diverted through a pipe elbow into the nearly horizontal pipe. An air vent at the upstream end evacuated some of the air entrained in the inflow. The inlet condition into the pipe was poor with this configuration, creating

waves on the upstream interface of the free surface flow in the pipe and some air entrainment, but the experimental objectives could not be easily met using a head box with significant storage at the inlet.

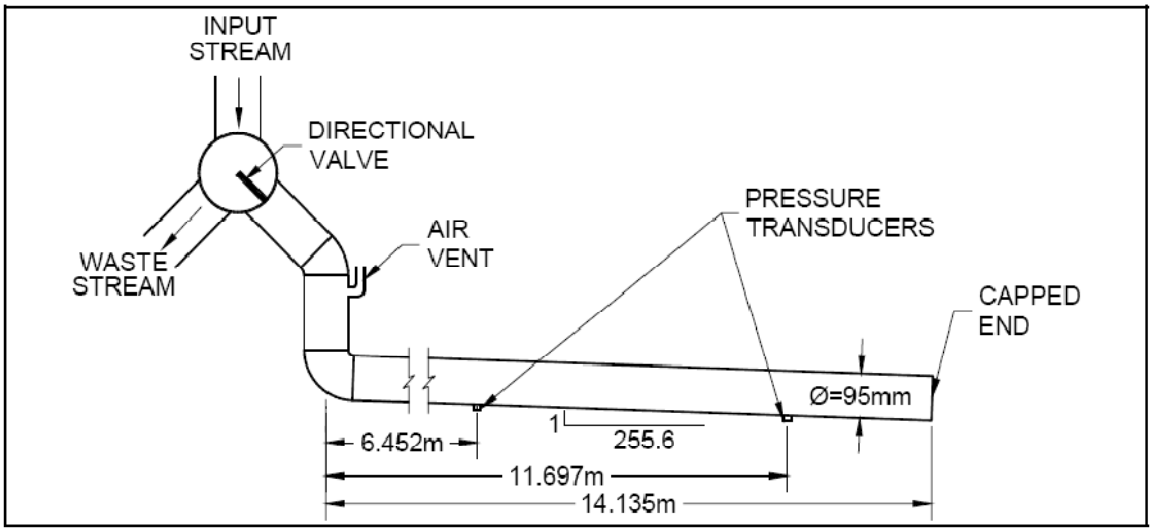

Figure 4.2 – Flow Regime Transition Experimental Setup

Flow was controlled upstream of the directional valve and metered to provide a range of flow discharges. The main objective in the reported experiments was to determine the influence of the discharge on the nature of the resulting bore. Table 4.1 provides the discharges for the different test conditions investigated. The specific choice of flow rates was dictated by a desire to reproduce a range of inflow rates up to a design flow rate appropriate for the combined overflow storage tunnel proposed for Washington, DC. The discharge range assumes the experiment to represent a Froude scaled model of the essential geometry of the proposed tunnel system. The controlled input stream came from a constant head reservoir tank located well above the lab setup. This flow upstream of the directional valve could be controlled and metered using a calibrated venturi meter and was essentially constant over the duration of the experiment. Two piezo-resistive

pressure transducers (Endevco model 8510B-1) were connected at the bottom of the pipe at distances of 6.45 and 11.70 m downstream of the center of the standpipe. Outputs from these transducers were sent to a data acquisition system (National Instruments DAQPad MIO-16XE-50) at a frequency of 10Hz for a total duration of 130 s, sufficient to capture both the initial filling front as well as the return of the bore to the upstream end of the system.

The pipe system was initially empty for each experiment and the directional valve was set to the waste stream. Once the desired discharge was established using a second, upstream control valve, the directional valve was quickly switched to allow flow into the pipe system. The sudden introduction of inflow at the upstream end created a filling front which propagated along the initially empty pipe. After the filling front had reflected off the downstream end and propagated back to the upstream standpipe, the flow was switched back to waste. The final steady level in the standpipe was recorded at the end of each 130 s experiment and used to determine the final hydrostatic pressure at each transducer by adding the difference in elevation (due to slope) between the standpipe and the transducer. This pressure (together with an initial pressure of zero gauge) was used to scale the transducer readings in order to obtain values of pressure throughout the duration of the experiment. A total of 13 experiments were conducted using the specified range of flows listed in Table 4.1. Each experimental condition was repeated three or four times to ensure repeatable measurement results and to permit video recordings of relevant aspects of the flow; the measured pressures were quite consistent among the different repetitions for a given discharge.

Table 4.1 Flow regime transition experiments

Label	Flow (L/s)	Slope (%)	Init. Water Level
1	2.36	0.3912	0
2	1.91	0.3912	0
3	1.34	0.3912	0
4	0.844	0.3912	0

4.4 Results

The following discussion of results focuses on the two types of propagating bores that were produced in the laboratory experiments; namely a pipe filling bore formed near the downstream end of the pipeline and a free surface bore followed by a gradual flow regime transition. It is noted that if even lower flow rates had been studied, the gradual flow regime transition would not have been observed due to the length of the pipe (the bore would reach the upstream end of the pipeline prior to the formation of the flow regime transition at the opposite end). Other bore formation scenarios are possible including the formation of a pipe filling bore following the reflection of the upstream propagating free surface bore from the upstream end of the system (see Vasconcelos and Wright, 2006 for a more detailed discussion of different mechanisms for air entrapment in filling pipelines). Although these additional flow conditions could potentially be relevant to a design analysis, the present results are restricted to the two more straightforward cases discussed below.

Pipe filling bore

For all experiments performed, the initial inflow generated a filling front similar to that formed for a dam break wave propagating on a dry bed, similar to the description by Bellos and Sakkas (1987), that propagated to the downstream, capped end of the

pipeline. The initial bore that formed upon reflection of the filling front off the downstream end was a free surface bore that relatively quickly evolved into a pipe filling bore for the flow rates of 2.36 L/s and 1.91 L/s. The distance from the downstream capped end to where the pipe filling bore formed was greater for the lower flow rate but still within 2 m from the downstream end of the pipe and before the bore reached either of the two pressure transducers. The pressure data for one experimental trial where a pipe filling bore formed is shown in Figure 4.3. The figure shows pressure records for both measurement locations. For this experimental condition, the water level for the initial front was somewhat greater than the centerline of the pipe at the time of bore arrival at the pressure transducers. This nearly vertical bore creates a surcharge condition behind the bore front; this is the type of bore assumed in most shock fitting numerical models. The pipe filling bore essentially acts as a "water piston" pushing the air in the pipe out ahead of it and so long as adequate ventilation is provided at the opposite end of the pipeline, the air does not become pressurized nor are any significant quantities trapped as discrete air pockets along the pipeline.

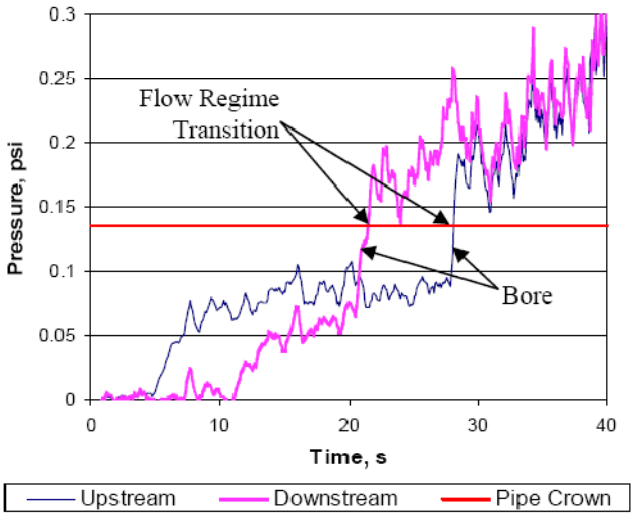

Figure 4.3 – Pipe Filling Bore, Q = 2.36 L/s

Free surface bore with a gradual flow regime transition

At lower flow rates, the free surface bore that formed persisted for the entire length of upstream propagation along the pipeline. Behind the bore, the water depth at a particular location increased gradually with time until it contacted the pipe crown. This type of flow condition is demonstrated by the pressure records in Figure 4.4 for a flow rate of 1.34 L/s. One can identify the initial filling front at each location, the returning bore, and the gradual increase in pressure until the hydrostatic pressure equals the pipe diameter. Once the bore reaches the upstream end of the pipe, the reflection at that location closes the flow cross-section resulting in the entrapment of air above the portion of the pipe not yet filled. Video observations for this flow rate showed large air pockets trapped in the pipe, which propagated upstream and eventually slugged up through the inflow standpipe. Previous work from the authors (Wright, et al. 2007) has indicated that geyser events may occur in this situation as the air rising through a vertical shaft partially filled with water displaces that water above it. That portion of the pressure record is not included in Figure 4.4, since the inflow was switched off as the reflected front arrived at the upstream end of the pipeline.

An additional case with a lower flow rate of 0.844 L/s is shown in Figure 4.5. The major difference between Figures 4.4 and 4.5 is the longer distance between the filling front and the flow regime transition. In Figure 4.5, the gradual flow regime transition observed by the upstream pressure transducer occurred almost exactly when the reflected front arrived at the upstream end of the system. Although the bore strength was less in this case, the volume of entrapped air was greater due to the longer distance

between the bore and the flow regime transition. Potentially this could result in a more severe geyser event in a prototype system if provisions are not made for venting this trapped air from the pipeline.

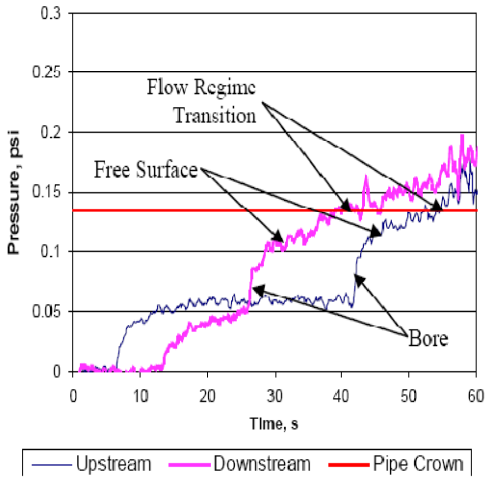

Figure 4.4: Free Surface Bore with a Gradual Flow Regime Transition, Q = 1.34 L/s

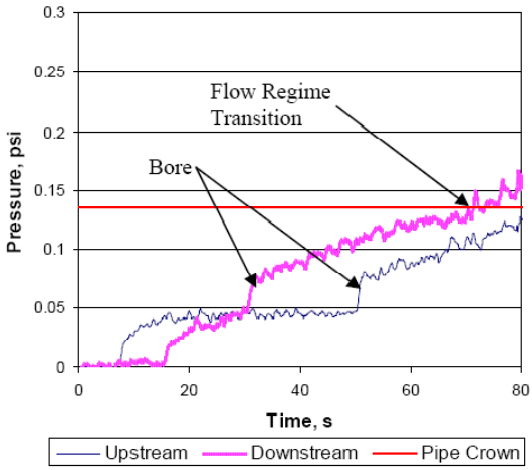

Figure 4.5: Free Surface Bore with a Long Transition Distance, Q = 0.844 L/s

4.5 Numerical Modeling Comparison

There are two general classes of numerical models that can be implemented to simulate the rapid filling problem; most of these do not simulate the role that the air can play in the filling process. Shock fitting methods involve tracking the bore through the pipeline. In principle, this could be implemented for both free surface and pipe filling bores, although the common application is only for pipe filling bores. A typical procedure is that of Cardle and Song (1988) in which different implementations of the Method of Characteristics are applied for the free surface and pressurized portions of the flow and the bore speed is computed by applying continuity and momentum equations across the bore allowing the location of the bore front to be updated throughout the simulation. However, this method or related ones relies on the presumption that the flow regime

transition from free surface to pressurized flow occurs as a pipe filling bore. Shock fitting methods of this type are therefore not appropriate for tracking gradual flow regime transitions following a free surface bore. In addition, the Method of Characteristics such as applied by Cardle and Song cannot accurately simulate a free surface bore. The more recent model by Politano, et al. (2007), while still based on a Method of Characteristics solution approach, includes a provision for explicitly accounting for the gradual flow regime transition interface condition, although it is not clear exactly how the model distinguishes between the two different types of flow regime transitions. It is noted that there are other numerical techniques available for more accurate simulation of free surface bores, including approximate Riemann solvers.

The second class of numerical models is referred to as shock capturing methods. Effectively, a single set of equations is applied to both the free surface and pressurized portions of the flow and a numerical scheme is required that is capable of numerically resolving the bore. This type of scheme has the potential to accurately simulate both types of bores. The Preissman slot scheme has traditionally been implemented in shock capturing schemes as typified by the model of Capart, et al. (1997). More recently, Vasconcelos, et al. (2006) proposed the two-component pressure (TPA) approach as an alternative; this method utilizes the concept of elastic pipe walls to provide the storage term necessary to simulate transient pressurized flow with the same equations as used for free surface flow.

In order to demonstrate the ability of a shock capturing numerical model to resolve the flow regime transition, computations of the two-component pressure approach of Vasconcelos, et al. (2006) were applied by others in the joint research to simulate the

experiments that were performed; results are presented for one each of the pipe filling bore and the gradual flow regime transition experiments in Figures 4.6 and 4.7 below. The model was implemented with a grid spacing Δx equal to the pipe diameter D. The Courant number $c\,\Delta t/\Delta x$ used in the simulation was 0.95, with c the appropriate wave speed (the maximum of either pressurized or free surface wave speeds that are relevant at any time in the simulation) and Δt the numerical time step. The simulation cannot proceed from empty pipe conditions so an initial depth equal to $0.005D$ was used to describe an initial condition for the simulation. The upstream boundary condition assumed a constant inflow rate into the upstream standpipe. The momentum of the falling water impinging on the pipe elbow was not included in the boundary condition formulation but the filling dynamics of the shaft were included by applying continuity and energy equations between the filling shaft and the first downstream computational node. In addition to these approximations, it is acknowledged that the use of the St. Venant equations assuming hydrostatic pressures is not strictly valid in simulating the initial filling front.

In spite of these limitations, there is a good agreement between the experimental data and the numerical simulations for both flow regime transitions, as indicated in Figures 4.6 and 4.7. The timing of the bore propagation as well as other features of the flow indicates that the numerical scheme is able to accurately resolve the free surface bore. The extreme nature of the flow introduction makes this a quite rigorous test of the numerical model framework. Both the simulation and experimental results indicate the bore strengthens as it propagates between the transducer locations. Thus, properly formulated shock capturing schemes can be used to simulate both pipe filling bores as

well as gradual flow regime transitions. It is noted that both cases are handled naturally within the framework of the numerical simulation and no special considerations need to be made to handle either outcome. In actual stormwater systems this may be of great importance as multiple inflow points and complex geometries could possibly allow many simultaneous bores of either type to occur in the system and thus be more problematic to account for with a shock fitting scheme.

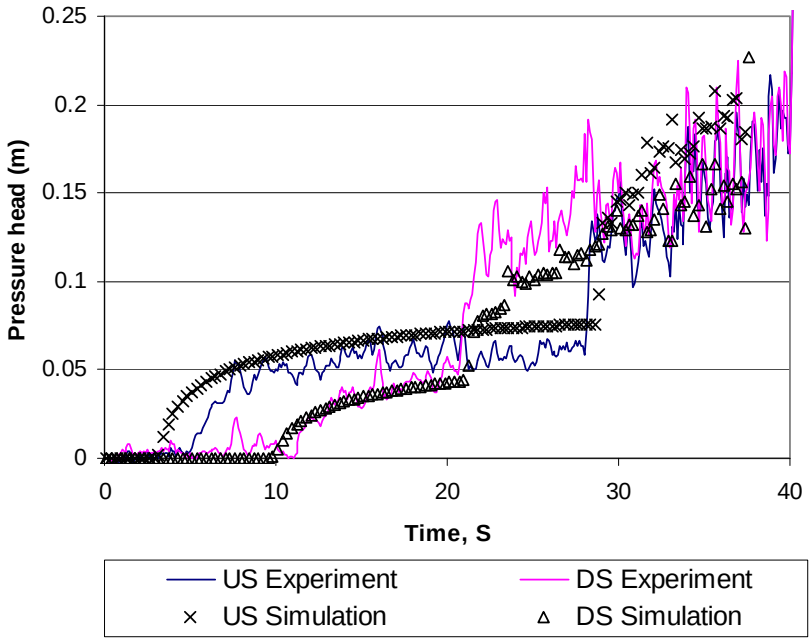

Figure 4.6 Two-Component Pressure Approach simulation results and experimental data for a pipe-filling bore (US = upstream pressure transducer location, DS = downstream transducer location, Q = 2.4 L/s (Run 1, see Table 4.1 for variable conditions)

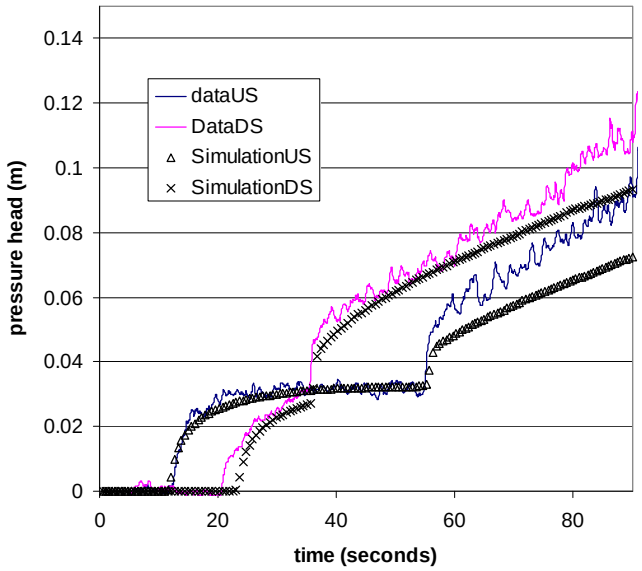

Figure 4.7 Two-Component Pressure Approach simulation results and experimental data of a gradual flow regime transition (US = upstream pressure transducer location, DS = downstream transducer location, Q = 0.844 L/s. Run 4b.

4.6 Bore collision experiments

Additional experiments to meet the remaining research objectives were made with minor modifications to the apparatus described above. The motivation for this investigation comes from the anticipation that the gradual flow regime transition provides a mechanism for entrapping air which can lead to geysers. A 0.044 m-diameter vertical standpipe was connected to the pipe at approximately the midpoint, as shown in Figure 4.8. The riser was 2.5 m tall and located 9.01 m from the upstream end. The ratio of the standpipe diameter to pipe diameter of 0.4 is intermediate in the range of values studied by Vasconcelos (2005). This choice was made to prevent the extreme geysering conditions Vasconcelos observed at small diameter ratios but still small enough to expect a significant effect. The main pipe was set in a horizontal condition and several experiments were performed with an initial level of stagnant water within the pipeline. The variables used in these experiments are shown in Table 4.2.

To initiate two different bore fronts, there needed to be two levels of inflow to the system. The flow was initially switched on to create a free surface bore that propagated to the

opposite end of the pipeline and became a gradual flow regime transition following reflection off the closed end of the pipe. As this bore was returning in the upstream direction, the inflow was increased to create a second free surface bore from the upstream end that collided with the first bore in the vicinity of the ventilation riser. Due to the method for initiating the second flow rate, the resulting bore front was not sharp but still served to meet the experimental objectives. As in the previous experiments, the inflow was switched back to waste stream once the filling front fully reached back to the upstream end.

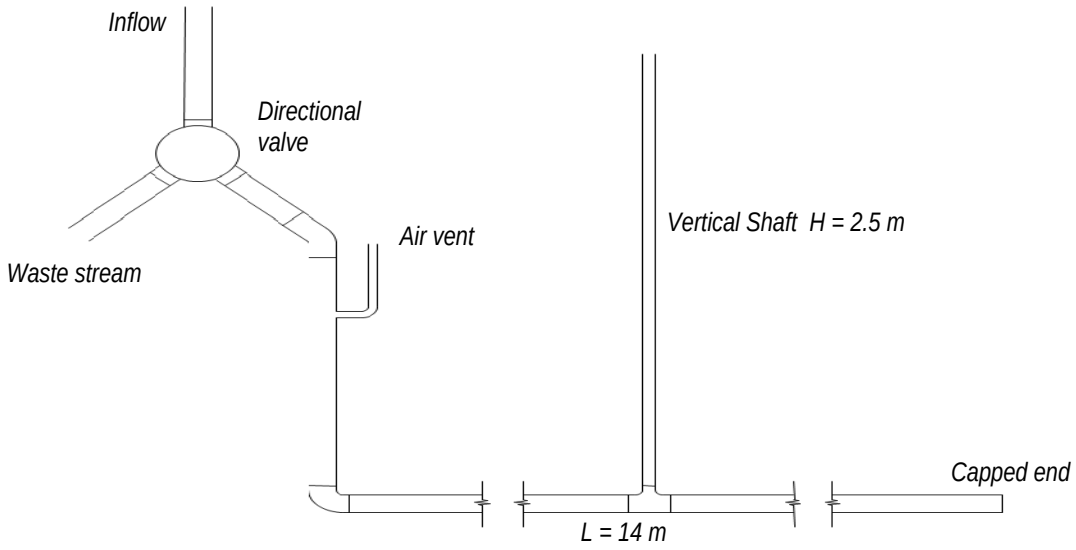

Figure 4.8: Experimental setup

Table 4.2 Bore collision experiments

Label	1st Flow (L/s)	2nd Flow (L/s)	Slope (%)	Init. Water Level (% Diameter)
S1	1.00	2.85	0.3912	0
F1	1.23	2.85	0	7
F2	1.00	1.60	0	15
F3	1.00	2.85	0	0
F4	1.00	2.85	0	15

4.7 Bore Collision Results

The experimental conditions were sufficient to trap sizeable air volume broken into several small air pockets at the crown of the pipe during the collision of the two free

surface bores. The trapped air pockets were larger than the volume of a length within the vertical riser equal to one pipe riser diameter but not significantly more. Figure 4.9 shows a schematic of the observations. The location of the collision occurred near the base of the vertical shaft and an initial column of water, perhaps 10-15 cm in height, was created within the riser due to the surcharged state. The gradual flow regime transition allowed for more air volume to be trapped at the crown of the pipe than would occur during a pipe-filling bore. The disturbance of the bore collision tended to break the air volume up into smaller pockets. As the discrete air pockets approached the riser, they began to lift the water upward in the riser. The 0.044 m diameter riser was 2.5 m tall, yet in spite of this large height, water spilled out the top of the riser in several experiments. Although a single air pocket was insufficient to lift the water the entire 2.5 m, another air pocket arrived to push the water still further up the riser. Air forced water upwards with a downward film flow around the perimeter until the water layer disappeared ahead of the air slug. The combined effect of a sequence of alternating air and liquid slugs moved rapidly up through the vertical shaft to create the geyser event up the entire riser height. This is apparently different than the Minnesota geyser event since the pressure record of the July 11 event (Figure 2.4) shows a steep pressure drop for each geyser occurrence which likely indicates a single large air pocket associated with each geyser occurrence.

A pressure trace of two different experiments is presented in Figure 4.10, one being where the vent riser was removed for the same experimental conditions. A geyser spilling out the top of the vent riser was observed for the vented trial. The large increase in pressure in each experiment is associated with the rise of the water at the inflow end of the system as the entire pipe goes full, as opposed to a pressure increase associated with

the collision of the bores or other transient effects within the pipeline. As the height of water in the stand-pipe rises, the inflow is switched off and the pressure begins to drop off as air pockets are released from the system. Regardless, the measured pressure head never approached the 2.5 m height of the riser and yet the water spilled out the top. One can see small pressure spikes (of about 10 cm amplitude) in the record, especially on the rising limb of the pressure trace. These pressure spikes are apparently associated with the release of air pockets from the system. Since the liquid was lifted in slugs with air pockets in between, a drop in pressure occurred each time an air pocket broke through the free surface within the riser. The behavior of these vertical interactions is studied further in later sections. Visual observations were consistent among the other trials, revealing that the air induced rise of water was well beyond the pressures recorded in the system. These results reinforce the hypothesis that trapped air in rapidly filling pipelines can produce a significant influence on the rise of water in vertical shafts attached to tunnels. It is stressed that because of the small scale of the laboratory experiments, no absolute correlation with large scale geyser events such as displayed in Figure 2.1 is possible. There may be several distinct mechanisms involving air that can lift water higher than would be indicated on the basis of static pressures alone.

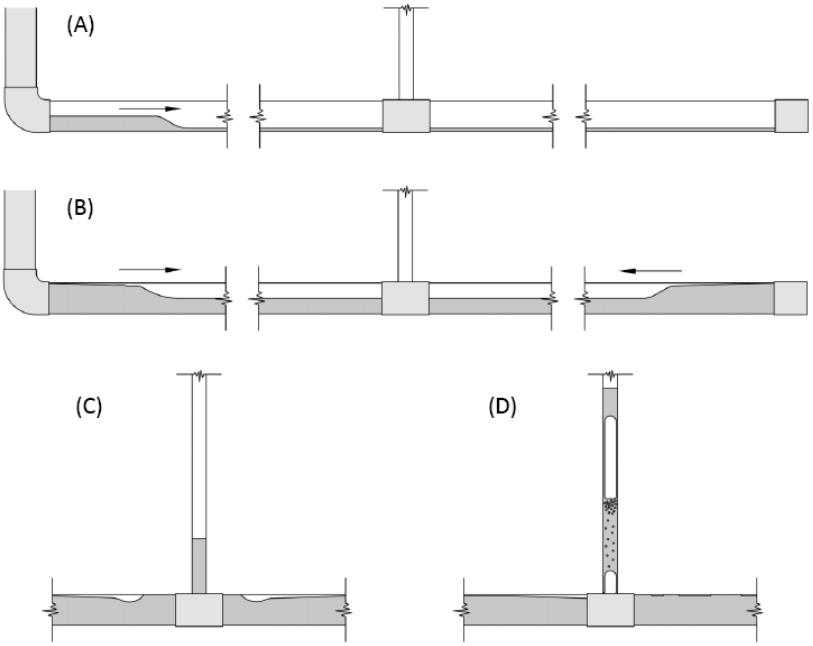

Figure 4.9 Schematic of bore collision experiments

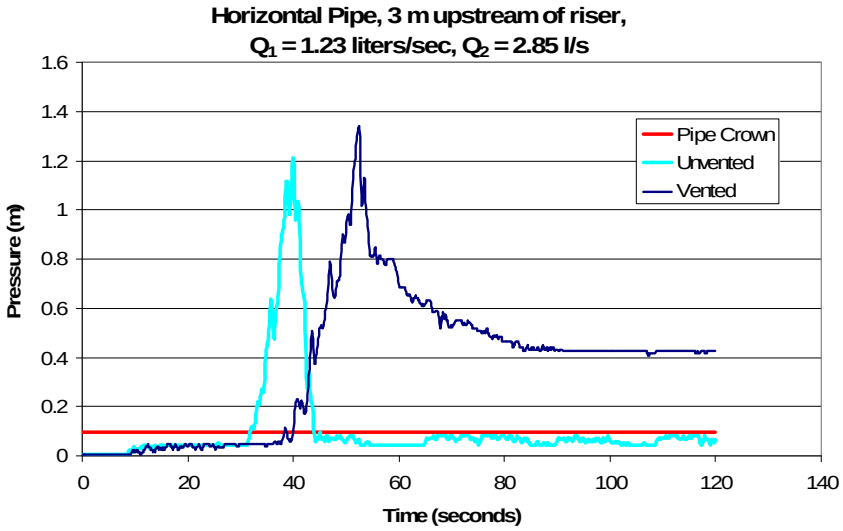

Figure 4.10 Pressure record for experiments with 2.5 m riser

4.8 Conclusions

Understanding the potential for a system to experience either large pipe surges or geyser events is important in the design of storm water or combined sewer overflow

systems. This work demonstrates that there is not a distinct bore type that will develop in the pipe under all conditions, and the flow regime transition may occur along with the passage of the bore or through the gradual increase in depth behind the bore. The type of bore expected is a function of the inflow hydrograph but will also depend on a number of other factors including system geometry but clearly filling rate is a key variable. Several additional conclusions may be drawn as a result of this work:

- Although many numerical models treat propagating bores in closed conduits as pipe filling bores, this is not necessarily the typical condition for a system, and free surface bores with long gradual flow regime transitions may exist within the system. Numerical simulations of the DCWASA system described in section 3.1 indicated that the presence of side tunnels and vertical shafts could also create a situation where an initially pipe-filling bore could devolve into a free surface bore with a gradual flow regime transition.
- The length of the gradual flow regime transition decreases with an increase in filling rate. The collected data indicate that a free surface bore tends to steepen with propagation distance but even for very long pipelines, gradual flow regime transitions are expected to occur.
- The gradual flow regime transition following a free surface bore is generally more conducive to air entrapment within a system compared to the pipe filling bore. Air is likely to be entrapped when a free surface bore with a gradual flow regime transition is reflected off a conduit transition and the reflection fills the pipeline. Alternatively, the collision of multiple bores is also very likely to entrap air.

Large volumes of trapped air may lead to geyser events in some systems where sufficient ventilation is not provided.

- Evidence is presented demonstrating that water can be lifted large distances in ventilation shafts by the release of air pockets trapped within the shaft. The combined effects of multiple small air pockets provides another mechanism beyond that discussed in Chapter 2 that could result in geyser formation. In either case, it is possible that large vertical lifts of water are not necessarily accompanied by large system pressures.
- Existing shock-fitting numerical methods are only capable of predicting the behavior of bores in systems where gradual flow regime transitions are unlikely to occur. A real system experiences many more lower flows than the largest ones, and attention should be given to gradual flow regime transitions which may occur. In general, models should at least be sufficiently accurate to predict the locations and amount of trapped air.
- Shock-capturing methods that can accurately predict bore characteristics for both free surface and pipe filling bores have significant utility in analyzing the extreme conditions that will control design of storm-water systems. The two-component pressure approach proposed by Vasconcelos, et al. (2006) is an attractive method for this purpose.

Since any physical system will experience a range of hydrological inputs, it is likely that both types of bores might be relevant in a general design analysis. There are some interesting similarities between the experimental results presented here and the field

measurements taken during the Minneapolis geyser example discussed in Chapter 2. Although details related to the propagation of filling fronts through the system cannot be determined, the pressure record in Figure 2.4 does show a flow regime transition prior to the geyser events. The source of the air for the Minneapolis geyser is unknown, but quick pressure drops are noticed in both Figures 2.4 and 4.10. The experimental pressure measurements of Figure 4.10 exhibit pressure drops which correspond to sequential air pockets breaking through the free surface water level within the vertical riser. Pressure drops in the field observations of Figure 2.4 correspond with geyser events at the ground surface. These similarities imply that the pressure drops during the Minneapolis geyser event are perhaps caused by the pressure of large air voids being relieved as they break through the water surface in the manhole. The laboratory work suggests methods in which sequential air pockets push water vertically to create a geyser event but that there are different mechanisms possible. The Minnesota data seems to suggest something different, something that cannot easily be resolved at the laboratory scale, but as discussed in Chapter 2 one should be aware that these are not surge related and cannot be computed with single phase (water) flow models.

Figures 4.11 and 4.12 show a comparison between the Minneapolis pressure data from Figure 2.4 and the laboratory data during the bore collision of Figure 4.10. For comparison, the horizontal axis of each figure has been normalized by $\sqrt{(gD_{ris})}$, an important quantity related to air rise velocity according to Davies and Taylor (1950) shown in Chapter 3. It is not expected that the pressure records would match in this comparison, remembering that the pressure in the bore collision experiments was driven by the inflow through the upstream stand-pipe and the subsequent discontinuation of the

inflow when the water level reached the stand pipe's air vent (see Figure 4.8 or 4.2 for a schematic). Nevertheless, a comparison may be attempted for the amount of time during the drop in pressure following the peak value. The drop occurs over a shorter time in the experimental data, lasting approximately 30 normalized time units from 780 to 810. The time for a pressure drop in the Minneapolis data is of the same order of magnitude but lasts longer, for example about 50 normalized time units from 1925 to 1975. Later sections of this dissertation will show that the air volume is an important factor in geyser formation, implying that since the geyser occurs over a longer normalized time frame in the Minneapolis data, this may represent a larger relative air volume. This seems reasonable since observations during the Figure 4.11 experiment revealed multiple, relatively small air pockets which did not occupy the entire height of the vertical riser. In general the similarity between the two figures suggests that both are due to the mechanism of air release. However, more measurements at a larger scale are necessary for a complete comparison with laboratory results.

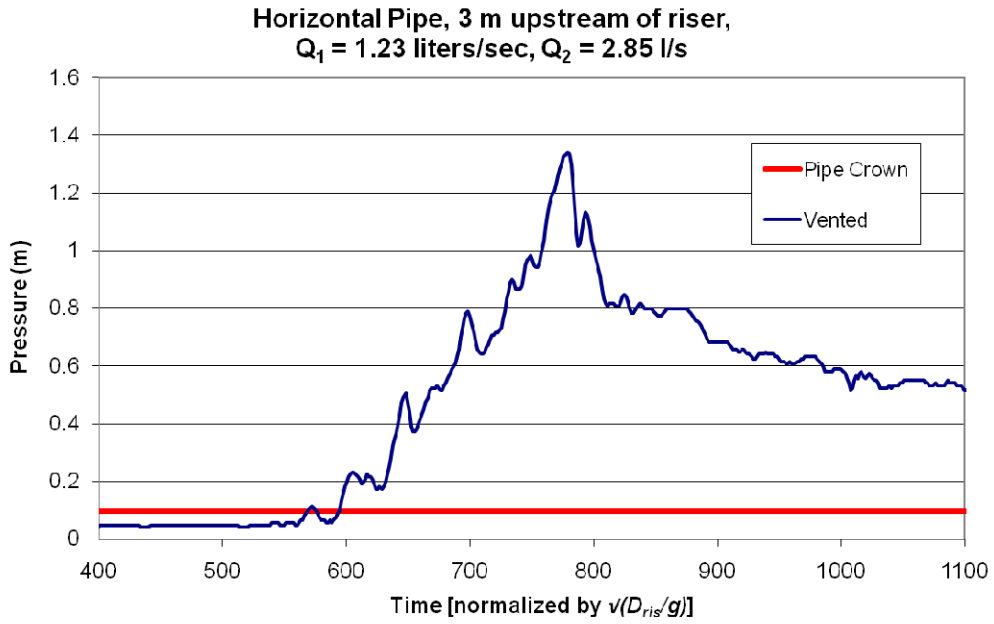

Figure 4.11 Pressure record from bore collision geyser with normalized time axis

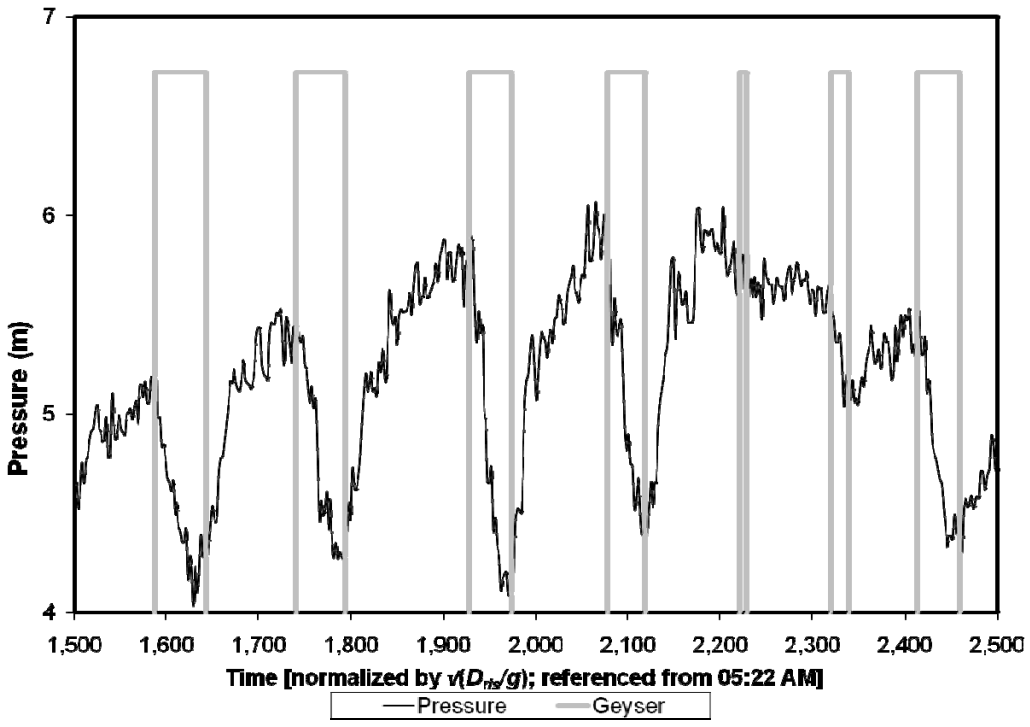

Figure 4.12 Minneapolis geyser pressure record with normalized time axis

Chapter 5

Air Pocket Migration

5.1 Objective

In order to develop general guidance for preventing geyser events due to air pocket release, the next consideration explored is how the air arrives at a vertical shaft. The previous chapter discussed the existence of gradual flow regime transitions and how they can potentially trap air pockets during the filling of a pipeline. This chapter will specifically examine the migration behavior of large discrete air pockets after they have formed inside of the system. For sloping pipelines it is less than straightforward to determine the best location for ventilation since the air pocket may migrate down the slope due to inertia effects or upslope due to air buoyancy or inertia. Furthermore, an experimental investigation will compare the migration velocities of discrete air pockets with those of infinitely long air intrusions studied previously in the literature for horizontal and sloping pipes.

5.2 Introduction

The system geometry and flow characteristics determine which direction an air pocket will migrate in a pipeline. A few initial considerations are presented for framing the problem of predicting air migration behavior. Buoyancy lifts the air pocket to the

crown of the pipe forming a nearly horizontal interface between the air and the liquid. For a horizontal pipeline containing stagnant liquid, the air will tend to spread along the crown of the pipe equally in both directions. For a sloped pipeline containing stagnant liquid, the buoyancy force acts in the direction of higher elevation to move the air up the slope. The migrating air pocket experiences shear forces in the opposite direction both along the upper pipe wall and along the liquid interface. When the liquid in the pipe is flowing in the direction of higher elevation, predicting the direction of air migration is straightforward because the liquid shear and the buoyancy act in the same direction. However, when the liquid is flowing down the slope of the pipeline, predicting the direction of air migration is more difficult because the buoyancy force and liquid shear force are acting in opposite directions. In general, if the flow of liquid is large enough it can push the air down the slope in the direction of liquid flow. Many CSO storage tunnels are constructed with relatively low slopes with liquid commonly flowing in the downward direction.

Studies related to the movement of air pockets in horizontal pipelines have shown that Froude number scaling is appropriate (implied by the results from Benjamin 1968 and Little, et al. 2008). Benjamin (1968) studied the migration of an air intrusion at atmospheric pressure into an emptying pipeline. Although Benjamin's analysis is for an air intrusion into an otherwise stationary liquid, the formulation of the problem was made in the frame of reference of the air intrusion, implying that the analysis can be applied to the relative velocity difference between the air and water. A dimensionless parameter C is used to represent the point at which the drag force from the liquid prevents the upstream air intrusion: $C = \frac{v}{\sqrt{(gD)}}$, where v is the relative liquid velocity upstream of

the intrusion and D is the pipe diameter. The air intrusion equations mentioned in Chapter 3 indicate that if $C > 0.54$ in a horizontal circular pipe, the drag force from the liquid prevents upstream migration of the air intrusion. The investigation of this chapter measures the migration behavior of a discrete pocket of air as opposed to Benjamin's quasi-infinite air intrusion of an emptying pipeline. Observations compare how near the air migration velocities of discrete pockets are to Benjamin's relation of $0.54\sqrt{(gD)}$. The study of Wickenhäuser and Kriewitz (2009) showed that larger air pockets migrate faster than smaller air pockets. Thus the influence of the air pocket's volume to the migration behavior is also examined within the experimental setup discussed below.

5.3 Experimental setup

The present study explores two experimental configurations for introducing air into the pipeline system. The first, a continuous air injection setup, is shown in Figure 5.1. Here, the volumetric air flow rate into the system was metered and adjusted. The second setup introduces the air by opening a valve separating a full pipe from a shorter length containing air. As shown in Figure 5.2, the air is located at the downstream end of the system and the large discrete air pocket migrates upstream toward the vertical shaft. For this setup, upstream means the reservoir end of the pipeline. In this situation, the volume of the discrete pocket of air is determined by adjusting the initial water level inside the short length of pipe beyond the valve. The main tunnel in both setups is constructed from 0.095 m diameter clear acrylic pipe with a horizontal slope. A large reservoir is connected to the upstream end of the tunnel where the water surface can be adjusted and maintained at a constant level. An elbow joint pointing downward is

located at the upstream end to prevent air from being released into the reservoir. Taking advantage of the clear acrylic pipe walls, the general behavior of the air and water was readily observed and recorded with a digital video camera at 30 frames per second.

For the continuous air injection setup, air was injected through a small hose located at the pipe invert connected to a constant pressure air supply tank. The location of air injection was 2.90 m away from the reservoir, or 4.42 m away from the vertical riser. A quarter-turn butterfly valve and a threaded PVC cap were located at the downstream end to regulate the flow through the tunnel (or to block it entirely). The water flow rate was measured at the downstream outlet by performing three repetitions of collecting a weight of water and a measured time. The water flow within the system was adjusted between a small number of quasi-steady-state flows, including a stagnant condition, as shown in Table 5.1. A T-joint was located immediately upstream of the butterfly valve where the vertical riser was attached. For the continuous air injection experiments reported in this chapter, the water level within the reservoir was held constant at 0.3 m above the pipe invert. A range of small air injection flow rates were used to produce a range of migrating bubble sizes for each trial. Air injection rates used to measure the migration velocities were less than 4 L/min. Two larger air flow rates were used to observe the behavior of large pockets. Rates larger than approximately 8 L/min occasionally produced a continuous layer of air along the crown of the pipe. Using video observations, the length of the bubble and the velocity of the nose were measured. The general procedure using this setup was: 1) establish the desired liquid flow rate by maintaining a constant reservoir level, adjusting the valve, and measuring the discharge; and then 2) begin injecting the air flow.

The air capsule experimental setup shown in Figure 5.2 measured the migration of a single air pocket from the downstream end to the vertical shaft located near the upstream reservoir. A quarter-turn butterfly valve was used to release the air pocket into the main tunnel. The short pipe downstream of the valve was 0.095 m diameter clear acrylic pipe with a length of 0.89 m. The vertical riser was 1.70 m downstream of the reservoir and the valve was 3.78 m downstream of the riser. Two small tubes were attached to a threaded PVC cap at the downstream end of the capsule. One tube was used to drain water out of the capsule while the other was connected to a pressurized air supply line. The air capsule was intended to be at the same pressure as the rest of the system, established by the reservoir level, but it was difficult to establish an air-tight seal within the capsule causing most experimental trials to begin with an air pocket near atmospheric pressure. The experimental procedure using this setup was to establish a constant reservoir level, close the butterfly valve, drain the liquid in the capsule until the appropriate volume of air exists, and release the air pocket by opening the valve. Table 5.2 shows the ranges of tested variables for the air capsule experiments.

A few experiments were performed similar to the continuous air injection setup using a 0.203 m diameter clear PVC pipe instead of the 0.095 m diameter pipe. The setup is very similar to Fig. 5.1, only the air injection location was 1.8 m downstream of the reservoir and the vertical shaft was approximately 9 m downstream of the air injection. Again, air was injected into the bottom of the pipe using a small tube connected to a pressurized air supply. The air migration velocities were again measured using the digital video camera and markings on the pipe walls.

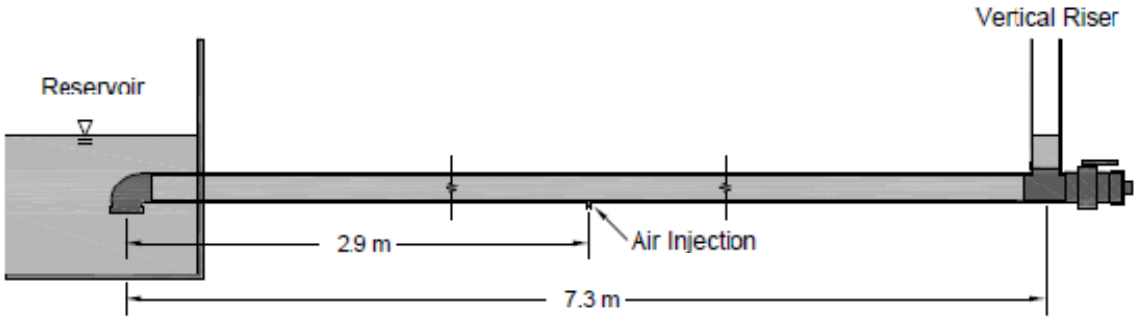

Figure 5.1: Continuous air injection experimental setup

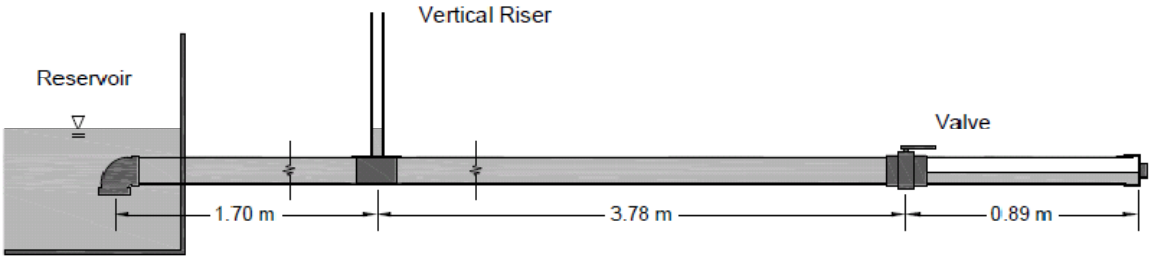

Figure 5.2: Air capsule experimental setup

Table 5.1: Continuous air injection experimental conditions

Tunnel diameter (m)	Water flow rate (m^3/s)	Equilibrium water level (m)
0.095	0.001	0.3
0.095	0.002	0.3
0.203	0.014	0.6
0.203	0.016	0.6

Table 5.2 Air capsule experimental conditions

Label	*Air volume (L)*	*Equilibrium water level (m)*
Low1	1.59	0.203
High1	1.59	0.457
Low2	3.14	0.203
High2	3.14	0.457
Low3	5.79	0.203
High3	5.79	0.457

5.4 Results

Many visual observations from previous studies in the literature were confirmed during this investigation; other observations added new insight. As observed in the study by Benjamin (1968), the general shape of a migrating air intrusion contained a nose region where the depth of air intrusion is the greatest. During both sets of experiments, the large air pockets were observed to have a distinct shape as shown in Figure 5.3 consisting of a nose, a transition region (or wake / hydraulic jump), and a tail. For the capsule experiment, the tail usually remained at the downstream end of the pipe as the air volume spread along the crown. The leading edge of the air pocket had a front or round head which typically was the thickest part of the air intrusion. A transition zone usually occurred for large air pockets located just behind the nose region. This can be thought of as a wake zone due to water flowing around the front of the air pocket; sometimes forming a distinct hydraulic jump. Next, the body of the air pocket generally stretched out along the crown of the pipe to form a long, narrow tail. Surface waves occurred in this region of the air flow and occasionally these waves reached all the way to the pipe

crown, breaking the air pocket into separate bubbles. Under certain circumstances, such as when the pressurized air pocket began to escape through the water free surface, the end of the tail region developed into a front similar to a pipe-filling bore. The reason is that the water within the tunnel is still at pressure and when a large enough air volume is exposed to atmospheric pressure the pressure drops such that a pressure gradient is induced toward the riser. The development of this front also created a significant surge potential due to the inertia of the advancing water column so that surges in the vertical shaft could be observed when the tail end of the air pocket was expelled.

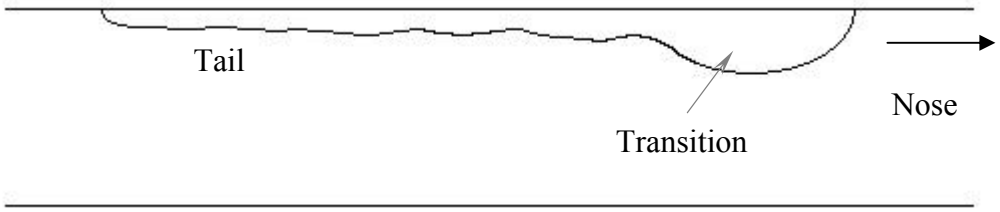

Figure 5.3: Shape of Large Migrating Air Pocket

The study of Wickenhäuser and Kriewitz (2009) observed that large bubbles overtake smaller bubbles leading to larger coalesced bubbles as the propagation distance increases; this was confirmed by observations during the continuous air injection setup. The relative velocity of the air is determined by subtracting the velocity of the water, determined from the measured flow rate through the system, from the velocity of the air pocket's nose, determined using frames of the video recordings. Figure 5.4 shows the relative velocity of air normalized by $\sqrt{(gD)}$ on the vertical axis and the bubble size on the horizontal axis, measured as the length from the nose to the tail normalized by the tunnel diameter. The data represents a sample of measurements over a range of conditions including both pipe diameter sizes. Though there is a significant scatter in the

data, a trend of increasing air velocity with increasing bubble size can be seen. Another observation is that air pockets in a horizontal pipe downstream of the injection point migrate both faster and slower than the water, depending on their size. Large air pockets downstream of the air injection point moved in the downstream direction at a greater velocity than the water. For this experimental setup the relative air migrations were substantially below the Benjamin limit of $0.54\sqrt{(gD)}$. This indicates that since the air starts out as small bubbles, it is essentially carried along with the flow. Even after coalescing into larger bubbles, the air tends to be transported by the water flow with some differential buoyant spreading. As mentioned earlier, the Benjamin solution is only applicable for situations where a large air pocket is intruding in the opposite direction of water flow. Therefore, the air migration in the capsule experiments is fundamentally different than the air injection experiments in this regard

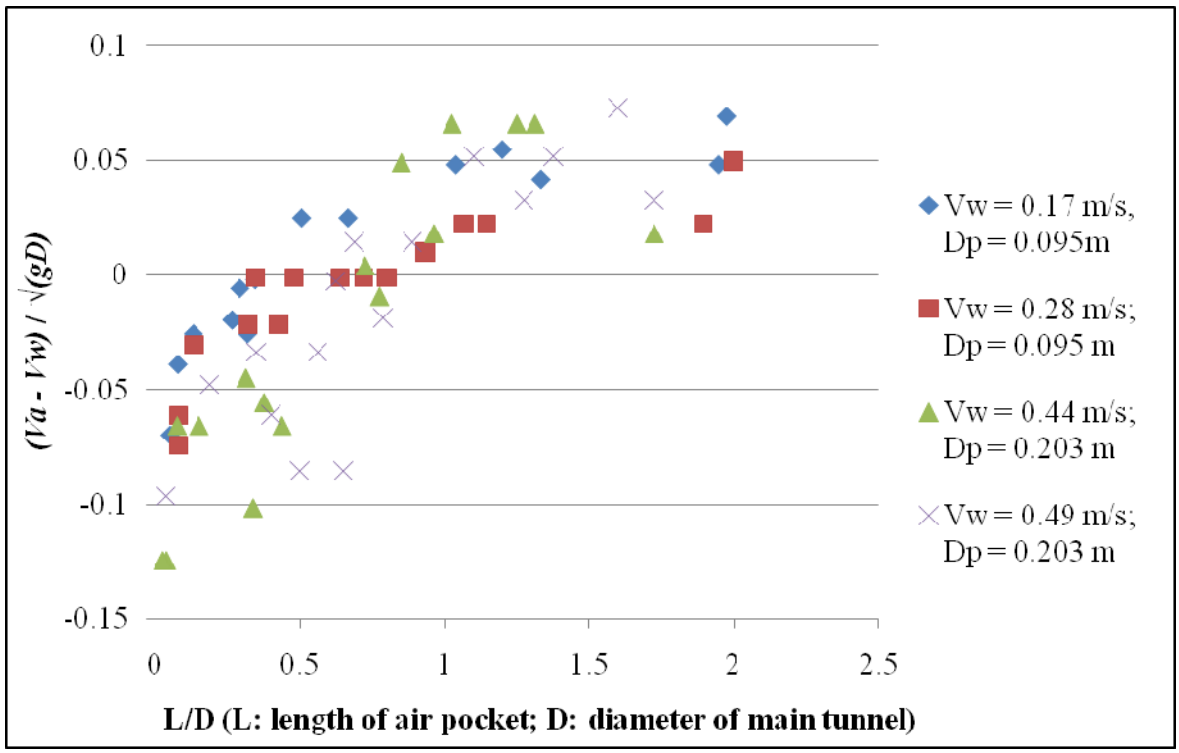

Figure 5.4: Air Pocket Migration Data

Some observations were made regarding the larger air injection rates. For the air flow rate of 8 L/min, the air occupied approximately the top 15% of the depth of tunnel diameter or 9% of the tunnel cross sectional area. The high air flow rate of 25 L/min occupied roughly 33% of the diameter or 29% of the area. These air flow rates represent a reasonable range of the expected air concentrations due to entrapment and are significantly larger than the expected concentrations due to air entrainment at a drop-shaft. An IIHR study (Odgaard and Lyons 2010; Lyons 2010) investigated the air entrainment rates within a drop-shaft designed for the Washington, DC Water and Sewer Authority CSO tunnel. For the range of drop-shaft geometries tested, the largest rate of air entrainment was roughly 0.31% of the cross-sectional area, an order of magnitude below the 9% air concentration during the 8 L/min trial of this study. A similar study for the Milwaukee storage system (Jain and Kennedy 1983) showed air entrainment near 0.48%. Roberts (2004) conducted an investigation for entrainment in a system proposed for Portland, Oregon and generally found air concentrations near the range of the present study. A maximum threshold of air flow within a tunnel system can be found using the Benjamin (1968) findings for air intrusions. The air may occupy a maximum depth of one half of the tunnel diameter with a relative intrusion velocity of $0.54\sqrt{(gD)}$, corresponding to an air flow rate of 112 L/min in the physical model or over four times the highest air flow rate tested in this study. Occasionally during these experiments, the air would form into a large discrete pocket having a distinct nose and tail region as shown in Figure 5.5. This behavior created a discontinuous air arrival into the base of the vertical riser. In general, it may not be possible to approximate the quantity of air that would need to be

trapped in discrete pockets during a single filling event in order to exhibit a comparable behavior of air release as observed in this continuous air injection analysis, as there is a fundamental difference in the migration behavior between the two cases.

(a) Tail of air pocket moving left to right *(b)* Head of next air pocket, taken 1.33 sec after (*a*).

Figure 5.5. Images of Air Pockets in Main Tunnel, air flow rate of 25 L/min.

Some interesting observations were made during the air capsule release experiments. As the valve opened, the nose of the air pocket migrated toward the vertical riser. Since the pipe was horizontal, the air spread along the crown of the pipe. The larger air volumes migrated faster and occupied more of the pipe depth than the smaller air volumes. The migration velocities of the air pockets are shown in Figure 5.6 along with an error bar representing one standard deviation of measurement in each direction. The dotted line in the figure represents Benjamin's migration velocity for an infinitely long air intrusion neglecting energy dissipation. The migration velocities of these experiments range between 9 and 22% below that of Benjamin's relation. Snapshot images of a typical air pocket are shown in Figure 5.7 (with a dotted line drawn to accentuate the interface). The depth of the interface between air and water was difficult to measure due to: 1) waves at the interface, and 2) usually a slightly larger air depth at the nose of the air pocket. The depth of air intrusion occurring just after the transition (as shown in the sketch of Figure 5.3) during these experiments was measured and is shown

in comparison to the Montes (1997) relation for an infinite intrusion in Figure 5.8. The data shows that for a given intrusion thickness ($1 - y/D$), the discrete air pockets migrate slower than the infinite intrusion. The difference here may be the finite air volume makes it only an approximation to use the Benjamin solution and also makes the definition of air layer thickness more subject to uncertainty. The thickness of the air layer would be somewhat controlled by the air volume and there is no particular reason for small air volumes to have a thickness as much as the limiting value. Also, since there is a finite volume of air spreading along the crown of the pipe, the migration velocity is not quite a constant value. The fact that some measurements of air intrusion thickness are greater than the maximum energy dissipation solution may suggest that the measurement of intrusion thickness in the experiments was not quite appropriate. In addition, there is a small velocity in the water under the air pocket to replace the forward moving air which would increase the relative velocity as well.

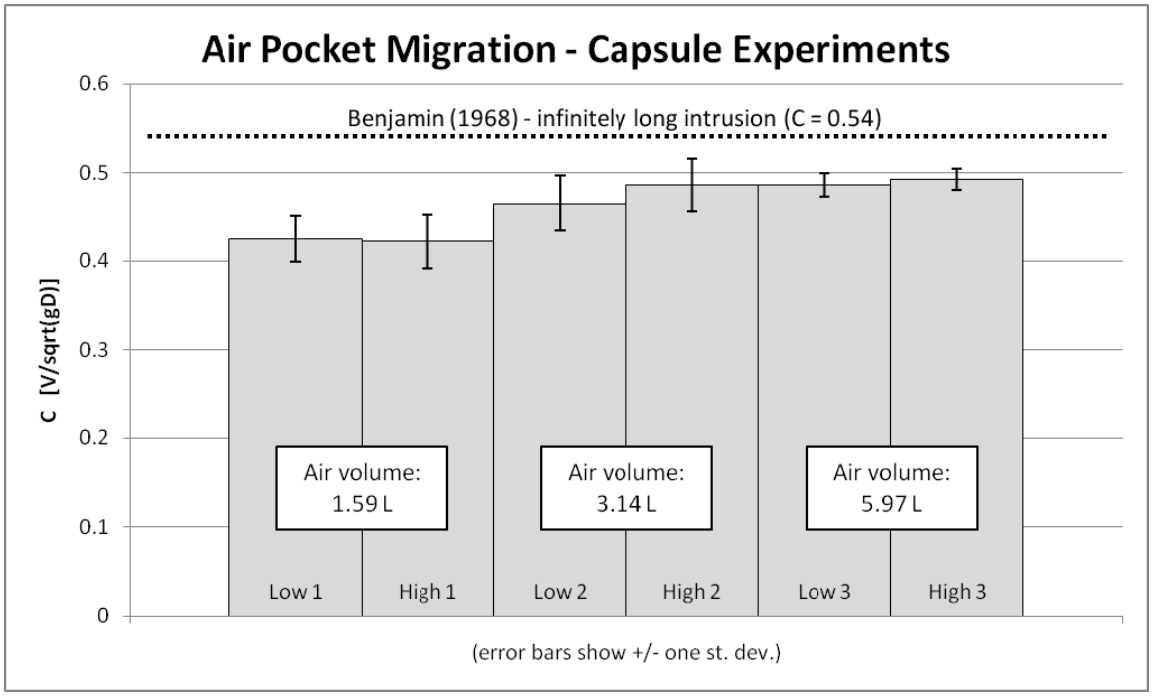

Figure 5.6 Air migration of discrete air volumes (see Table 5.2 for specific values)

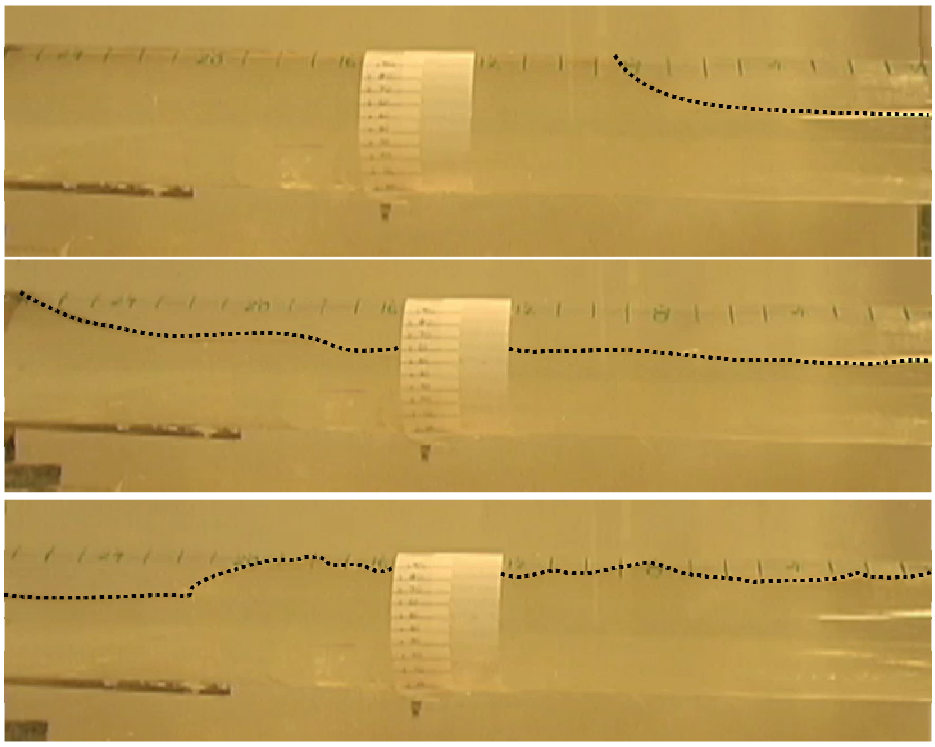

Figure 5.7 Video snap-shot images during air capsule experiments

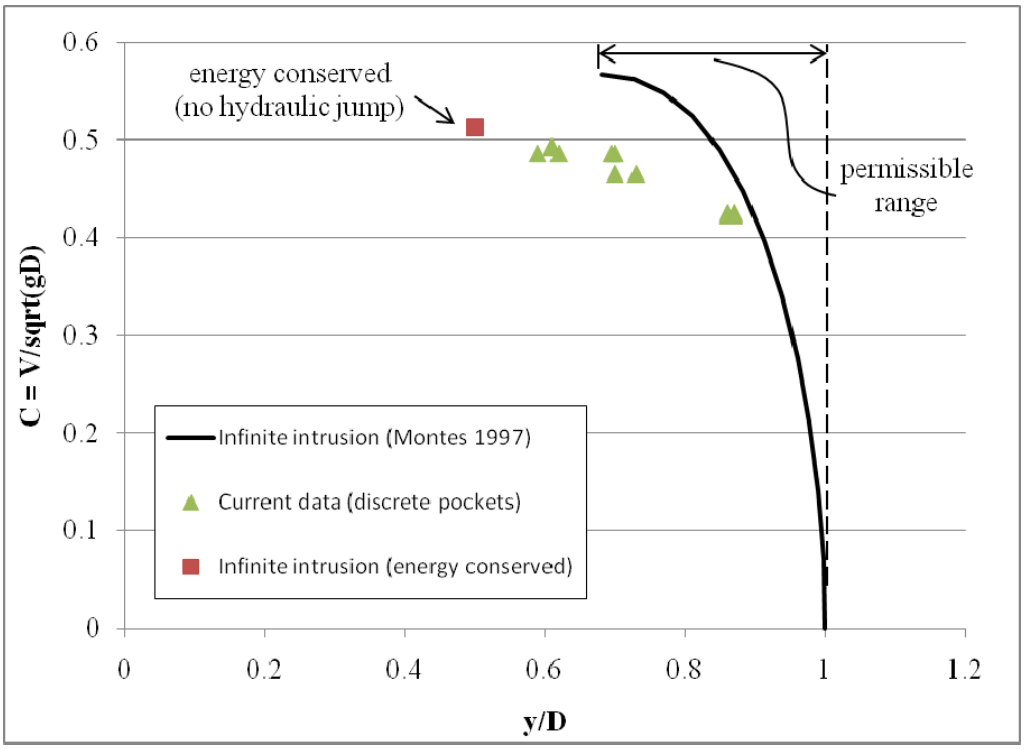

Figure 5.8 Air migration data in comparison to Montes 1997

5.5 Conclusions

Some general conclusions can be made regarding the results of this experimental investigation:

- Air in a horizontal pipe will have a tendency to migrate in both directions, especially with a low water velocity. The result of larger air pockets migrating faster than smaller ones was confirmed by these experiments. Larger air pockets migrating in the direction of flow were capable of moving faster than the water velocities utilized, while small air pockets generally moved slower than the water velocity. Since these are moving in the direction of flow, they are apparently unrelated to the Benjamin study. In general, the horizontal movement of air entrained at drop-shafts will behave differently than air pockets trapped during filling.
- All air migration velocities fell below a threshold of $C = 0.54$ corresponding to the Benjamin relation for the migration of an infinitely long air intrusion at atmospheric pressure. The large air pockets created in the capsule release experiments were within 22% of the Benjamin loss-free solution, with the largest air pocket migration velocity within 9%. There exists a small backflow in the water which replaces the forward moving air, which would slightly increase the relative velocity of the air migration from the observed measurements.
- For a given air intrusion thickness, observed migration velocities of discrete pockets were less than the Montes (1997) relation for an infinite intrusion. The measurement for air intrusion thickness contains uncertainty due to waves and curvature along the interface between the air and water. Also, it is possible for an

air volume to have a thickness much less than the limiting value, resulting in a lower velocity.

In relation to the real application discussed in Chapter 2, the investigation of this section can provide a few insights. Regarding the direction of air migration, the required water velocity to prevent upstream migration is roughly $0.54\sqrt{(gD)}$. At the location where the Minnesota geyser event occurred, the diameter of the main tunnel was 3.7 m. From this, the required water velocity to prevent air pockets from migrating up an incline would be 3.3 m/s, or a flow rate of 34 m^3/s. This flow is greater than the largest velocity measurement of 1.2 m/s taken by the St. Anthony Falls Laboratory. Therefore, the air which created the Minnesota geyser event seems to have originated from the lower elevation downstream. In general, air pockets trapped in CSO systems will typically migrate up a slope due to the large tunnel diameters unless there is a significantly large flow rate. Experiments clearly showed that large pockets of air are able to intrude into the water with relative velocities approaching the infinite intrusion relations. There was a fundamental difference between this and air injected as small bubbles, which effectively moved with the flow of liquid. Air entrained at drop-shafts essentially resembles the air injection experiments, and the movement of large trapped air pockets may be similar to the capsule experiments. This difference also impacts the assessment of vertical air/water behavior between these two experimental scenarios are investigated in Chapter 7.

Chapter 6

The Initial Rise of an Air Pocket

6.1 Objective

In sequential order, this chapter and the next two chapters will investigate the initial rise of the air pocket, the splashing which occurs once the air breaks through the surface, and the surge oscillations created by the change in water level. As the air pocket begins to rise within the vertical shaft, two interfaces develop between the air and water phases. The interface at the bottom of the vertical shaft is located at the nose of the air pocket and rises vertically. The second interface is occurs at the top of the liquid phase and is referred to as the free surface. A numerical model proposed by Vasconcelos and Wright (2011) is implemented to predict the movement of these two interfaces between the air and water. Experimental results are compared with the numerical model and a modification is suggested for an alternative method of approximating the air pocket pressure.

6.2 Introduction

The previous chapter discussed how air pockets arrive at the base of vertical shafts. The remainder of this dissertation is focused on the interactions between air and water as air pockets are ventilated in the vertical direction. There are three distinct

phases that were observed during previous experimental observations. The first phase is the slug flow regime of the air pocket's well-rounded nose pushing up a column of liquid and will be labeled the "initial rise". Once the air pocket breaks through the free surface of the liquid, a chaotic behavior ensues which will be referred to as "splash". Finally, the liquid level in the vertical shaft will drop due to the air release and this initiates an inertial oscillation referred to as "surge". This chapter and the next two chapters will consider initial rise, splash, and surge mechanisms, respectively.

In a relatively horizontal system, the filling process may cause pressurization leading to liquid surcharge at vertical shafts and pressurization of air pockets in the system. If the air arrives at the surcharged shaft, nearly hydrostatic pressures throughout the system permits the buoyancy of the air relative to the liquid to force the air upwards in the shaft. As the air rises, it generally occupies the center of the shaft while the liquid flows downward along the perimeter of the shaft in a thin film flow. The rise of an air pocket within a vertical shaft is initially slug flow regime because a slug of liquid exists above the slug of air. According to Davies and Taylor (1950) the front of the air pocket forms a well-rounded nose as it rises within the liquid. Davies and Taylor also predicted that an air pocket rises in an emptying, vertical, cylindrical container with a velocity of $v = 0.35\sqrt{(gD)}$. The cylinder used in the Davies and Taylor experiments was sealed at the top, which is a significant difference from the experimental setup used in this investigation. In most collection systems the vertical shafts are not sealed from above and are not water-filled in any case.

Vasconcelos and Wright (2011) developed a numerical model for the vertical air / water interactions and compared the model with experimental results. The Davies and

Taylor rise velocity was used as the initial velocity of the air pocket as it begins to move upward into the vertical shaft. Vasconcelos and Wright studied the upward air flow through an initially hydrostatic water column with a free surface. During this process, momentum may be transferred from the rising air to the surrounding liquid. If air continues to arrive as the liquid begins rising, the air velocity may significantly exceed that of Davies and Taylor. The experimental setup used in the Vasconcelos and Wright (2011) investigation included only one vertical shaft connected to a main tunnel sealed at both the upstream and downstream ends. For this confined system with only one shaft, the pressure within the air pocket is essentially equivalent to the column of water above it in the vertical shaft. Therefore the water level in the shaft has a direct influence on the pressure elsewhere in the system. In an actual filling tunnel, where the system is becoming surcharged by the inflow, the water level in the shaft is responding to this rather than the other way around. If a rising air pocket has a large portion of its volume in the main tunnel, the air pressure is influenced by the dynamics of the flow in the main tunnel. The main issue, then, is whether there are significant horizontal pressure gradients as the air pocket begins to be released.

The experimental investigation of this chapter measured the air/water interface velocities during the ventilation of a large air volume. The velocity of the nose of the air pocket was compared with the Davies and Taylor rise velocity. This velocity as well as the free surface velocity was compared with the numerical model proposed by Vasconcelos and Wright (2011). A few variables were adjusted to observe their influence on the magnitude of geysering.

6.3 Experimental Setup

The air capsule release experimental setup, as discussed in Chapter 5, was used for these experiments. The sketch of the experimental setup can be seen in Fig. 5.2. The horizontal 0.095 m diameter clear acrylic pipe was connected to a constant pressure head reservoir. Two different vertical riser diameters near the upstream reservoir were used, namely 0.095 m and 0.044 m. In addition, the reservoir level was adjusted between the values of 0.203 m and 0.457 m above the invert of the main tunnel. Also, three different volumes of the air capsule were used, namely 1.59, 3.14, and 5.97 L. The values of the variables are presented in Table 6.2 and each combination of the values was tested with four repetitions. Frames from the video camera were used to measure the vertical positions of the nose of the air pocket and the liquid free surface at each time step (30 frames/sec or Δt = .033 sec). The average experimental error, estimated from the standard deviation of the repetitions, was 0.04 m. Two experimental scenarios, namely the two larger air volumes with the small shaft diameter and higher reservoir level, had significantly greater errors than the other measurements, an estimated 0.15 m, due to the higher rise and necessary zooming out of the camera. Nevertheless, these were included in the overall average error of 0.04 m for these experiments.

Table 6.1 Experimental variables tested

Variable	Range of values tested	Normalized values
Vertical shaft diameter	0.044 and 0.095 m	0.47 and 1.0 [D_{riser}/D_{tunnel}]
Reservoir level	.203 and .457 m above invert	2.13 and 4.80 [H_{res}/D_{tunnel}]
Air capsule volume	1.59, 3.14, and 5.97 L	1.84, 3.64, and 6.91 [Vol_{air}/D^3_{tunnel}]

6.4 Results

The initial rise of the air pocket within the vertical shaft was capable of lifting water significant distances. As expected, the free surface water level moved upward as the air pocket rose within the shaft. Generally, the free surface continued to rise as the nose of the air pocket, moving faster than the free surface, caught up to the free surface and broke through the interface as expected. In this chapter, the geyser strength is defined as the elevation of the free surface level at the instant that the air pocket's nose reached it, relative to the tunnel invert. Later chapters will discuss other possible definitions when referring to the strength of a geyser. Table 6.2 reveals a fairly clear influence of each variable on the rise of the liquid due to the initial air release through the vertical shaft.

For all of the experiments, the geyser strength increased as the volume of the air pocket increased. One reason is that if there is less air than is necessary to completely fill the shaft cross-section, the buoyancy force is greater for larger air pockets since the volume of displaced liquid is greater. However, if there is more air than is necessary to fill the shaft, this physical principle may not be important since any remainder of the buoyancy force is exerted on the tunnel crown. A second important factor is related to the arrival of the air at the base of the vertical shaft. The previous chapter showed that the larger air pocket is able to migrate at a slightly greater velocity and greater depth through the tunnel. This allows the air to arrive at the base of the vertical shaft at a greater rate than the smaller air pockets. In particular, this distinction in air flux would be especially noticeable with regards to whether or not the rising air is capable of filling most of the shaft cross section. If the air flux is small enough, air just bubbles up in the

vertical shaft, which will still lift water as in an air-lift pump. However, a rising bubble that fills most of the cross section will lift the liquid much higher. Another critical factor in the influence of the air pocket's volume is the ratio of the volume of air to the volume of liquid in the vertical shaft. If the air pocket is large enough to rise through the entire column of liquid while still having a significant tail remaining in the main tunnel, this will create a higher rise than an air pocket which exists solely within the vertical shaft prior to reaching the free surface. This influence is clearly noticed in the case of the smaller diameter riser (0.044 m) and the higher reservoir level of 0.457 m. The air volume of 1.59 L is initially 2.8 times the volume of the surcharged liquid, but the migration process causes it to break into smaller pockets which spread across the top of the tunnel. Video observations in Figure 6.1 show that the vertical movement of the interface begins to decelerate starting at around 0.7 seconds, back to the Davies and Taylor velocity, which is most likely caused by a discontinuation of the air arrival into the base of the riser. The velocities of the 3.14 and 5.97 L air pockets did not level off, meaning that the air arrival was sufficient to continue forcing the water upward.

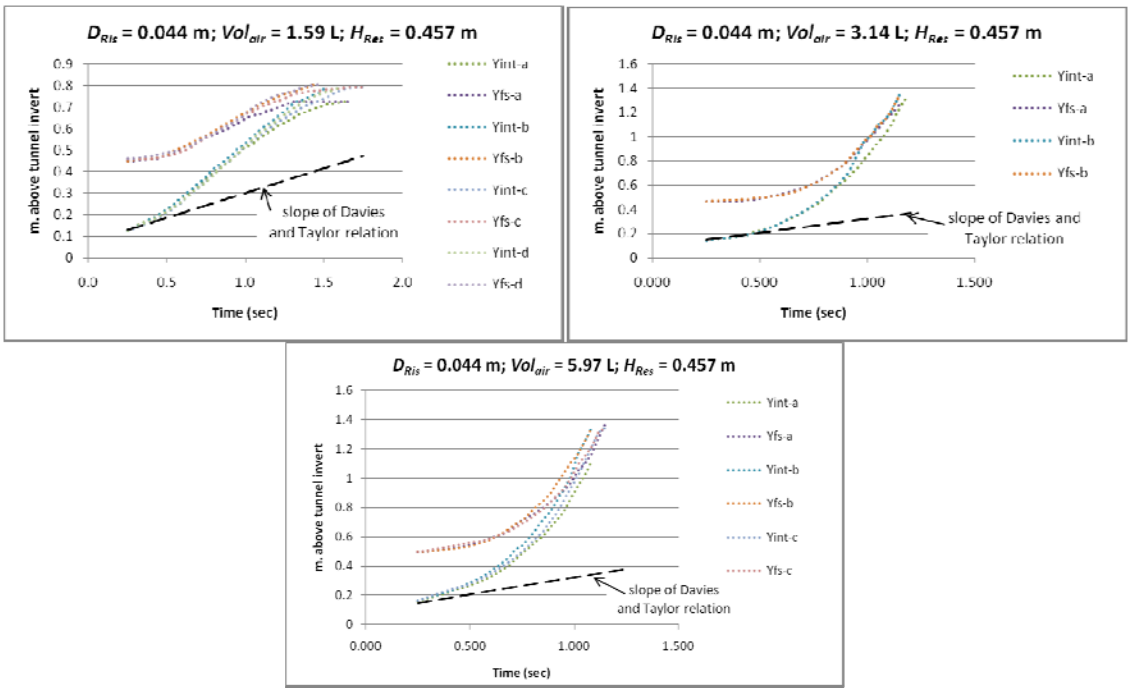

Figure 6.1 Video observations of the free surface level (Y_{fs}) and the air / water interface at the nose of the air pocket (Y_{int}) [The letters a, b, etc. represent trials for the same conditions]

Table 6.2 also shows that increasing the reservoir level increased the height of water rise. The reservoir level determines the volume of liquid that is surcharged initially within the vertical shaft and this volume of liquid must flow downward around the perimeter of the rising air pocket. When the reservoir level is higher, there is a greater volume of liquid which has to flow through this film region and this takes more time. If the air continues to arrive at the base of the vertical shaft and if the free surface level continues to rise, then the longer rise time associated with the higher reservoir level creates a higher level of liquid when the air reaches the free surface. The dimensionless rise of liquid, normalized by the reservoir level, was relatively the same for the experimental conditions involving the larger diameter. For the 0.095 m diameter riser, the rises of the 1.59 L air pocket through the 0.203 and 0.457 m reservoir levels were

1.16 and 1.11; the 3.14 L air volume through the lower and higher reservoir levels were 1.30 and 1.29; and the 5.97 L air volume through the lower and higher reservoir levels were 1.30 and 1.34. Figure 6.2 shows the video observations of the 1.59 L air volume rising through the 0.457 m initial water level for the larger diameter (0.095 m) riser, with multiple repetitions of the same conditions labeled "a", "b", "c", or "d". The rise velocity appears very close to the constant Davis and Taylor velocity as there seems to be a lack of a strong driving force to accelerate the air upward. This provides an explanation for how the large diameter dimensionless geyser strengths in Table 6.2 are similar between the two reservoir levels for each experiment. This also implies that the vertical air flow is constrained by the horizontal air arrival rate from the tunnel. The dimensionless rise heights of the smaller diameter shaft are clearly not similar, because the velocity (or slope in Figure 6.1) of the air rise through the higher initial water level is not constant. The larger air volumes are especially high because the air pocket continues to accelerate until it reaches the free surface. It is unknown whether a reservoir level much greater than the relative conditions of this experiment would continue to have an influence of increasing the rise height of the liquid. It is doubtful that the air would continuously accelerate for a "very high" column of liquid.

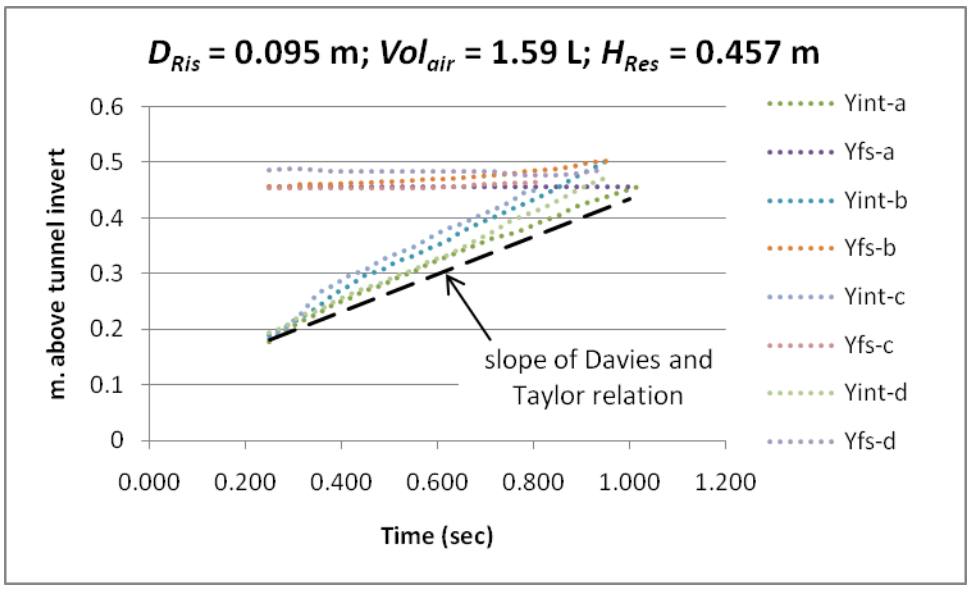

Figure 6.2 Video observations of the free surface (Y_{fs}) and the air / water interface at the nose of the air pocket (Y_{int}); shows a nearly constant velocity of rise for the larger diameter shaft.

Finally, of significant importance, the smaller riser diameter resulted in a higher liquid rise than the larger diameter for these experiments. The greater film flow around the perimeter of the larger diameter partially contributes to this influence. Another factor, though, could be the relative arrival rate of the air depending on the air volume and migration. Although it was not evident for these experiments, the air flow could be broken up if it rises faster through the vertical shaft than it migrates through the horizontal tunnel.

Overall, some of the vertical velocities of the air / water interfaces clearly achieved greater speeds than was expected from the Davies and Taylor (1950) expression. However, not all experiments exceeded the Davies and Taylor velocity, especially experiments with smaller air volumes. An air volume much larger than the surcharge volume of liquid within the shaft appears to be a key factor in creating strong vertical accelerations. Figures of the rise velocities can be seen in the Appendix.. In

particular, the releases of the 3.14 and 5.97 L air volumes through the 0.044 m diameter shaft with a reservoir level of 0.457 m (shown in Figure 6.1) created rise heights greater than 4.5 times the initial water level. The Davies and Taylor velocity is 0.23 m/s for this diameter riser, but for these two scenarios the air interfaces reached velocities greater than 3 m/s. Comparing the air volume to the liquid surcharge volume in Table 6.2, the major accelerations all occur for air volumes noticeably larger than the initial surcharge volumes.

Table 6.2 Geyser strengths for each set of variable conditions.

Riser diameter (m)	Reservoir level (m)	Air capsule volume (L)	Initial liquid surcharge volume (L)	Geyser strength (m)	Geyser strength (normalized by reservoir level)
0.044	.203	1.59	0.31	0.33	1.63
0.044	.203	3.14	0.31	0.37	1.82
0.044	.203	5.97	0.31	0.40	1.96
0.044	.457	1.59	0.69	0.78	1.72
0.044	.457	3.14	0.69	2.07	4.54
0.044	.457	5.97	0.69	2.23	4.88
0.095	.203	1.59	1.44	0.24	1.16
0.095	.203	3.14	1.44	0.26	1.30
0.095	.203	5.97	1.44	0.26	1.30
0.095	.457	1.59	3.24	0.51	1.11
0.095	.457	3.14	3.24	0.59	1.29
0.095	.457	5.97	3.24	0.61	1.34

6.5 Numerical Modeling

A rigid column formulation for predicting the vertical behavior of the air and water was developed by Vasconcelos and Wright (2011). The model calculates the film flow downward around the perimeter of the vertical shaft, similar to that proposed by Batchelor (1967), by solving Equations 6.1 and 6.2 and assumes that this film thickness remains constant.

$$Q_{displaced} = Q_f \qquad [6.1]$$

$$\frac{\pi}{4} U_B \left(D_{ris} - 2\delta\right)^2 = \frac{\pi}{3} \frac{g D_{ris} \left(\rho_w - \rho_a\right) \delta^3}{\mu_w} \qquad [6.2]$$

Where $Q_{displaced}$ is the water displaced by the upward moving air pocket, Q_f is the film flow around the air pocket, U_B is the rising velocity of a bubble according to Davies and Taylor, δ is the film flow thickness, ρ_w and ρ_a are water and air densities, and μ is the dynamic viscosity of water. For each time step, the changes in mass and momentum of the liquid column are calculated to determine the location of the free surface and the change in air pressure. The location of the air interface is also calculated. The experimental setup used to test this model in the Vasconcelos and Wright study included a main tunnel capped at both ends with a single vertical shaft. As the valve separating the air and water was opened, the water level in the shaft quickly responded to a level required to satisfy hydrostatic pressure variation requirements until the air pocket arrived at the shaft and began to rise, at which point the water level in the shaft started to rise at a somewhat lower rate to satisfy the imbalance between the film flow and the air rise. For that experimental setup, the pressure throughout the entire system, including the pressure within the air pocket, can be assumed to be directly related to the liquid level within the

vertical shaft assuming hydrostatic pressure variation. Therefore, the pressure within the air pocket drops as the air begins to rise due to the displacement of the water by the air and the resulting film flow. Although this assumption is appropriate for the Vasconcelos and Wright (2011) setup, the setup used in this investigation is somewhat different. The reservoir at the upstream end of the setup imposes a pressure which may keep the pressure within a large air pocket approximately constant.

Figures 6.3 and 6.4 show the results of this experimental investigation compared with the Vasconcelos and Wright (2011) numerical model for some experimental conditions; the others are presented in the Appendix. For most of the experimental conditions, the numerical model predicts nearly constant vertical velocities of the air / water interface and the free surface, with an air/water interface velocity near the Davies and Taylor relation. The model shows very little movement of the free surface as the air / water interface rises to meet it. This behavior is clearly observed with the 0.095 m diameter vertical shaft as opposed to the 0.044 m diameter shaft. The experimental results with the smaller diameter shaft typically show the air having a positive acceleration which causes them to be under predicted by the numerical model. In particular, the predictions of a large air pocket through the smaller diameter shaft at the higher initial water level deviated the most from the observed data. Care should be taken when implementing the model for air volumes which may be smaller than required to occupy the vertical shaft, as is probably the case for the top left image of Figure 6.3. Although the initial capsule volume is larger than would occupy the 0.8 m height, the slope levels off in this image implying that the air arrival rate is too small. This is plausible since the air spreads along the crown of the tunnel between the downstream end

and the vertical riser, limiting the air arrival. Also, the implementation of the numerical model is consistent here since the simulation only reaches a height of approximately 0.5 m above the tunnel invert, an air volume in the shaft which is less than half of the original air capsule volume.

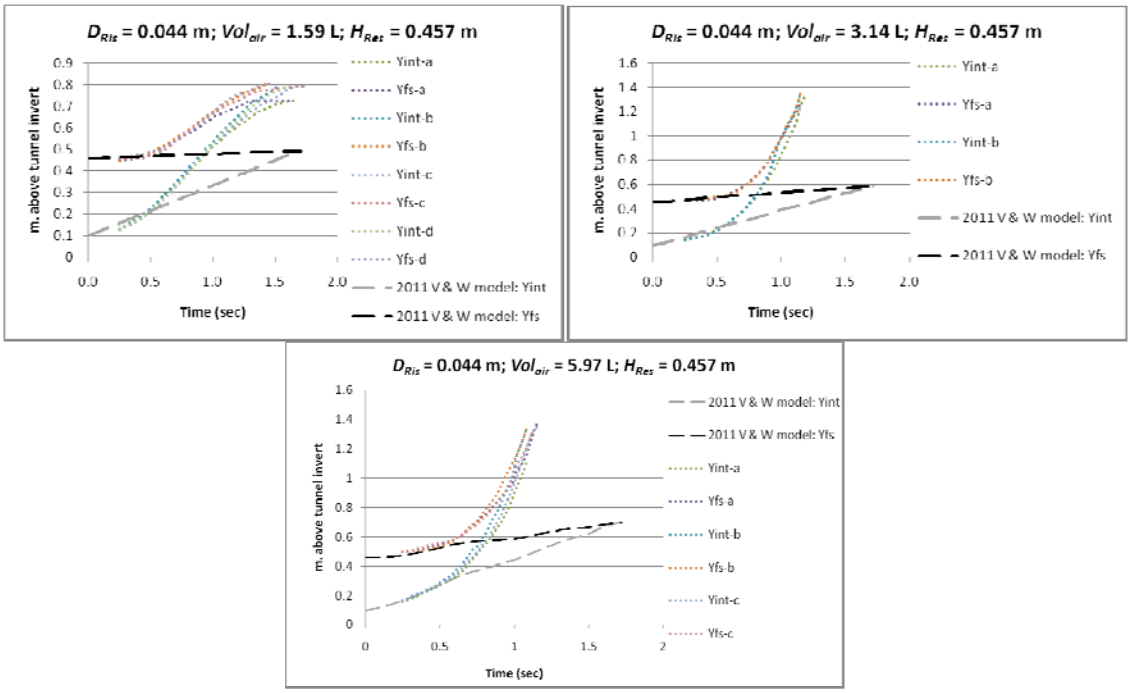

Figure 6.3 Numerical results and video observations (same conditions as Figure 6.1)

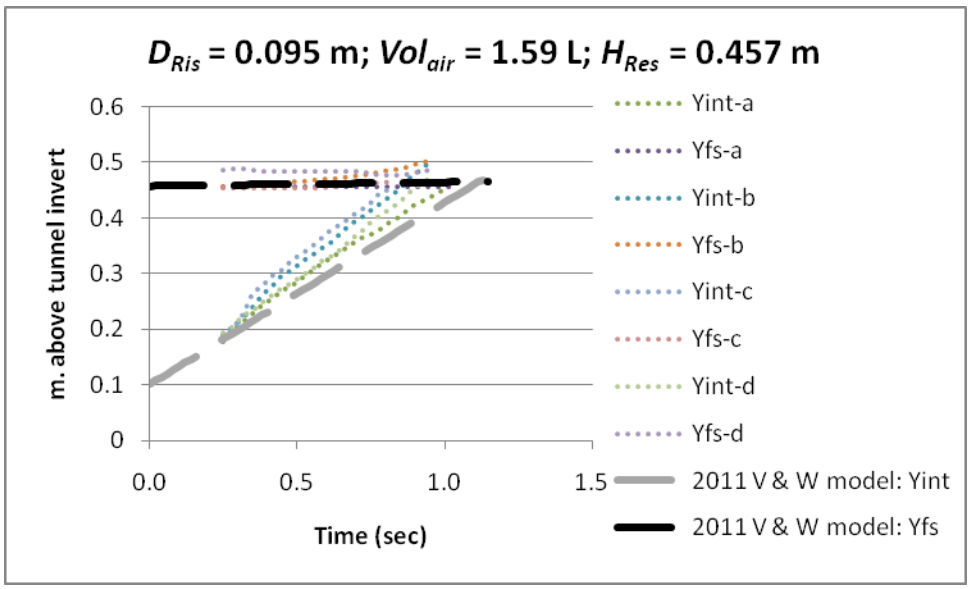

Figure 6.4 Numerical results and video observations (same conditions as Figure 6.2)

In general, the numerical model under predicts the rise heights and velocities, when compared with the observed data. As mentioned above, the numerical model assumes that the pressure within the air pocket is directly related to the water level above it in the vertical shaft. In reality, the pressure of a large air pocket may also be influenced by the flow conditions within the main tunnel, specifically the surcharge pressure after the tunnel goes full. In the present study, the main tunnel pressure is held nearly constant by the upstream reservoir and this pressure is greater than the water level above the air pocket due to the film flow downward. Therefore the air pressure is being under predicted by the numerical model which leads to the under prediction of the interface rises. A revision is suggested to the numerical model in which the pressure within the air pocket remains equal to the reservoir pressure throughout the rise process. This is implemented by assuming $\frac{dH_a}{dt} = 0$, which will not be exactly correct but serves as a reasonable first approximation. Again, careful implementation of the numerical model

must consider the possibility that the finite air pocket volume could be smaller than exists within the vertical shaft; this would cause the vertical velocity to level off presumably to the Davies and Taylor velocity. Figure 6.5 below shows the comparison between the experimental results and the two numerical alternatives for modeling the air pressure: first using the Vasconelos and Wright (2011) formulation (labeled "2011 V & W model" in the figure) and the second using the reservoir pressure (labeled "Revised" in the figure). The data is more closely aligned with the revised framework in which the air pressure is determined by the reservoir, rather than the initial assumption that it is equivalent to the liquid in the vertical shaft. However, this revised simulation rises too quickly, accelerating to speeds greater than the experimental measurements. Most likely, the air pocket experiences drag as it accelerates which has not been included in this numerical model. Further investigation would be required to include the drag acting on the air pocket as it rises. The assumption of constant reservoir pressure is not quite valid when the air is in motion, but it should over-estimate the vertical acceleration. In a real system, one would need to consider the conditions that would define the local pressure within the tunnel adjacent to the shaft.

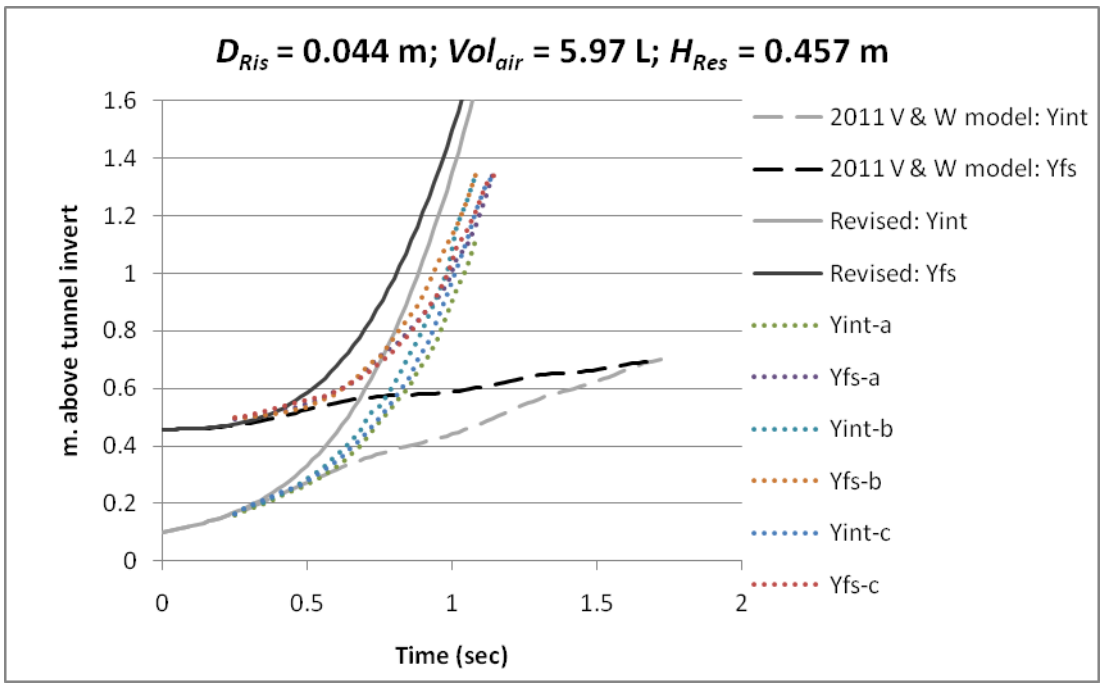

Figure 6.5 Comparison between experimental results and revised numerical model

6.6 Conclusions

- The higher reservoir level increased the height of rise of liquid measured from the location of the main tunnel as the air is initially released. It also increased the total change in water surface elevation, i.e. relative to where it started from.
- The larger air pocket volume increased the liquid rise during the initial air release.
- Rise velocities exceeded the Davies and Taylor relation for many of the experiments, in one case roughly an order of magnitude greater. Small diameter shafts were subject to greater accelerations, and thus are more prone to flooding instabilities and geyser occurrences. Also, geysering should be more likely with large trapped air pockets, since a large air volume relative to liquid surcharge volume is needed to produce significant acceleration.

- The Vasconcelos and Wright (2011) numerical framework was developed for an experimental setup with a single vertical shaft. The experimental setup used in the present study included a reservoir at the upstream end. Nevertheless, the results compare fairly well with the experimental data for the larger vertical shaft diameter. However, for the smaller diameter shaft the model predicts much slower interface and free surface rises when compared with the observed data.
- Considering the differences in the experimental setup, a modification to the numerical model is suggested. The air pressure within large air pockets can be modeled using the constant reservoir head. The experimental measurements were more nearly represented by this revised model, although the revised model over-predicts the water rise. Real systems experience surcharge during the filling process and the pressure of a trapped air pocket is largely influenced by the dynamics of the flow in the main tunnel, not quite matching either of the numerical implementations since horizontal pressure gradients are not taken into consideration.

The initial rise of an air pocket in the Minneapolis, MN system discussed in Chapter 2 can be modeled with the two numerical alternatives suggested here in this chapter. As the initial air pocket rises, both numerical models assume that the air pocket will occupy the shaft cross-section with a liquid film flow around the perimeter. The air will initially rise at the speed of the Davies and Taylor (1950) solution, calculated from the diameter of the shaft. The nose of the air pocket may rise at a greater volumetric flow than the liquid film flow downward, thus causing the liquid free surface level to rise.

Since it is difficult to know the potential air volume trapped in this system, Figure 6.6 below shows the results of an assumed 100 m^3 air pocket rising within the vertical shaft. The ratio of this air volume to D_p^3 is similar to that of the experimental setup of this chapter. The assumed initial water level is 1.5 m above the base of the vertical shaft, based on transducer measurements discussed in Chapter 2. As before, the numerical model results show only the predicted initial rise of the nose of the air pocket, not the behavior which may occur after the air breaks through the free surface. In these scenarios, the interface between the liquid and the air pocket reaches velocities of 8.5 and 6.8 m/s for the air pocket pressure alternatives using the tunnel pressure and water above the air pocket, respectively. These are high velocities, yet not as high as estimated in Chapter 2 to produce the geyser height observed. Once the air pocket breaks through the free surface, the pressure difference between the tunnel conditions and atmospheric pressure can accelerate the continued air release even faster, as discussed more in the next chapter. It is likely that the interfacial shear stress between the rising air and falling water will create instabilities which are not accounted for in the numerical framework. These flooding instabilities would likely change the air/water interactions of the geyser significantly from the experimental observations. This effect is not included in the model and a more detailed modeling framework would be required. It has not been explored in the present study due to the complexity of air density increases if water droplets are entrained, among other reasons. Observations from laboratory experiments suggest that the air arrival rate is an important factor in determining the vertical behavior. If the air arrival is insufficient to supply the upwards air flow, then the velocity is not as high and a lower water rise is expected. Certainly, if the air arrival rate is less than the Davies and

Taylor velocity (multiplied by the shaft cross-section minus the perimeter film), a reasonable outcome would be air pocket break-up and lower geyser strengths given the present understanding of geyser events.

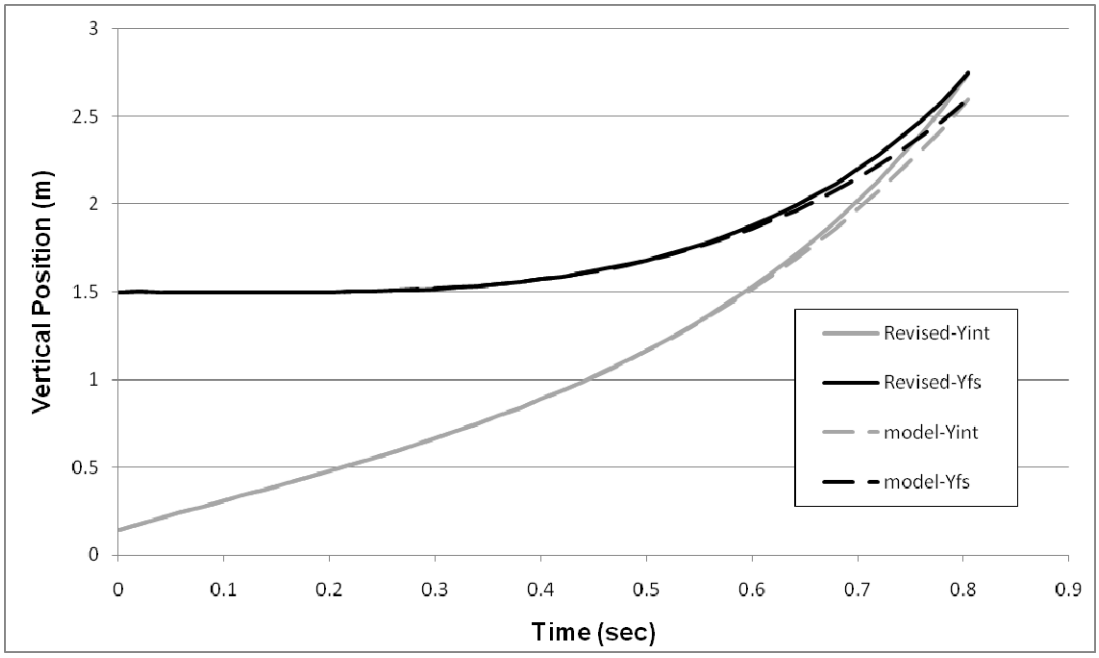

Figure 6.6 Free surface and air/water interface positions from the crown of the tunnel during an initial air pocket release in the Minneapolis, MN system (Vol_{air} = 100m^3; H_{Res} = 5.2m from tunnel invert; D_{Ris} = 2.4 m)

Chapter 7

Continued Air Release

7.1 Objective

The next stage of air release occurs while air continues to arrive at the vertical shaft after the nose of the air pocket has reached the free surface. At this point, the liquid is flowing downward around the perimeter of the shaft while air is flowing upward through the center. The behavior of the air and water may become chaotic as the two fluid phases churn together, flowing past one another within the shaft. An experimental investigation is conducted to demonstrate the continuous release of air through a vertical shaft surcharged with liquid. The objective of this section is to measure how liquid may be lifted during the continued release of air.

7.2 Introduction

The previous chapter discussed the initial rise of the air pocket's nose through the vertical shaft of a CSO storage tunnel. This chapter will focus on the subsequent release of air after the nose of the air pocket reaches the free surface. As mentioned previously, the liquid tends to flow around the perimeter of the shaft while the air flows upward through the center. Momentum may be transferred from the rising air to the surrounding liquid. Small amounts of liquid may be projected upward at the moment that the air

pocket breaks through the free surface. In this dissertation, this process is referred to as "splashing" although the potential implications of this process may be much more significant than the name implies. Real systems may move water much higher than the splashing levels indicated by the laboratory scale results as the water may be entrained into the upward air flow through the flooding phenomenon discussed previously.

A large volume of air may still exist within the main tunnel as the nose of the air pocket breaks through the free surface. If the main tunnel is in a surcharged state, a pressure gradient will exist within the air pocket between the surcharged pressure in the main tunnel and the atmospheric pressure where the air pocket broke through the free surface of the liquid in the shaft. Since the air has such a low density, even a small pressure is capable of accelerating the air significantly. For example, the potential air velocity can be calculated from an approximate energy balance based on a water pressure head driving the air flow:

$$v \approx \sqrt{\frac{2g\rho_w(\Delta H)}{\rho_a}} \qquad [7.1]$$

where v is the air velocity (m/s), g is the gravitational acceleration (m/s^2), ρ_w is the density of water (kg/m^3), ρ_a is the density of air (kg/m^3), and ΔH is the pressure difference (m, water). From this, a water pressure head of 0.1 m is capable of producing an air velocity near 40 m/s. In reality, the potential air velocity in this scenario would be lower due to energy losses caused by air/water and air/conduit shear stresses. Also, if the air entrains water droplets as discussed below, then ρ_a should actually be the density of the air/water mixture and this would reduce the velocity further. Nevertheless, it appears

that air being vented through a surcharged system can reach very high velocities and this effect may ultimately control the strength of the geysers that are depicted in Figure 2.1.

As the air accelerates, the vertical two-phase flow regime may transition from an initially presumed slug flow to semi-annular or annular flow. Nicklin (1963) discusses the different vertical two-phase flow regime categories. For the scenario of air being vented through a surcharged vertical shaft, the semi-annular or annular flow regime is not stable. There are two factors which could create instabilities. First, surface waves may develop at the interface between the air and water as observed by Hewitt and Wallis (1963), known as flooding. If the air velocity past these liquid surface waves is great enough, the shear between the air and water is capable of entraining liquid into the upward air flow. In essence, liquid particles are ripped from the wave crests and carried upward. Guedes de Carvalho, et al. (2000) derived approximate scaling laws relating the effect of air phase pressure to the velocity threshold for flooding instability.

The second factor which causes the annular flow regime to be unstable is the return of liquid to the base of the vertical shaft. As the air pocket breaks through the free-surface of the liquid within the shaft, a local low pressure is created within the liquid as well as the air. The liquid pressure in the system relative to the pressure relief within the air pocket causes the liquid in the main tunnel to accelerate toward the vertical shaft. The liquid flow into the base of the vertical shaft is capable of temporarily choking off the flow of air. This choking mechanism may only last a split-second such that the overall process appears as a chaotic burst of an air / water mixture as observed by Tramba, et al. (1995), disrupting the continuous outflow of a single large air pocket. The inertial surge

created by the acceleration of the liquid mass within the tunnel is discussed in more detail in the following chapter.

7.3 Experimental setup

The experimental procedure of this section is focused on the rise of an air/water mixture through a vertical shaft during a continuous injection of air. The experimental setup is the same as the continuous air injection setup shown in Figure 5.1. The downstream end of the tunnel was completely closed for the entirety of this investigation.

Table 7.1 Experimental Conditions

Label	Riser Diameter (m)	Air flow rate (L/min)	Initial water level (m, above tunnel invert)
1A	0.095	8	0.104
1B	0.095	25	0.104
2A	0.095	8	0.143
2B	0.095	25	0.143
3A	0.095	8	0.198
3B	0.095	25	0.198
4A	0.095	8	0.287
4B	0.095	25	0.287
5A	0.044	8	0.314
5B	0.044	25	0.314

The reservoir level at the upstream end was adjusted between five levels. Two air flow rates were used, namely 8 and 25 L/min. A 0.095 m diameter clear acrylic pipe was used as the vertical riser for most of the experimental trials, but another diameter of 0.044 m

was also used for two of the trials. Table 7.1 shows the combinations of the experimental conditions below. The air injection was maintained for three to five minutes for each trial. The digital video camera was used to measure the height to which the water was lifted by the continuous air release.

7.4 Results

Prior to measuring the air release through the vertical shaft, the migration of the air after injection was observed. The movement of the air through the main tunnel behaved in a similar manner for each trial. Since the liquid flow through the tunnel was zero, the air initially spread across the crown of the pipe in both directions. The elbow at the upstream end of the tunnel prevented air from being released into the reservoir. After approximately 30 seconds, a continuous pocket of air developed between the air injection location and the upstream elbow. The injected air bubbles continuously coalesced into this large pocket. Downstream of the injection location, discrete pockets of air were observed breaking off of the large pocket and migrating toward the vertical shaft. Once this behavior was established after approximately 30 seconds, the air injection rate into the tunnel was the same as the time-averaged air release rate through the vertical shaft. The air injection rate was very regular while the air release through the riser was intermittent due to the arrival of the discrete air pockets and the choking mechanism described in the Introduction. Arrival of the air pockets occurred on average approximately every 2 – 3 seconds for the high air flow and every 7-8 seconds for the low air flow. During the release of a single large air pocket, the air flow was occasionally choked off in a chaotic churning behavior of the air/water mixture as both

phases flowed into the vertical riser. The frequency of large air pocket arrival was the main factor in determining the frequency of extreme events.

The continuous injection of air was capable of lifting water over 1 meter beyond the equilibrium water level. Two possible ways of defining the geyser height for each experiment are given. The first method, labeled the "inertial surge" level, measured the elevation of the near-horizontal water surface which fluctuates due to inertial oscillations following the drop in pressure from the air release. The second method for defining the geyser height, labeled the "splash" level, measured the elevation reached by the splash of varying amounts of water particles. In small diameter risers, the splashing effect is less noticeable because the rising air tends to form a distinct interface with the water flowing downward around it. However, for large diameter risers the air does not necessarily fill the cross section and the large air pockets project water droplets significant distances into the air as they break through the free surface. The chaotic behavior which developed after the air broke through the free surface raised the water much higher than the surface level. The highest splash and surface levels during the entire 3-5 minute video clip for each trial were recorded. The surface level for the 0.044 m diameter riser was difficult to distinguish accurately from the video, so only the splash height has been recorded. Table 7.2 shows the measurements relative to the main tunnel invert and normalized by the equilibrium water level.

A comparison can be made between Table 7.2 and Table 6.2. The experiments labeled 3A and 3B from Table 7.2 have a similar reservoir level to experiments using the lower reservoir level in Table 6.2. The initial rise heights of the air pockets from Table 6.2 are 0.24, 0.26, and 0.26 m, depending on the air volume, while the surge values from

Table 7.2 are 0.30 and 0.39 m, depending on air injection rate, and the splash values are 0.51 and 0.53 m for the 0.095 m diameter riser. The air pockets created in the tests of Table 6.2 were much larger and for a real system would more likely represent the situation where a large air volume may be trapped during the filling process as opposed to multiple smaller air bubbles entrained at drop-shafts. On the other hand, the air pockets created in the tests of Table 7.2 were much smaller but more numerous. In a real system, this may likely correspond to the situation of significant air entrainment from a drop shaft. A brief comparison shows that both scenarios lead to results on the same order of magnitude, with the results of Table 7.2 showing a higher geyser height than Table 6.2. Since the rises are higher, which is unexpected if everything else is the same, there must be a physical difference in the behavior between the two cases. As will be studied later, the effect of inertial surge within the system during the experiments of Table 7.2 potentially combines with the process of air release. This implies that multiple mechanisms of air release exist which may potentially lead to geysering, in this case a single large air pocket and repetitive smaller air pockets.

An observation was made during the measurement of the surface level movement and the splash levels. Oscillations in the water surface level occurred separate from the physical process of air release. These oscillations were due to inertial surge in the system created by an interaction between the air being ventilated through the shaft and the water in the tunnel, even though the net water flow through the tunnel was zero. The arrival of an air pocket at the free surface relieved the pressure within the air pocket and caused the surface level in the riser to drop below the equilibrium level. This pressure gradient initiated a flow of water toward the riser which subsequently surged beyond the

equilibrium level due to the inertia of the flowing water. Video observations confirmed that the largest surge levels for each experiment immediately followed the end of a large air pocket release, leaving the surface level low within the riser to create the surge, as will be discussed further in Chapters 8 and 9.

Table 7.2 Recorded Heights (all distances are measured from the invert of the tunnel)

Label	Equilibrium level (m)	Max surface level (m)	Max splash level (m)	Max surface level divided by equilibrium water level	Max splash level, divided by equilibrium water level
1A	0.104	0.18	0.22	1.7	2.1
1B	0.104	0.23	0.29	2.2	2.8
2A	0.143	0.22	0.37	1.6	2.6
2B	0.143	0.28	0.46	2.0	3.2
3A	0.198	0.30	0.51	1.5	2.6
3B	0.198	0.39	0.53	2.0	2.7
4A	0.287	0.39	0.66	1.3	2.3
4B	0.287	0.46	0.69	1.6	2.4
5A	0.314	N/A	0.78	N/A	2.5
5B	0.314	N/A	1.52	N/A	4.8

The influence of each of the variables can be seen from the maximum elevations shown in Table 7.2. The effect of increased air flow rate is to increase both the surface level and the splash level. In general, the higher air flow rate created larger air pockets although the configuration of this setup did not allow the measurement of this relationship. The previous chapter showed that an increase in volume of the air pocket increased the water rise during the initial rising process, which is confirmed by these

observations. The influence of shaft diameter size caused the splash level to increase as the shaft diameter decreased. The third variable tested, equilibrium level, increased both of the maximum heights as it increased. This is similar to the results of the previous chapter that the air takes longer to rise through the higher equilibrium level, allowing more time to transfer momentum from the air to the water. In addition, the inertial surge was greater for the higher equilibrium level because the pressure gradient was larger following the release of a large air pocket.

Since the splashing effect may occur as air is released through the surface level which, in turn, may occur during any phase of the surge process, in reality, the observations cannot be totally uncoupled. In general, the maximum height of water was reached when the surge level and splash mechanism combined with one another. Figure 7.2 shows a timeline of tracking the splash elevation of water within the shaft for part of experiment 5B (see Table 7.1 for experimental conditions). As can be seen, most of the peak elevations reached by the water are between 0.75 and 1.0 m. Out of the 50 seconds of video shown in the figure, only two events reach beyond 1.25 m, representing 4% of the rise maximums. Careful observation of the video reveals that during the two extreme events, the surge level was rising quickly at the same moment that a large air pocket arrived at the base of the vertical shaft. This implies that each of the physical processes, surge and air release, are important in contributing to the maximum geyser potential. A more detailed discussion of this issue occurs in section 9.5 as well as related numerical modeling results.

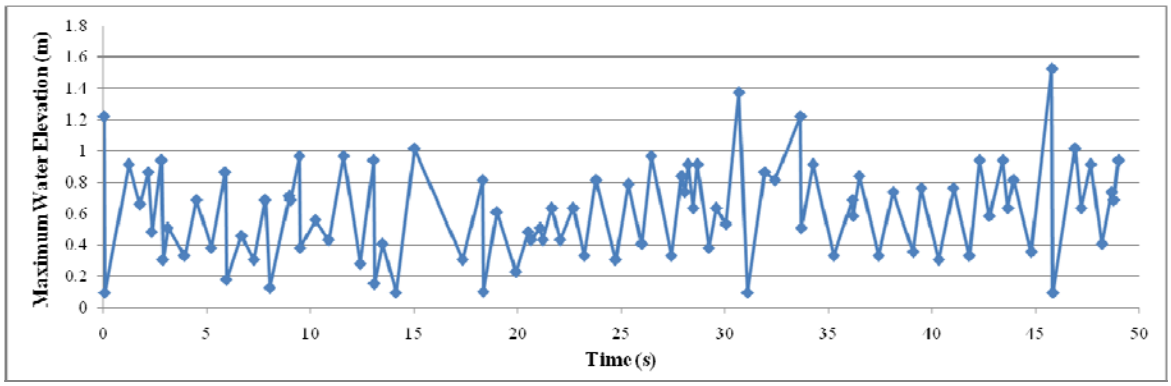

Figure 7.1 Time history of water level changes during experiment 5B

7.5 Conclusions

Some general conclusions can be made regarding the maximum water levels caused by repetitive air release:

- During the continuous air injection experiments, arrival of the air pockets at the base of the vertical riser occurred approximately every 2 – 3 seconds for the high air flow and every 7-8 seconds for the low air flow on average. The frequency of air arrival was the main factor in determining the frequency of geysering.
- Increasing the air flow rate increased the volume of the air pockets reaching the vertical shaft and thus increased the maximum surface and splash levels.
- The highest geyser heights were observed for the smaller riser diameter. As discussed in Chapter 6, the smaller diameter causes higher initial rises of the air/water interfaces as an air pocket moves toward the free surface.
- Increasing the equilibrium level caused higher maximum surface and splash levels.
- The release of a large air pocket initiated a low pressure in air remaining in the tunnel at the location of the vertical shaft which is transmitted locally to the water.

This pressure gradient initiated inertial surge oscillations within the system independent of the air release process. The highest splash levels were reached when the timing of these two processes, maximum surge rebound velocity and the release of another large air pocket, matched one another.

A real collection system, such as the one mentioned in Chapter 2, would have some similarities to these experimental results, yet also a key difference. In general, the influence of air arrival rate and equilibrium level would be the same. However, an important phenomenon known as flooding is difficult to produce at the laboratory scale, at least with the experimental setup used here. The velocity of the escaping air would be greater in the real system due to the scaling between the model and the prototype shaft diameter. Therefore, the fast moving air in a large system could create enough shear at the interface with the water to entrain the water upward. The rise of this air and water mixture would therefore increase the height of the maximum water rise compared to the laboratory observations. It is difficult to determine the potential for this phenomenon, but it is believed to be very important based on visual observations from the Minnesota geyser event of Chapter 2. The maximum velocity of the air can be estimated from an energy balance by using the system surcharge pressure, similar to the discussion in Chapter 2. Approximating the rise distance of the water, however, is difficult because it is dependent on how much water is entrained; i.e. the density of the air/water mixture. This is a different mechanism for water rise that is not directly accounted for in the laboratory experiments. In general, though, the results of this investigation show that both inertial surge and air release are important. A problematic scenario which could

lead to a strong geyser occurrence would be for a large air pocket to arrive at the moment that the vertical velocity from surge is the highest.

Chapter 8

Inertial Surge Caused by Air Release

8.1 Objective

The inertia of the liquid as it rapidly fills the pipeline is an important physical property of the collection system. Indeed, much of the literature explains this single mechanism as the cause of past geyser events. The previous chapters discussed how the air pocket can influence the rise of liquid within the vertical shaft by various mechanisms. The release of the air pocket also lowers the pressure of the tunnel at the shaft location. The inertia of the liquid refilling the vertical shaft can cause the water level to exceed the equilibrium level significantly. This mechanism was observed during the dissertation research of Vasconcelos (2005) studying rapid filling and air entrapment, where geyser events occurred at both the nose of an air pocket as well as the tail of the same air pocket, as mentioned in Chapter 3. The objective of the experiments in this chapter is to study the interaction of a surge front with a vertical shaft in a rapidly filling pipeline to evaluate the potential for causing a geyser event. Two possible scenarios can lead to the arrival of a filling front at an empty vertical riser. The first is due to a pipe-filling bore, as discussed in Chapter 4, and the second is due to the tail end of a large air pocket as witnessed by Vasconcelos (2005). The similarities between these two types of

conditions were exploited to simplify the experimental setup for this study discussed below.

This laboratory investigation aims to understand the variables that are most influential in determining the peak of the pressure surge and to compare the results with a simplified numerical model. The bore front is also expected to entrain air as it propagates through the main tunnel. It is also unknown whether the reduced density of the air/water mixture in the shaft could result in a significantly different rise due to pressure surge compared to what would occur with the water phase alone.

8.2 Experimental setup

The experimental setup in this investigation was very similar to the setups discussed in Chapter 5. A length of 7.79 m of the 95 mm diameter clear acrylic pipe was used as shown in Figure 8.1. Video observations were made for each trial as well as three continuous pressure recordings. The locations of the pressure transducers are shown in Figure 8.1 on either side of the riser, yet not right next to it. The butterfly valve was located at the upstream end of the pipeline to create the pipe-filling bore by sudden opening of the valve. At the downstream end of the system, a weir controlled the initial water depth within the system as well as the flow through the system once the bore arrives downstream. The vertical riser was located 3.47 m downstream of the valve.

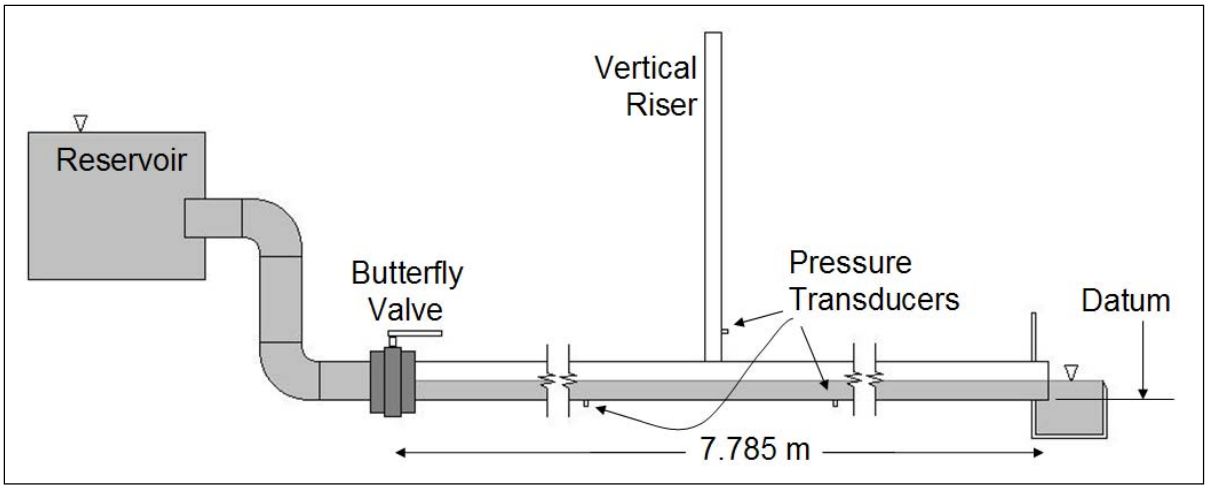

Figure 8.1 - Experimental Setup

The reservoir elevation, initial depth, riser diameter, and ventilation were adjusted through the ranges presented in Table 8.1. The upstream reservoir was adjusted to elevations of 0.627 m, 0.703 m, and 0.822 m above the main horizontal pipe invert (datum). The reservoir consisted of a large Plexiglas box in the center of a large cylindrical tank. An inflow source was provided into the reservoir so that water flowed over the top edges of the reservoir to maintain a nearly constant pressure head over the duration of the experiment. The elevation of the reservoir was adjusted by adjusting the elevation of the Plexiglas box.

Table 8.1 - Experimental Variables

Variable	**Values**
Initial Depth	50%, 70%, 95%, 100% of pipe diameter
Ventilation	Open, closed, ~ 5% open
Riser Diameter	44.4, 25.4, 12.7 mm
Reservoir Elevation	0.627, 0.703, 0.822 m to pipe invert

Secondly, the initial water depth in the horizontal pipeline downstream of the valve was adjusted to the various levels of 50%, 70%, 95%, and 100% full with respect to pipe diameter. The weir box at the downstream end of the system had base dimensions 0.240m by 0.240m. The weir crest elevation was adjusted by installing sharp-crested Plexiglas pieces of different heights into the end wall of the weir box. The weir crest height produced the desired initial water depth in the pipeline while the water flow over the crest was sufficient to maintain a full pipe condition after the pipe-filling bore arrived at the downstream end of the system.

Three different vertical riser diameters were used, namely 12.7 mm, 25.4 mm, and 44.4 mm. The pressure transducer was mounted in the same vertical location for each of the three diameter risers and in such a way as to be unobtrusive to the flow within the riser. Each riser consisted of clear acrylic tubing of height greater than 1.8 meters, sufficiently tall that all surges were contained within the riser.

The final variable was the degree of ventilation within the riser. Open ventilation simply meant that the top of the riser was open to the ambient air. Closing off the top of the vertical riser created closed ventilation conditions. Under these conditions, the air contained within the riser became pressurized as the surge was initiated and the compressed air limited the height of the water rise. The other ventilation setting was an intermediate condition in which an opening at the top of the riser provided a small ventilation area. From previous experiments, this was considered to be restrictive to air escape such that some air pressurization would develop as the surge rose in the riser shaft. This ventilation condition was produced by placing a plug at the top of the riser with a smaller diameter hole, such that the opening was roughly 5% of the cross-sectional

area of the riser. The opening was adjusted for each riser diameter to maintain the 5% ratio.

Three repetitions were performed for each experimental trial in order to ensure repeatability of experiments that involved a manual valve opening. The butterfly valve was slowly closed preceding each repetition. The slow closure allowed the system to gradually come to rest at an initial depth based on the downstream weir height. The initial still-well water level was recorded for each set of experimental conditions for calibrating the transducers. The butterfly valve was opened rapidly, allowing the surge front to propagate through the system. The system usually reached steady-state equilibrium within 15 seconds with the water level and the flow passing through the system controlled by the weir in the discharge outlet box. The final still-well water level in the riser for this equilibrium state was recorded for calibration as well. Individual experiments were performed for each permutation of the values listed in Table 8.1 with the exception of the 100% initial depth scenario. Only eight experimental combinations were performed for the 100% initial depth in addition to the 81 other experimental combinations. These full pipe experiments were primarily performed to gain a better understanding of energy losses within the system.

8.3 Results

General observations

Visual observations of the experiments showed that a pipe-filling bore formed for all trials that were not initially full at the start of the valve opening. Furthermore, air became entrained within the pipe filling bore in the form of many very small bubbles.

Two different flow behaviors existed for the air in the experiments, based only on the initial depth of the system. For initial depths of 50 and 70 percent with respect to pipe diameter, the flow exhibited that of a moving hydraulic jump, as seen in Figure 8.2a. The surge front consisted of an air/water mixture entraining small diameter air bubbles. The other behavior, exhibited for the 95% full case, involved the movement of larger air pockets instead of an air/water mixture, as seen in Figure 8.2b. These air pockets generally moved with the flow of water which was significantly slower than the movement of the pipe filling bore. The 95% initial depth case had a very small gap in the top of the circular pipe, which did not allow for the rolling or churning behavior observed with the bore motion observed with the lower initial depths tested. Instead the air at the crown of the pipe formed discrete bubbles, possibly due to the fact that the pipe was not entirely level. The increased pressure moved through the liquid very quickly, similar to a water-hammer transient. As air flowed through the system, some of it moved up into the vertical riser while a significant portion flowed downstream. As expected, there were no visual signs of air moving through the system during the 100% initial depth experiments.

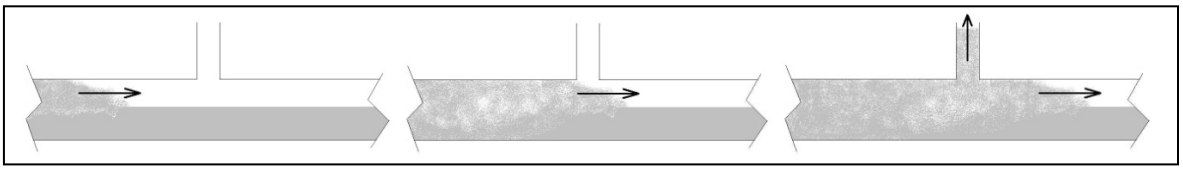

Figure 8.2a - Moving Hydraulic Jump With Air Entrainment

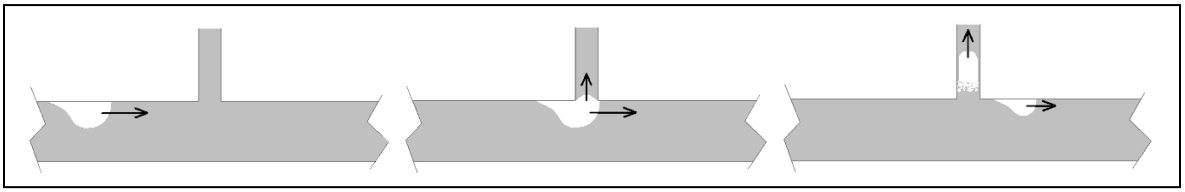

Figure 8.2b - Moving Discrete Air Pocket

From the video recordings, the visual observations of the maximum water level were compared with the pressure readings from the transducer within the riser. The objective of this comparison was to determine if the presence of the air bubbles was sufficient to alter the pressure distribution within the riser due to a reduction in density of the air/water mixture. Equivalence between the observed water level and the corresponding pressure head would indicate that the air bubbles have a negligible effect. Figure 8.3 shows a comparison. If the air bubbles have an impact, the visual water level should be higher than the recorded pressure head; the experimental data show no such effect and the two values are the same, apparently within measurement accuracy. The measurement error from the three pressure transducers, estimated using the average standard deviation of the repetitions for all experimental conditions, was 0.034 m. The measurement error using the video snapshots was larger, approximately 0.08 m, due to the zoom of the video camera and the small diameter sizes of the vertical riser. The perhaps systematic deviation for the 95 % full case is likely due to the discrete air pockets in the riser. The important thing to note about the small differences is that a numerical correction for the change in density due to the presence of the air bubbles seems unnecessary.

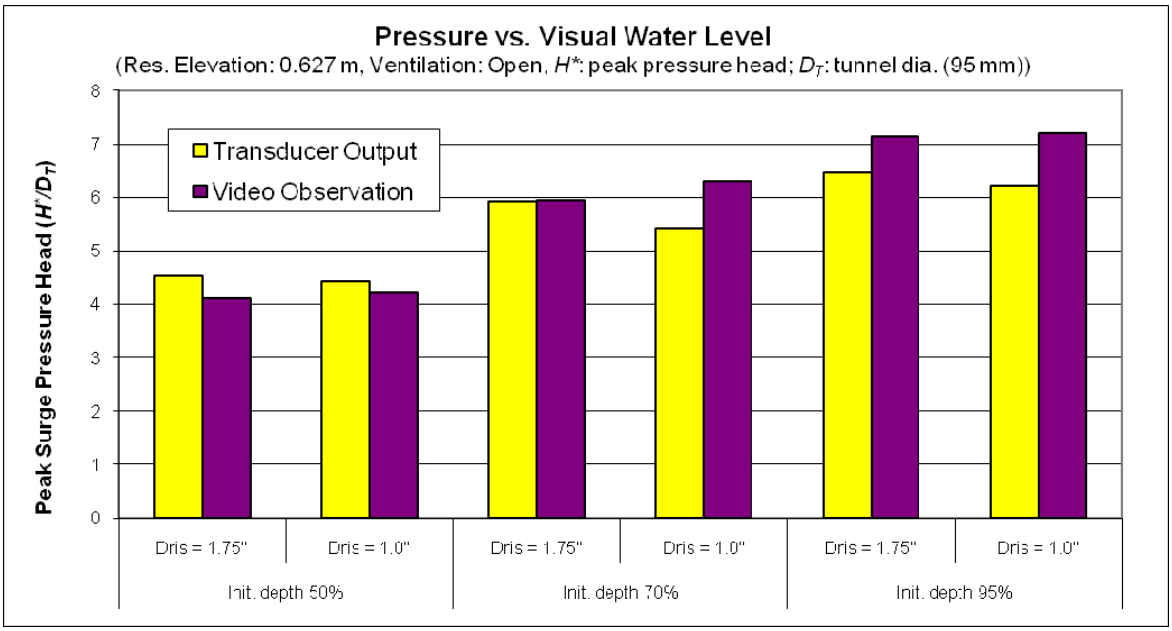

Figure 8.3 - Visual Comparisons With Peak Pressures

Variable adjustments

The experimental results were influenced strongly by changing some variables, but they seemed unaffected by changing others. As the bore progressed forward, it moved in a shape similar to that sketched in Figure 8.4, depicted in a frame of reference moving with the bore that is assumed to have a quasi-steady speed of propagation.

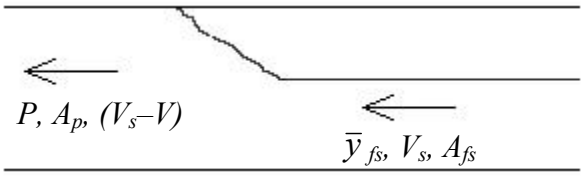

Figure 8.4 - Surge front schematic (frame of reference moving with the bore)

Conservation of mass and momentum can help qualitatively explain the expected behavior across the bore front:

Cons. of Mass: $$(V_s - V) \cdot A_p = V_s \cdot A_{fs} \qquad [8.1]$$

Cons. of Momentum: $$P \cdot A_p + \rho \cdot (V_s - V)^2 \cdot A_p = \rho \cdot g \cdot \bar{y}_{fs} \cdot A_{fs} + \rho \cdot V_s^2 \cdot A_{fs} \qquad [8.2]$$

where P represents the gage pressure behind the bore front, A_p is the area of the full pipe, V_s is the bore velocity, V is the fluid velocity behind the bore, $\bar{y}_{fs}$ is the centroid depth in the downstream free-surface portion of the flow, A_{fs} is the area of the free surface portion, g is gravity, and ρ is the density of the fluid. From the conservation equations we can solve for a parameter Z representing the pressure head behind the advancing bore which will influence the magnitude of the riser surge.

Substitute Equation 8.1 into 8.2:

$$P \cdot A_p + \rho \cdot (V_s - V) \cdot A_p \frac{V_s \cdot A_{fs}}{A_p} = \rho \cdot g \cdot \bar{y}_{fs} \cdot A_{fs} + \rho \cdot V_s^2 \cdot A_{fs}$$

Dividing the above by ($\rho g A_p$): $$\frac{P}{\rho g} + \frac{V_s (V_s - V) \cdot A_{fs}}{g A_p} = \bar{y}_{fs} \cdot \frac{A_{fs}}{A_p} + \frac{V_s^2 \cdot A_{fs}}{g A_p}$$

Rearranging: $$\frac{P}{\rho g} = \bar{y}_{fs} \cdot \frac{A_{fs}}{A_p} + \frac{V \cdot V_s \cdot A_{fs}}{g \cdot A_p}$$

Equation 8.1 can be rearranged to: $$V_s = \frac{V A_p}{\left(A_p - A_{fs}\right)}$$

Finally, letting $Z = (P/\rho g)$: $$Z = \bar{y}_{fs} \cdot \frac{A_{fs}}{A_p} + \frac{V^2 \cdot A_{fs}}{g \cdot \left(A_p - A_{fs}\right)} \qquad [8.3]$$

From this equation we see that an increase in velocity V would increase Z. One of the effects of raising the reservoir elevation is to increase the fluid velocity and therefore raise the surge pressure. Increasing the reservoir elevation of the system did indeed result in an increase of the maximum peak pressure for all but one of the nine experiments shown in Figure 8.5; the case of 50% initial depth and 5% ventilation. In this particular case, there is less than one standard deviation of measurement accuracy (0.034 m or

$0.36D_T$) between the two experiments. Therefore an overall trend of increasing peak pressure with increasing reservoir elevation is clearly observed.

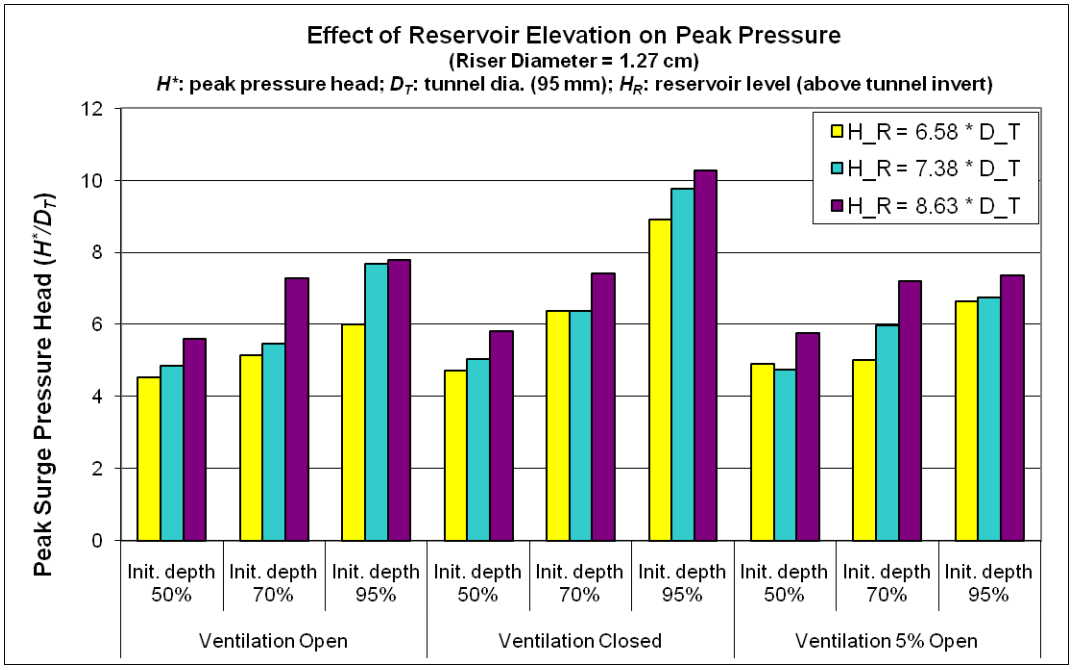

Figure 8.5 - Influence of Reservoir Elevation

A bore moving in a real tunnel usually encounters a partially filled collection system and the experimental results show that a higher initial depth results in an increased velocity of the bore (based on bore arrival times at the first and second transducers) and higher maximum peak pressure. From Equation 8.3, as initial depth increases, both terms in the equation will increase due to an increase in A_{fs} and $\bar{y}_{fs}$. Therefore we can qualitatively predict that increasing the initial depth will increase the peak surge pressure, assuming all other variables are unchanged. This coincides with the experimental results for all 27 experiments, as shown in Figure 8.6. The vertical axis shows the dimensionless peak surge pressure head normalized by the tunnel diameter.

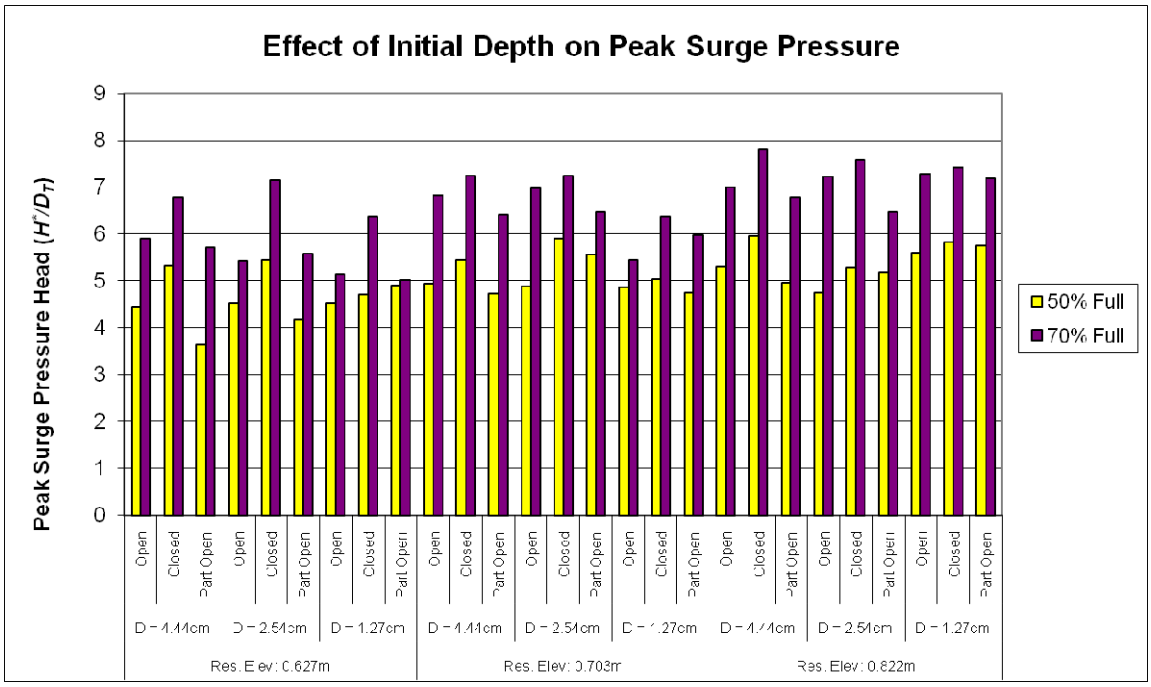

Figure 8.6 - Influence of Initial Depth

The ventilation was discovered to have little impact on the maximum peak pressures in the system. From Figure 8.7 it is observed that there is no significant variation apparent with respect to the degree of ventilation. The partially open ventilation scenarios generally behaved similar to the open ventilation scenarios, implying that a small cross-section of the riser was sufficient to adequately ventilate the air without air pressurization. Visually, there was a large difference in the riser water level between the open and closed scenarios. The transducer pressure ouputs, however, were very nearly the same between both situations due to air pressurization in the closed ventilation case or water column pressure in the open ventilation case.

The open ventilation case consistently resulted in a slightly lower maximum peak pressure presumably due to extra energy losses involved in the greater movement of the water column up into and within the riser. On the other hand, the degree of ventilation had a very strong impact on the oscillation characteristics. The pressure output for the

closed ventilation scenarios resulted in a higher frequency and smoother behavior, as can be seen in Figures 8.8 and 8.9. The oscillating frequency of a surge tank and that of an accumulator can be compared using relevant time scale relationships. Wylie and Streeter (1993) recommend $f_{s,accumulator} = \frac{1}{2\pi}\sqrt{\frac{H_A g A_T}{\forall L}}$ (Hz) as the frequency of an air accumulator within a pipeline and $f_{s,surge} = \frac{1}{2\pi}\sqrt{\frac{gA_T}{LA_S}}$ (Hz) for a surge tank, where f_s is the frequency of oscillation, H_A is the absolute pressure within the accumulator, A_T is the area of the tunnel, A_S is the area of the surge tank, $\forall$ is the volume of the accumulator, and L is the length of the tunnel. For these experiments: H_A is approximately the height of the reservoir, 0.7 m on average, plus the 10.33 m atmospheric pressure; the volume of the accumulator, $\forall$, is A_S*H_R where H_R is the height of the riser. The riser height was approximately 1.8 m for all of the experiments. Other variables in the equations are common to both relationships. Due to the cancellation of most of the terms, the ratio of the accumulator frequency to the surge tank frequency can be represented by $\frac{f_{s,accumulator}}{f_{s,surge}} = \sqrt{\frac{H_A}{H_R}} = \sqrt{\frac{11}{1.8}} = 2.5$. This shows that the frequency of an air accumulator is roughly 2.5 times higher than the frequency of the surge tank, which is supported by the comparison between Figures 8.8 and 8.9. At the end of the pressure record of Figure 8.9, one of the repetitions trends to a higher level. This is presumably caused by a measurement error of the piezo-resistive transducer occurring part way through the trial. Occasionally, an air bubble stuck to the face of the transducer yielding erroneous results and this may have occurred here. When this situation was noticed during the experimental procedure, the trial was repeated.

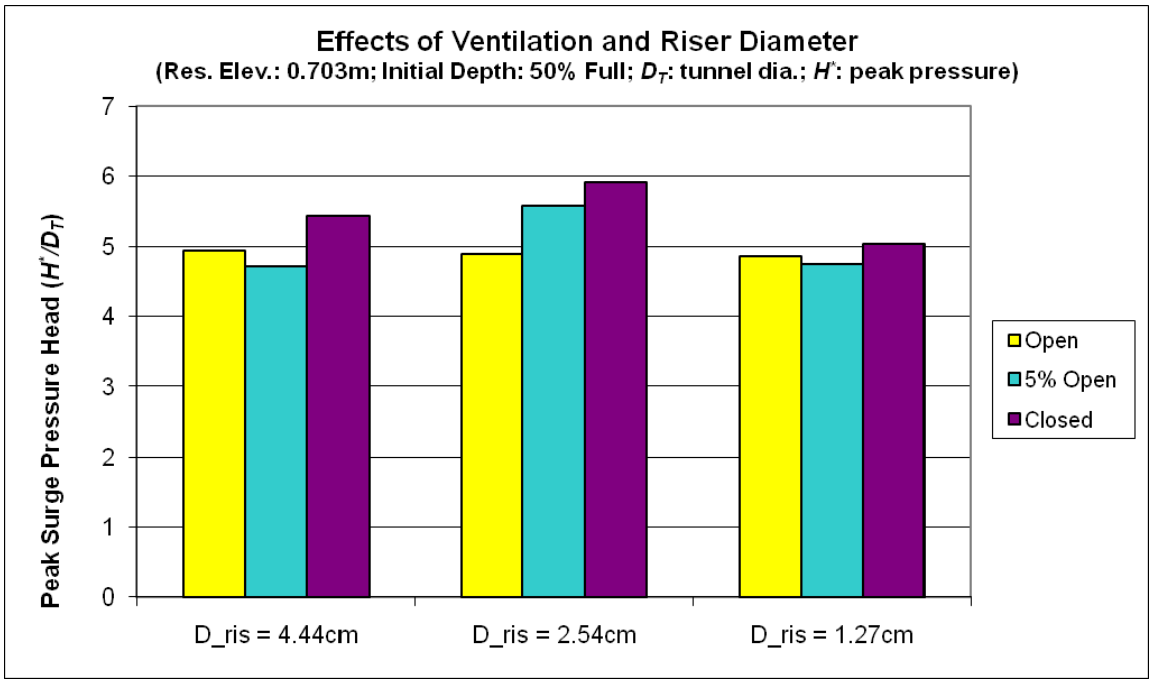

Figure 8.7 - Lack of influence for ventilation and diameter

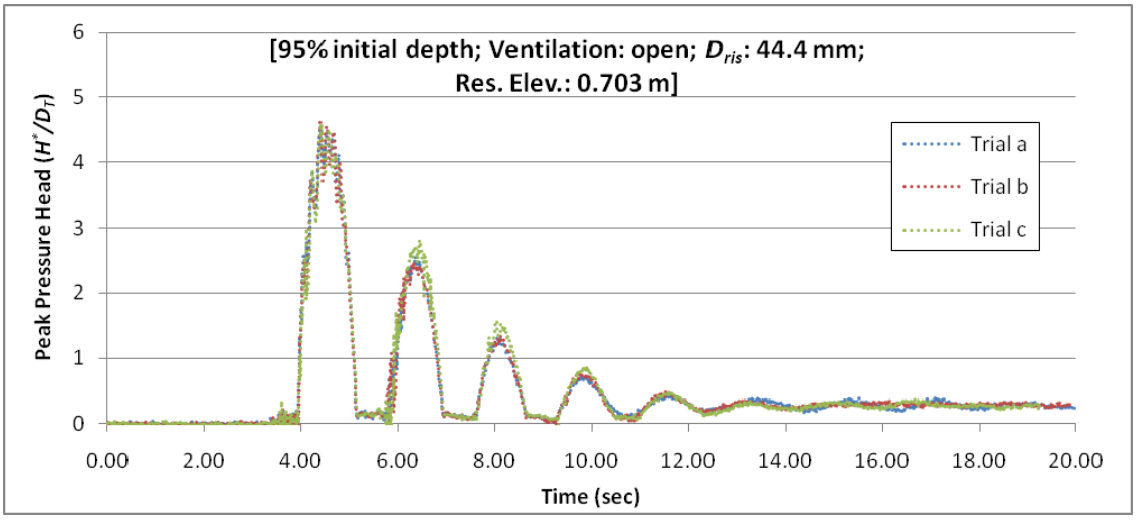

Figure 8.8 – Example of pressure frequency oscillation for open ventilation

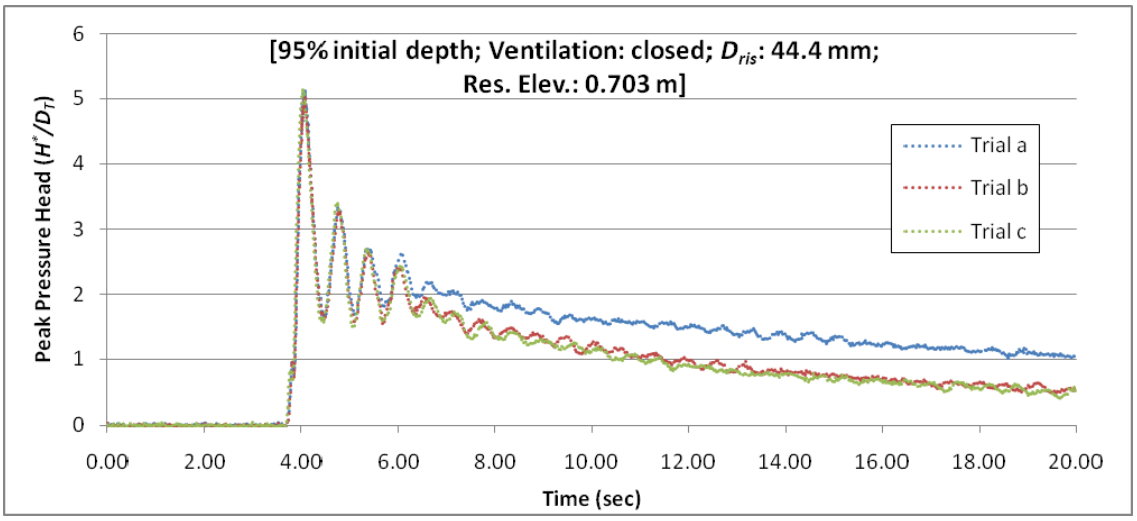

Figure 8.9 – Example of pressure frequency oscillation for closed ventilation

There are two minor effects which are influenced by the diameter of the vertical riser: friction and inertia. An equation for momentum, below in Equation 8.7, shows that although A_2 is present, it cancels out in the dominant terms and is only left in the smaller term of the minor loss into the riser. Therefore the riser diameter is not expected to be critical. This is in opposition to the air entry process where the diameter size is very influential to the vertical air and water velocities. This suggests that the air entry is more important in smaller diameter shafts than surge. As the riser diameter decreases, more energy will be lost to overcoming friction along the vertical pipe walls. Therefore, as the water moves up into the riser, the friction from a smaller diameter would cause the maximum peak water heights to be less. The other effect that would be influenced by the vertical riser diameter is the inertia of the liquid in the horizontal pipe. Upon the arrival of the bore, the water will be accelerated up into the riser due to pressure forces originating from the elevated reservoir. Once the water level within the riser reaches that equilibrium elevation, the fluid will have a velocity upwards that will then decay due to the force of gravity. The larger the diameter, the more the fluid entering the riser shaft

should influence the remaining flow in the pipeline, effectively reducing the inertia of the surge. The effects of these two phenomena were sufficiently small that they do not significantly affect the riser surge.

8.4 Rigid column modeling approach

A simplified numerical model which considers the inertia of the liquid in the system can be implemented to compare with the experimental results. Three control volumes can be drawn as shown in Figure 8.10; two around the liquid in the main tunnel on each side of the riser and one in the riser. The liquid in each control volume is assumed incompressible and represented by a single velocity. The numerical model represents the upstream section of the tunnel with a straightened control volume, but includes the energy losses of the 90° elbows in the friction representation discussed later. The length of the control volume in the riser changes as the water level within the riser changes. A conservation of mass equation can be formulated discretely at the base of the vertical riser using these control volumes to obtain Eq. 8.4.

Cons. of Mass (at the base of the riser): $\rho v_1 A_1 = \rho v_2 A_2 + \rho v_3 A_3$ *[8.4]*

where ρ is the density of water, v is the fluid velocity, and A is the cross-sectional area of the control volume perpendicular to the velocity. The cross sectional areas of the control volumes are known.

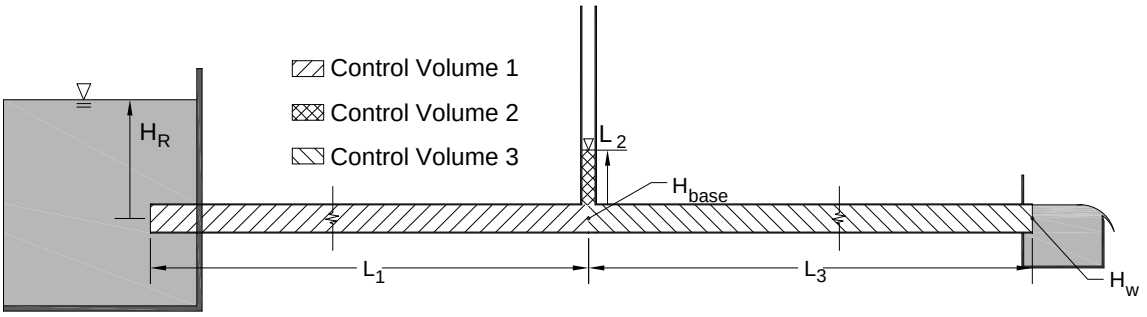

Figure 8.10 Sketch of the control volume used in the rigid column method

The rigid column approach uses the conservation of momentum principle within each control volume to solve the system of equations. The first control volume could be broken up into multiple control volumes based on the elbow connections turning the flow from the horizontal to vertical direction, then back to the horizontal direction. However, since the diameter of these sections are the same, the velocity in each section is also the same due to the conservation of mass, and the multiple sections can be represented by a single control volume with additional energy losses associated with the bends. Equations 8.6, 8.7, and 8.8 show the momentum relations for each of the three control volumes:

Conservation of Momentum: $$\frac{d}{dt}\int_{V}\rho\vec{v}dV+\int\rho\vec{v}\left(\vec{v}\cdot\hat{n}\right)dS=\sum\vec{F} \qquad [8.5]$$

$$\rho A_1 L_1 \frac{dv_1}{dt} = \rho g A_1 \left(H_R - H_{base} - \frac{f_1 L_1 v_1^2}{D_1 2g} \right) \qquad [8.6]$$

$$\rho A_2 L_2 \frac{dv_2}{dt} + \rho A_2 v_2 \frac{dL_2}{dt} - \rho A_2 v_2^2 = \rho g A_2 \left(H_{base} - L_2 - K \frac{v_2^2}{2g} \right) \qquad [8.7]$$

$$\rho A_3 L_3 \frac{dv_3}{dt} = \rho g A_3 \left(H_{base} - H_w - \frac{f_3 L_3 v_3^2}{D_3 2g} \right) \qquad [8.8]$$

where H_R is the reservoir pressure head at the upstream end of the tunnel, H_{base} is the pressure head at the base of the riser, H_w is the pressure head at the riser expansion, and f is a representative friction factor. A conservation of mass equation within the riser is used to cancel the middle two terms of Eq. 8.7:

$$\frac{dL_2}{dt} = v_2 \qquad [8.9]$$

Equations 8.6 – 8.9 can be used with Equation 8.4 to solve for the five unknowns, namely v_1, v_2, v_3, L_2, and H_{base} for each time step. The friction in the main tunnel is calculated using the Jain explicit expression of the friction factor as a function of material relative roughness (ε/D) and Reynolds number as shown in Equation 8.10:

$$f = \frac{0.25}{\left[\log_{10}\left(\frac{\varepsilon}{3.7D} + \frac{5.74}{\mathrm{Re}^{0.9}}\right)\right]^2} \qquad [8.10]$$

This model assumes that all of the local losses in control volumes 1 and 3 can be represented by wall shear through a single representative roughness value in the form of a material roughness variable. The scenarios with an initial depth of 100% were used to calibrate the representative roughness in the main tunnel for control volumes 1 and 3. Control volume 1 is expected to have a much larger representative roughness than control volume 3 due to the presence of the entrance, the elbows, and the valve at the upstream end. More recent experiments performed by others at the University of Michigan suggests that the loss coefficient for the fully open valve is on the order of about 6, implying that this is the major loss in the system. The model also assumes that all of the losses in control volume 2 can be modeled with a local loss coefficient in the T-shaped

junction at the base of the riser, ignoring the friction within the riser. This coefficient applies only when $v_2 > 0$ and is also calibrated using the 100% initial depth scenarios.

Initially, the experimental conditions with 100% initial water depth are used to compare the rigid column numerical method with the experimental measurements. These trials were simpler to model than the other trials because they did not include the propagation of a pipe-filling bore. As mentioned above, they were also helpful in establishing the friction and local losses within the system. The representative ε/D roughness values for the first and third control volumes are chosen as 0.16 and 0.0001, respectively to match the 100% initial depth results. Again, the energy loss through the first control volume is greatest due to the entrance, the elbows, and the valve in that section. The local loss coefficient within the riser was influenced by the diameter of the riser and is therefore chosen as $K = 0.5/D_2$.

Using a simple forward difference for the time derivative terms, the calculation procedure can be seen for two important variables, v_1 and L_2 below in *Eqs 8.11* and *8.12*.

$$v_1^{n+1} = v_1^n + \Delta t\left[\frac{dv_1}{dt}\right]^n \qquad [8.11]$$

$$L_2^{n+1} = L_2^n + \Delta t\left[v_2^n\right] \qquad [8.12]$$

where n is a time index. The initial conditions are $v_1 = v_2 = v_3 = 0$, $L_2 = 0.001$ m, and $H_{base} = L_2 + D_1/2$ (here the pressure head is relative to the center of the main tunnel cross section). A small initial length of L_2 was chosen to prevent dividing by zero when calculating dv_2/dt.

As shown in Figure 8.11, the rigid column model explains the behavior of the experimental results by matching both the frequency and peak pressure fairly well. Since

the pressure transducer is located 0.203 m above the base of the riser, all model results have been translated accordingly. The timing of the model has also been adjusted to visually line up with the start of the pressure rises in the experiments and the numerical model, since the valve opening is manual and cannot be easily registered to the timing of the pressure transducer measurements. The matching of the frequency between the numerical and experimental results implies that the inertia included in this model is appropriate. The alternative method of only considering the inertia within the vertical shaft, while ignoring the inertia of the main tunnel, is incorrect because it would result in an oscillation frequency which is too high. The peak surge pressures match relatively well, especially in Figures 8.6a and b. For the experiments performed in Figure 8.6c, the piezo-resistive pressure transducer within the riser was noticed to have an error, a drift downward in the pressure trace. Since the transducers measure the relative change in pressure and have been calibrated independently for each trial based on the starting and ending levels in the still-well, this downward drift creates an unexpected error for this experiment. Another difference is that the numerical model does not react sharply enough to match local extrema following the initial peak, e.g. the second peak of Figure 8.6a. This discrepancy is likely caused by the simplified method for handling energy losses within the system.

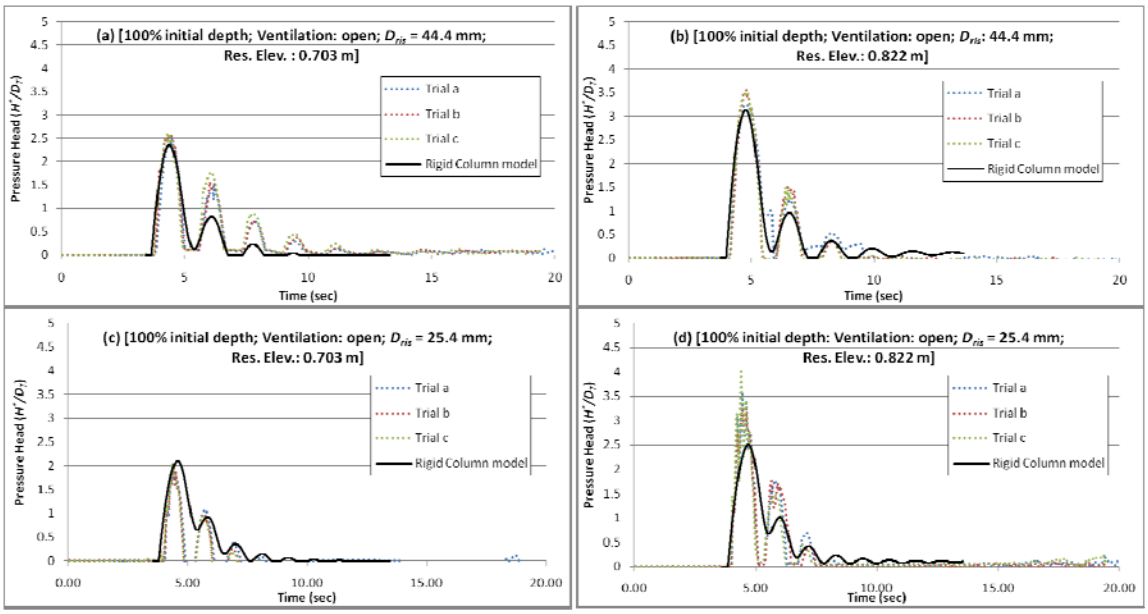

Figure 8.11 [(a), (b), (c), and (d)] Comparison of numerical and experimental results

The numerical computation for the pipe-filling bore propagation was similar to the 100% initial depth scenarios, with the exception of the initial conditions within each control volume. The system was initially at rest with an initial depth in the main tunnel of 50%, 70%, or 95% of the tunnel diameter. The numerical model begins with the valve opening at time $t = 0$. Since computing the propagation of the pipe-filling bore is required, the first part of the simulation begins by splitting the control volume which was previously labeled "1" into two parts (i.e. ahead of and behind the bore) as shown in Figure 8.4 and mathematically in Equations 8.1 and 8.2. The control volumes previously labeled 2 and 3 are ignored until the bore arrives at the riser location. Equation 8.13 gives the conservation of momentum to the left of the pipe-filling bore, where x represents distance from the upstream end to the bore location:

$$\rho A_1 x \frac{dv_1}{dt} = \rho g A_1 \left(H_R - H_{bore} - \frac{f_1 x v_1^2}{D_1 2g} \right) \qquad [8.13]$$

The numerical procedure is as follows:

1) Equation 8.1 is used to calculate the propagation speed of the pipe filling bore by conservation of mass.
2) Equation 8.2 is used to find the H_{bore} value by conservation of momentum across the pipe-filling bore front using a frame of reference moving with the bore.
3) A forward difference is used to calculate dv_1/dt at each time step using Equation 8.13. From this, the variables v_1 and x can be updated for the next time step.

After the bore reaches the base of the riser, control volumes 1 and 2 are then calculated as in the full-pipe scenario explained above. The bore location, x, still represents the distance from the upstream end, now splitting the third control volume into two parts using Equation 8.14 for momentum conservation and the numerical procedure similar to the steps above until the bore reaches the downstream end:

$$\rho A_3 (x - L_1)\frac{dv_3}{dt} = \rho g A_3 \left(H_{base} - H_w - \frac{f_3 (x - L_1) v_3^2}{D_3 2g} \right) \qquad [8.14]$$

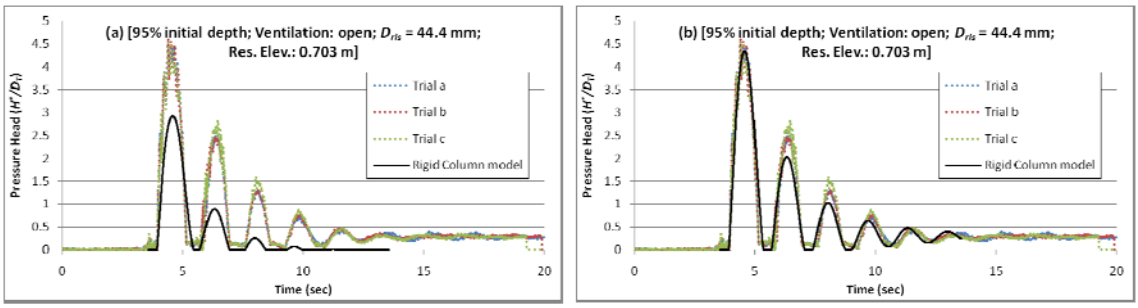

Figure 8.12 Comparison and recalibration of the numerical model. (a) Results using the roughness values from the 100% initial depth calibration. (b) Recalibrated to match the experimental results of the trial shown (95% initial depth, D_{ris} = 44.4 mm, Res. Elev. = 0.703 m)

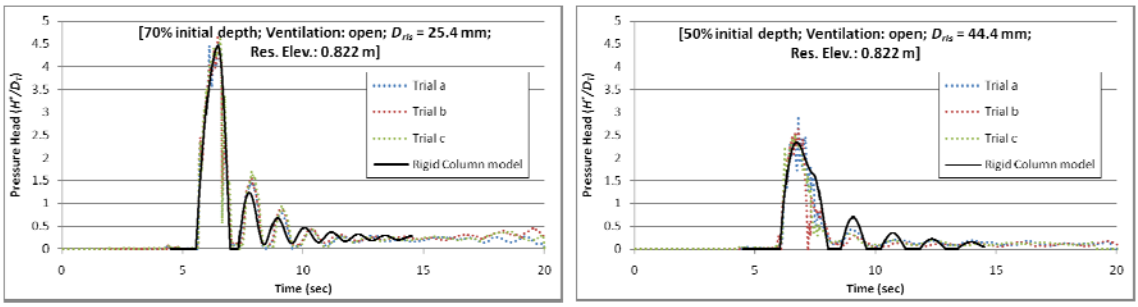

Figure 8.13 Comparing the recalibrated model with other experimental results.

The numerical model can be compared with the experimental results, as in Figures 8.12 and 8.13. Figure 8.12a shows that the roughness values which were previously calibrated using the 100% initial depth scenarios are too large. The peak pressure and the final equilibrium pressure are under-predicted in the model. This implies that the losses in the 100% initial depth trials are greater than those of the other initial water depths. The relative roughness parameter is likely an oversimplified representation of the energy losses during these transient flow conditions. The relative roughness parameters for control volumes 1 and 2 were recalibrated using a single trial of 95% initial depth, a riser diameter of 44.4 mm, open ventilation, and a reservoir elevation of 0.703 m as shown in Table 8.2 below. The recalibrated model is compared with other experimental results as shown in Figure 8.13. The peak pressure head and the frequency match between the model and experimental results.

Table 8.2 – Calibrated relative roughness parameters

	Calibrated using the 100% initial depth trials	**Recalibrated parameters using the single trial described in Fig. 8.12**
ε_1/D_1	0.16	0.06
K (entrance loss at base of riser)	$0.5/D_2$	$0.2/D_2$
ε_3/D_3	0.0001	0.0001

In general, a rigid column numerical framework such as this is appropriate in understanding the inertial oscillations within a vertical riser caused by a propagating pipe-filling bore. The frequency of oscillation is captured well by including the inertia of the entire system as opposed to just the inertia within the riser. Matching the peak pressure value is more of a challenge, however. Knowledge of the energy losses in these transient flow situations is needed, since they have an important effect.

8.5 Conclusions

Some general conclusions can be made concerning the behavior of surges within systems containing vertical shafts.

- As the bore front propagates through the system, a noticeable amount of air becomes entrained within the flow. However, the magnitude of the surge does not appear to be influenced by the presence of air entrained within the flow. This implies that numerical models which consider the air and water as distinct phases should be able to predict the surge magnitudes.
- The maximum peak pressures are influenced by the main system properties rather than the riser characteristics. In other words, the main controlling factors are the nature of the flow regime transition, related in these experiments to reservoir elevation and initial depth in the experiments studied.
- As the reservoir elevation increases, the pipe-filling bore is stronger and the maximum peak pressure within the riser increases.

- A higher initial depth within the main tunnel results in a higher peak pressure in the vertical shaft after the pipe-filling bore arrives. This is apparently caused by a higher pressure behind the bore front.
- Peak pressures in the riser did not vary in any significant fashion with riser diameter or degree of ventilation, which is to be expected since the behavior is determined by the fluid inertia moving through the main tunnel.
- The relative roughness behaves differently between the 100% initial depth trials and the trials of other initial depths. It is necessary to understand the energy losses occurring for transient flow conditions, which were appropriately represented by a single relative roughness parameter in the numerical model presented.

Chapter 3 mentioned a video taken during the course of work by Vasconcelos and Wright (2005) showing a geyser event of what appears to be the same strength for both the nose and tail of an air pocket. Even though water jetting appears to be about the same for both arrivals in the video, this should not be taken to imply that the two effects would always be equal. The mechanisms for lifting water are different for these two situations, as demonstrated by the results in this and previous chapters. For the nose arrival of the air pocket, the air displaces water by the processes discussed in Chapters 6 and 7. Given the discussion of the surge process in Chapter 7 and the current chapter, the rise of water in the shaft after the expulsion of air is essentially an inertial surge process. In the particular experiment that was recorded in the video, the high rise in the surge chamber at

the downstream end of the pipeline created a large pressure that subsequently caused a large inertial surge at the shaft as the air was expelled.

The results of this chapter, especially the comparison between the numerical model and the experimental measurements, reveal that the behavior of the main tunnel is important when studying the behavior in the vertical shaft. If the details of the system geometry are known, one could assess the extent to which surge is an important process. Even though inertial surge is an important physical process during rapid filling, it is possible that it may have been insignificant during the formation of the Minneapolis geyser events. A number of arguments presented throughout this dissertation indicate that the geysers depicted in Figure 2.1 are associated with the entry of air into the vertical shaft as is depicted in Figure 2.6 and mechanisms discussed in Chapters 6 and 7. Relating the experimental results of this chapter to the Minneapolis geyser example discussed in Chapter 2, the arrival of a pipe-filling bore is not sufficient to lift water to the ground surface in that system. The lack of strong pressure oscillations in Figure 2.4 implies that this does not have an effect in forming the Minneapolis geyser. There is also no indication of significant bore propagation from the pressure data in Figure 2.4, suggesting that the source of air is not from filling, but likely caused by the specific geometry of this tunnel system.

Chapter 9

Geyser Reduction

9.1 Objective

The previous chapters have discussed the physical mechanisms of air / water behavior which can lead to geyser events in CSO storage tunnels. Usually, a major purpose of vertical shafts is to eliminate air from the system, promoting as fast of an escape as possible. However, results from previous chapters show that the release of air can lead to the possibility for geysers. The objective of this section is to investigate methods of allowing air escape while also disrupting problematic air/water interactions in order to reduce the strength of potential geyser events. The hypothesis is that geometric adjustments to the vertical shaft can reduce the vertical momentum of the air / water mixture, thus mitigating the geyser strength. The first method is the addition of two 90° bends within the vertical shaft to create a near-horizontal section with the intent of separating the air phase from the liquid. The second strategy is a diameter expansion within the vertical shaft. This method is expected to require fewer resources to construct than the first method due to the smaller land-area footprint. For this reason as well as preliminary success of the diameter expansion, the second method is studied more thoroughly. The vertical location of the diameter expansion as well as the expansion ratio of shaft diameters was explored with respect to reducing the negative effects of air-

release. Since the laboratory geysers discussed in previous chapters cannot exactly replicate a real geyser event, an absolute statement about the effectiveness of possible mitigation strategies cannot be certain.

9.2 Introduction

The observations of the previous sections have revealed the physical mechanisms of air-release which could lead to geyser events within a CSO storage tunnel. The severe negative consequences of these events motivate the investigation of possible ways to mitigate geyser formation. One impression is that sufficient ventilation to completely eliminate the interactions between air pockets and water in vertical shafts is probably not feasible. The work by Zhou, et al. (2002) concluded that lack of adequate ventilation at the end of the system studied led to large pressure rises. The solution to this situation is straightforward; just add sufficient ventilation at the downstream end. However, if problems arise due to entrapped air pockets, the ventilation apparently needs to be added close to the location of air entrapment. The variable location where this occurs makes this practically impossible to accomplish so some method for mitigating geyser formation must be sought. Although increased ventilation may be beneficial in reducing the total volume of trapped air, the dilemma is that tunnel filling is largely beyond the control of the designer and can be highly variable due to spatial and temporal variations in actual rainfall events. Consequently, solutions that allow air pockets to be ventilated without lifting liquid beyond the ground surface are desired. This chapter describes two approaches that were investigated and the observations from the experimentation.

The specific issue is the release of pockets of trapped air from the tunnel through a riser that is in a surcharged state, such that the bubble must pass through water that stands in the riser shaft. Adjustments which disrupt the interaction of an upward accelerating air slug and a thin film of downward water flow around the perimeter seem advantageous. The first approach modified the vertical riser by placing a near-horizontal segment a short distance above the pipeline connection. The schematic is shown in Figure 9.1 and a description of the details is provided in the Experimental Setup section below. The concept behind this approach was that a vertically stratified flow would develop with the air flowing along the top of the horizontal segment and water flowing in the opposite direction along the bottom. This design could potentially boost the air flow rate out of the system and reduce the amount of water lifted vertically through the riser. An additional consideration is that since most storage tunnels are constructed well below grade, there are constructability issues with such a configuration. Also if the shaft is used for access, this is not likely a convenient configuration.

A second mitigation approach involved a riser consisting of a small diameter segment near the bottom expanding to a larger diameter shaft a short distance above the pipe connection. In other words, the diameter at the ground level is larger than the diameter at the connection to the main tunnel. Figure 9.2 shows a schematic of this approach and the Experimental Setup section describes the tested variations of this strategy. The results of Chapters 6 and 7 show that small diameter shafts provide a problem in the vertical acceleration of large air pockets as they rise. This design was chosen based on a couple of potential advantages: the diameter expansion within the shaft could disrupt the jet of air/water mixture as the flow expands to the larger cross-section

and the material costs of the shaft in comparison to a constant large diameter would be less. However, the latter reason is likely outweighed by costs of constructing the shaft with two different sizes. Physically, the expansion in the vertical shaft will produce two positive benefits. First, the upward momentum of the air and water slug mixture will be somewhat dissipated because the increased cross-sectional area will essentially slow down the velocity. Using conservation of mass at the expansion, the velocity of the mixture through the larger diameter section will be lower than the velocity through the smaller diameter section. In terms of momentum, the radial movement of the air at the diameter expansion will reduce the upward velocity. The second positive benefit is that the expanded section will allow extra capacity for the potential spillage volume. More water can exist within the film flow instead of being pushed above the air pocket because the expanded diameter has a larger perimeter. The experiments will investigate the benefits of the expansion by varying both its vertical location and ratio of shaft diameters.

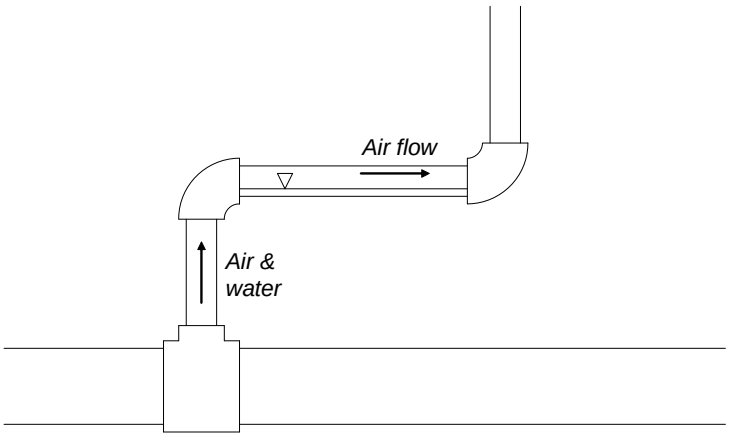

Figure 9.1 Mitigation of geysers by addition of a horizontal section to vertical riser.

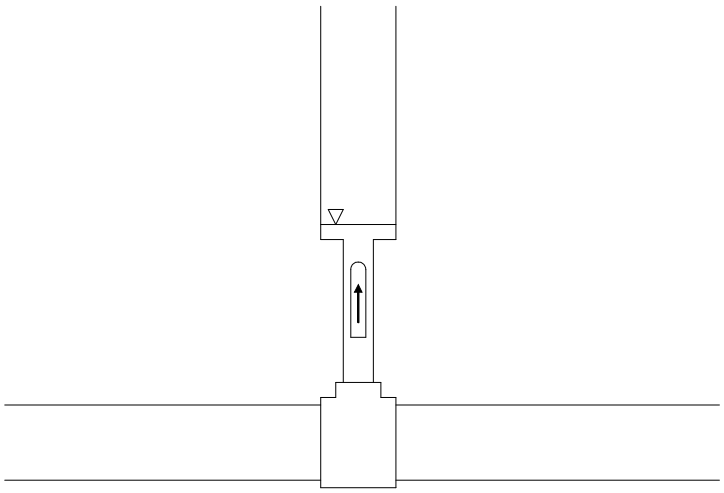

Figure 9.2 Mitigation of geysers by addition of a larger diameter section to vertical riser.

9.3 Experimental setup

The three setups used for the experiments in this section were similar to the setups described in previous sections. The only difference between the setups of the previous sections and those studied here was the adjustment to the vertical riser. In each setup, the main tunnel consisted of 0.095 m diameter (I.D.) clear acrylic pipe. Taking advantage of the clear acrylic pipe walls, the general behavior of the air and water was readily observed and recorded with a digital video camera at 30 frames per second.

The first experimental setup testing geyser mitigation was the same setup as that described in Chapter 4 for the bore collisions. The horizontal main tunnel was 14.14 m in length and capped at the downstream end. The upstream end allowed for a sudden introduction of inflow through a vertical inlet pipe using the directional valve. A sudden second inflow was introduced shortly after the first inflow to create a bore collision near the base of the vertical riser as discussed in Chapter 4. Both mitigation strategies were studied with this setup. First, two 90° elbows were installed to create a near-horizontal

section within the vertical shaft. The first bend was approximately 0.3 m above the crown of the main tunnel to connect the first vertical section with the near-horizontal section. The horizontal section was approximately 0.6 m long and the other 90° elbow was connected to a 0.6 m long vertical section. The diameter of the shaft was 0.044 m and constant through each section. The diameter expansion was then installed using the same general setup. The expansion occurred at a vertical location of 0.3 m. The expanded section was 0.133 m diameter and approximately 1.5 m long. The shaft diameter below the expansion was again 0.044 m. For both the bend and expansion experiments, the same filling scenario was used. The initial depth of water within the main tunnel prior to the introduction of the bore-forming flow was 7% of the tunnel diameter. The first inflow rate of water was 1.23 L/s and then the inflow rate was increased to 2.85 L/s. Three repetitions were performed for each experimental scenario. A comparison is made in the results section between each of the mitigation strategies and the 0.044 m diameter straight-vertical riser condition.

The second setup was the same as the continuous air injection setup discussed in Chapter 5. A large constant-head reservoir was located at the upstream end and a 0.10 m butterfly valve at the downstream end. For the tests discussed in this study, the downstream valve was fully closed in order to emphasize the effects of air release. An air injection hose was connected to the invert of the main pipe at a distance of 2.5 m from the upstream end. Adjustments to the air inflow rate were used to vary geyser strengths. Two specific air flow rates were chosen for measurement: 0.136 L/s and 0.87 L/s. The 0.044 m diameter vertical riser was located 4.4 m downstream of the air injection point. A schematic of the diameter expansion is shown in Figure 9.3. Expansion ratios (D_2/D_1)

were varied among values of 1.00, 1.29, 2.14, ad 3.00. Two values for the vertical location of the expansion (Z) were used: 0.40 m and 1.01 m from the tunnel invert. Peak geyser strengths were observed using video recordings 3-5 minutes in length for each test.

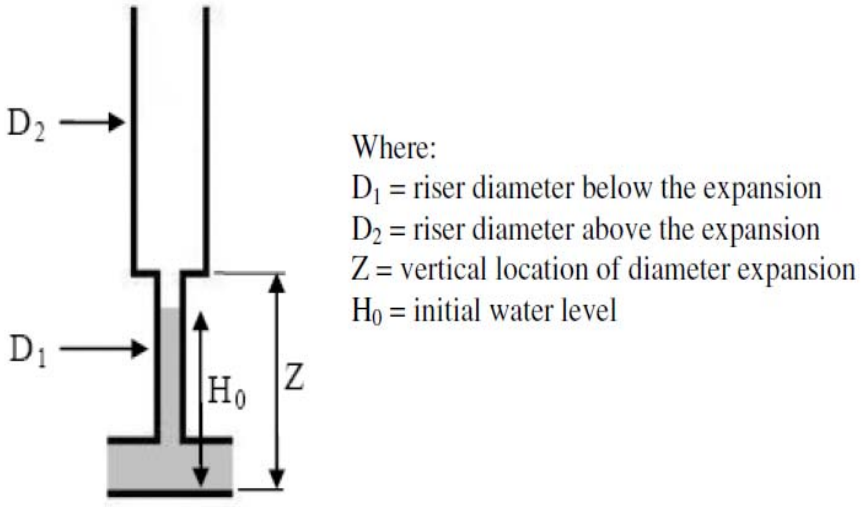

Figure 9.3 Schematic of riser diameter expansion and variable descriptions

Another set of experiments was performed using the continuous air injection setup to test the diameter expansion among larger diameters. The lower vertical shaft diameter (D_1) for these experiments was 0.095 m and the expansion occurred at a vertical location of 0.095 m above the crown of the main tunnel ($Z = 2*D_1$). The expanded diameter was also fixed for these experiments at a size of 0.19 m (I.D.). Two variables were adjusted for these tests: namely the air injection rate and the initial water level. Table 9.1 shows the combinations of four water levels and two air flow rates tested. The lowest water level corresponds to a slightly surcharged main tunnel. The second surcharge level is halfway between the main tunnel and the location of the riser

expansion. The third level is just slightly above the expansion location and the fourth level is one tunnel diameter above the expansion.

Lastly, the diameter expansion was constructed within the air capsule experimental setup which is also discussed in Chapter 5. Using the schematic of Figure 9.3 as a reference, the vertical location (Z) was constant at 0.41 m. Both diameters were constant, with D_1 = 0.044 m and D_2 = 0.095 m. Two water levels were tested, namely 0.203 and 0.457 m above the main tunnel invert. Three air volumes were released from within the capsule: 1.59, 3.14, and 5.97 L. A comparison was made between the expansion strategy and the constant diameter vertical shaft results for the 0.044 m and 0.095 m diameters.

Table 9.1 Conditions tested for the expansion strategy

Label	Air Injection Rate (L/min)	Equilibrium water level [EWL] (m)
1A	8	0.104
1B	25	0.104
2A	8	0.143
2B	25	0.143
3A	8	0.199
3B	25	0.199
4A	8	0.286
4B	25	0.286

9.4 Results

The preliminary investigation of the mitigation strategies within the bore collision experimental setup revealed positive results. As mentioned in Chapter 4, the release of sequential air pockets each pushed the water within the riser higher until it projected out of the top of the 2.5 m tall constant diameter riser (0.044 m). The bend configuration reduced the height of the geyser in the riser, but vertical interactions leading to the geyser phenomenon still developed. As the initial rise of the air/water mixture reached the first bend, the water settled to the bottom of the horizontal section to promote a safe air release. However, the riser diameter was not sufficient to prevent water from occupying the entire length of the horizontal segment of the pipe while the air was being released; this water surcharged into the higher vertical section. Therefore, the free escape of air along the top of the horizontal section was prevented and continued air release formed geysering in the final section of the riser. This process might only be associated with the release of multiple air pockets where a single large air pocket may be able to escape past the water spreading in the horizontal section. The process also depends on whether the volume of water above the air pocket is greater than would occupy roughly the bottom half of the horizontal section. The configuration was altered so that the horizontal segment was sloped slightly upwards and this was noticeably more successful in venting air, but residual problems existed. In particular, the geysering phenomenon took slightly more time to develop in the final vertical section compared with the previous configuration. Although the bend mitigation approach reduced the initial rise of the air/water mixture, a geyser event was eventually observed out of the top of the riser. The total vertical height was only 0.9 m for the bend configuration setup since some of the

riser length was used for the horizontal section: 0.3 and 0.6 m before and after the horizontal section, respectively. Further optimization of the lengths and diameters of each section could potentially lead to better results, but overall this strategy was not very successful in preventing a geyser event. The diameter expansion strategy was very successful in reducing the strength of the geyser. Only small water level fluctuations within the large diameter segment of the riser were observed as several air pockets were expelled. Violent accelerations were still witnessed through the small diameter pipe, but were mostly dissipated at the expansion.

The diameter expansion measurements within the continuous air injection setup also revealed some positive results. Table 9.2 shows the results in comparison to the control condition of a constant diameter, labeled as an expansion ratio of 1.00. For the control case, an air inflow rate of 0.136 L/s produced geyser strengths of 0.78 m, or 4.9*D* (where *D* = horizontal tunnel diameter) beyond the static water level, and the air inflow rate of 0.87 L/s produced geyser strengths of 1.52 m, or 12.7*D* beyond the static water level. Larger expansion ratios are compared with these two measurements to evaluate their success in mitigating the geyser strength. The expansion ratio of 1.29 at a vertical location of 0.40 m above the tunnel invert successfully reduced the geyser strength from 0.78 m to 0.58 m. Expansion ratios of 2.14 and 3.00 further reduced the geyser strengths to 0.45 m and 0.44 m respectively, just a short distance beyond the expansion location. For the higher air inflow rate of 0.87 L/s, the expansion ratios of 1.29, 2.14, and 3.00 successfully reduced the geyser strength from 1.52 to 1.01, 0.71, and 0.61 m respectively. Next, each diameter expansion was installed at a vertical location of 1.01 m above the tunnel invert. Since the lower air inflow rate did not create geyser strengths which

reached this vertical location of the expansion, only the higher air inflow rate was used. The expansion ratios of 1.29, 2.14, and 3.00 all resulted in the same geyser strength as the control test. As an important note, for the two larger expansion ratios the geyser rise was observed as only a spray reaching the measured height as opposed to a horizontal water level. There seems to be a vertical location within the shaft where the air/water mixture reaches a peak velocity, and the peak velocity was reached prior to the location of the expansion. A simple energy balance of $H_{rise} = v^2/2g$ (where H_{rise} = the 0.51 m geyser height beyond the expansion, v = velocity of water at the expansion, and g = gravitational acceleration) suggests that the water velocity at the 1.01 m vertical location is roughly 3.2 m/s for these conditions. Velocity measurements can be extracted from frames of the video recordings with an error of about +/- 0.4 m/s. The maximum upward velocity observed was 3.0 m/s, confirming the magnitude of the energy balance calculation. Overall, geyser strengths were reduced for the vertical location of 0.40 m but not for the vertical location of 1.01 m. Placing an expansion above the location of peak velocity will apparently do very little to solve geyser problems. In other words, constructing a diameter expansion just below the ground surface will not significantly reduce the geyser strength. The vertical placement of the diameter expansion should be relatively low, prior to the air bubble having a sufficient chance to reach a peak upward velocity, thus reducing the geyser strength.

Table 9.2 Expansion Measurements

D_1 (cm)	D_2 (cm)	Expansion Ratio	Z (cm)	Air Injection (L/s)	Water Flow	H_0 (cm)	Peak Geyser Height (cm)
4.45	4.45	1.00	40.3	0.136	0	31.4	78
4.45	5.72	1.29	40.3	0.136	0	31.4	58
4.45	9.53	2.14	40.3	0.136	0	31.4	45
4.45	13.34	3.00	40.3	0.136	0	31.4	44
4.45	4.45	1.00	40.3	0.87	0	31.4	152
4.45	5.72	1.29	40.3	0.87	0	31.4	101
4.45	9.53	2.14	40.3	0.87	0	31.4	71
4.45	13.34	3.00	40.3	0.87	0	31.4	61
4.45	4.45	1.00	101.3	0.87	0	31.4	152
4.45	5.72	1.29	101.3	0.87	0	31.4	152
4.45	9.53	2.14	101.3	0.87	0	31.4	152
4.45	13.34	3.00	101.3	0.87	0	31.4	152

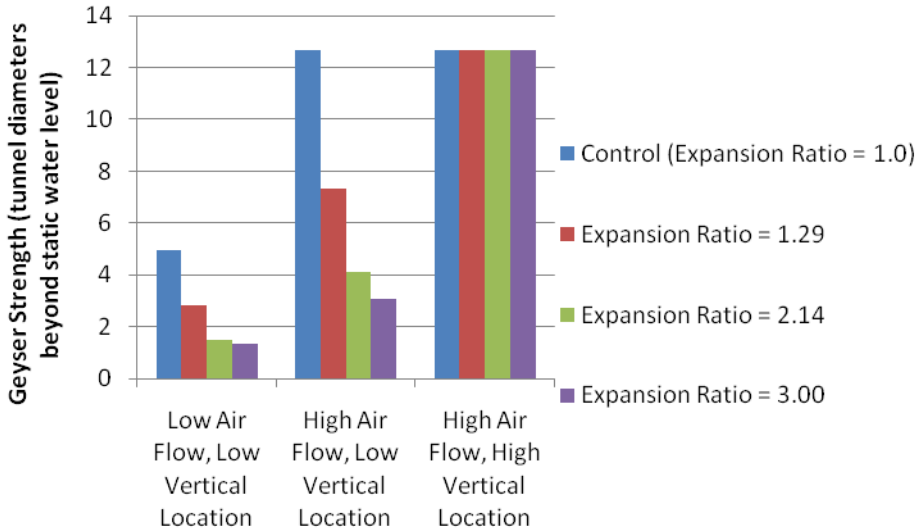

Figure 9.4 Geyser strengths for diameter expansion experiments.

The results for the diameter expansion experiments using larger diameters (D_2) with a low vertical location are shown in Table 9.3. It is possible that the behavior of this

setup is qualitatively different from the experiments discussed in the previous paragraphs since the diameters were larger for these experiments and the expansion occurred much nearer to the main tunnel. The larger diameters also allowed for the level of the inertial surge height to be clearly measurable apart from the maximum splash level. Figure 9.5 shows the maximum splash and inertial surge levels for the expansion scenario compared with the constant diameter scenario. For all of the scenarios, the diameter expansion reduced the maximum splash level. Table 9.4 shows the percent reduction in maximum splash and inertial surge heights due to the diameter expansion. The maximum reduction in the "splash" height, during experiment 4A, was 37 % and the average splash reduction for all experiments was 17%. The maximum reduction in the inertial surge height was 49% during experiment 4B and the average inertial surge reduction for all experiments was 22%. One could interpret the relative influence of both inertial surge level and splash level among the various experiments by comparing the results in the third and fourth columns of Table 9.3 to the relative changes in the second column (EWL). For example, the static equilibrium level change between the 3 and 4 series of experiments is 0.09 m while the change in maximum inertial surge heights are less than this change, but the maximum splash height increases are greater than the equilibrium level change. Conversely, the static level change between the 1 and 2 series of experiments is only 0.04 m while the increase in splash height between the two is roughly 0.12 m and in free surface height is 0.05 to 0.08 m. These counteracting trends between the two series are presumed to be related to free surface dynamics as discussed in more detail below. The water level drop which initiates the inertial surge in the series 1 experiments is low since

the equilibrium level is close to the tunnel crown and the resulting inertial surge height is influenced by this.

Table 9.3 Results of diameter expansion experiments

Label	Equilibrium water level [EWL] (m)	Max inertial surge height (m)	Max splash height (m)	Max inertial surge height, divided by EWL	Max splash level, divided by EWL
1A	0.104	0.18	0.21	1.7	2.0
1B	0.104	0.19	0.28	1.8	2.7
2A	0.143	0.23	0.33	1.6	2.3
2B	0.143	0.27	0.41	1.9	2.8
3A	0.198	0.29	0.42	1.4	2.1
3B	0.198	0.30	0.50	1.5	2.5
4A	0.287	0.34	0.52	1.2	1.8
4B	0.287	0.37	> 0.61	1.3	> 2.1

Figure 9.6 shows a large air pocket spreading in all directions as it enters the larger diameter of the riser expansion. This volumetric expansion in the radial direction limits the continued increase of upward momentum of the rising air, thus decreasing the strength of the geyser event. This transition also serves to allow water to flow around the rising air pocket more easily than for a constant diameter riser. The figure shows what appears to be an expanding bubble but the system pressures are so low that compressibility effects are negligible and the air is simply being fed from the air remaining in the horizontal pipeline.

Table 9.4 Geyser strength reduction caused by diameter expansion

Label	% Reduction in splash (beyond EWL)	% Reduction in free surface (beyond EWL)
1A	4	0
1B	7	30
2A	18	-15
2B	16	9
3A	28	19
3B	11	45
4A	37	42
4B	20	49
Average	**17**	**22**

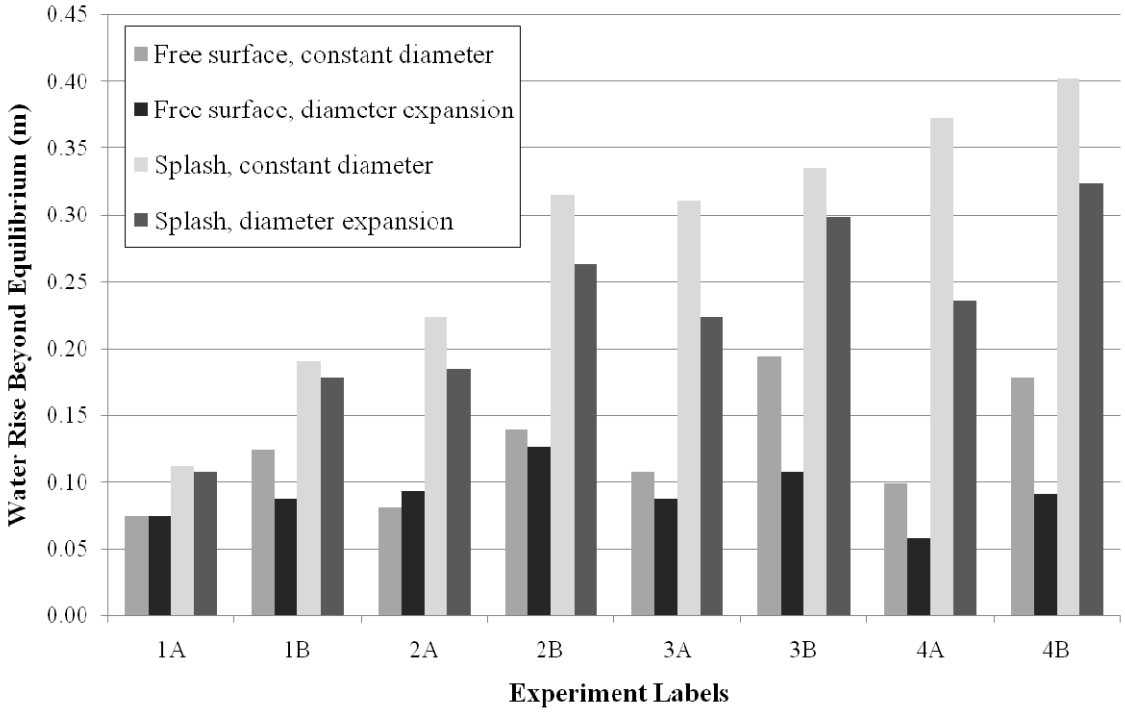

Figure 9.5 Geyser strengths relative to the initial water level

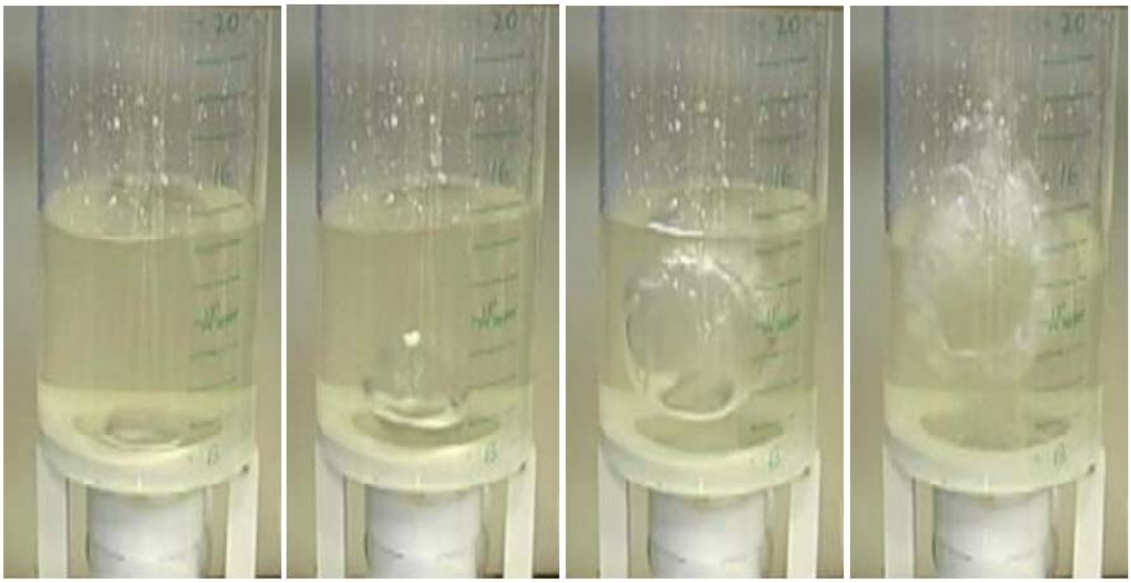

(a) 0.0 sec *(b)* 0.1 sec *(c)* 0.2 sec *(d)* 0.3 sec

Figure 9.6 Images of air pocket expansion within vertical riser

The reduction in geyser strength due to the diameter expansion is also seen in the air capsule experimental results. Figures 9.7 through 9.9 show the geyser strengths, according to different processes within the geyser event. Figure 9.7 shows the initial rise height of the air pocket's nose as discussed in Chapter 6. Figure 9.8 shows the measurements of the subsequent maximum inertial surge levels after the initial air pocket broke through. Figure 9.9 shows the maximum splash level measured during the experiment. The diameter expansion reduces the maximum rises of all experimental scenarios relative to the constant 0.044 m diameter condition. This suggests an importance of avoiding a small diameter, and this is consistent with the conclusions of Chapter 6. Comparing those results with Figure 9.7 below shows again that the worst case scenarios are associated with air volumes much larger than the liquid surcharge volume; these are capable of driving strong upward accelerations. Furthermore, the results in the figure confirm that this mechanism of upward acceleration was disrupted by

a diameter expansion at a sufficiently low vertical location. However, in general the 0.095 m diameter scenarios behave very similar to those of the diameter expansion scenarios.

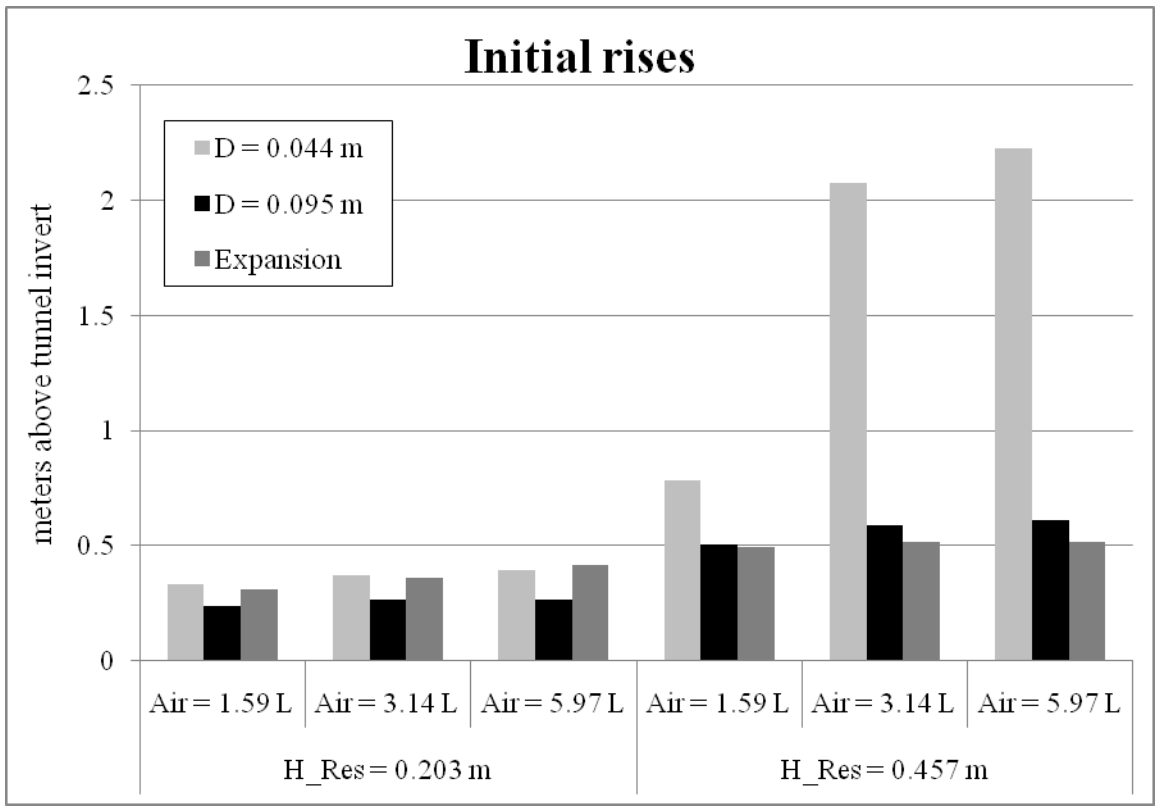

Figure 9.7 Levels measured for initial rise of an air bubble (as discussed in Chapter 6)

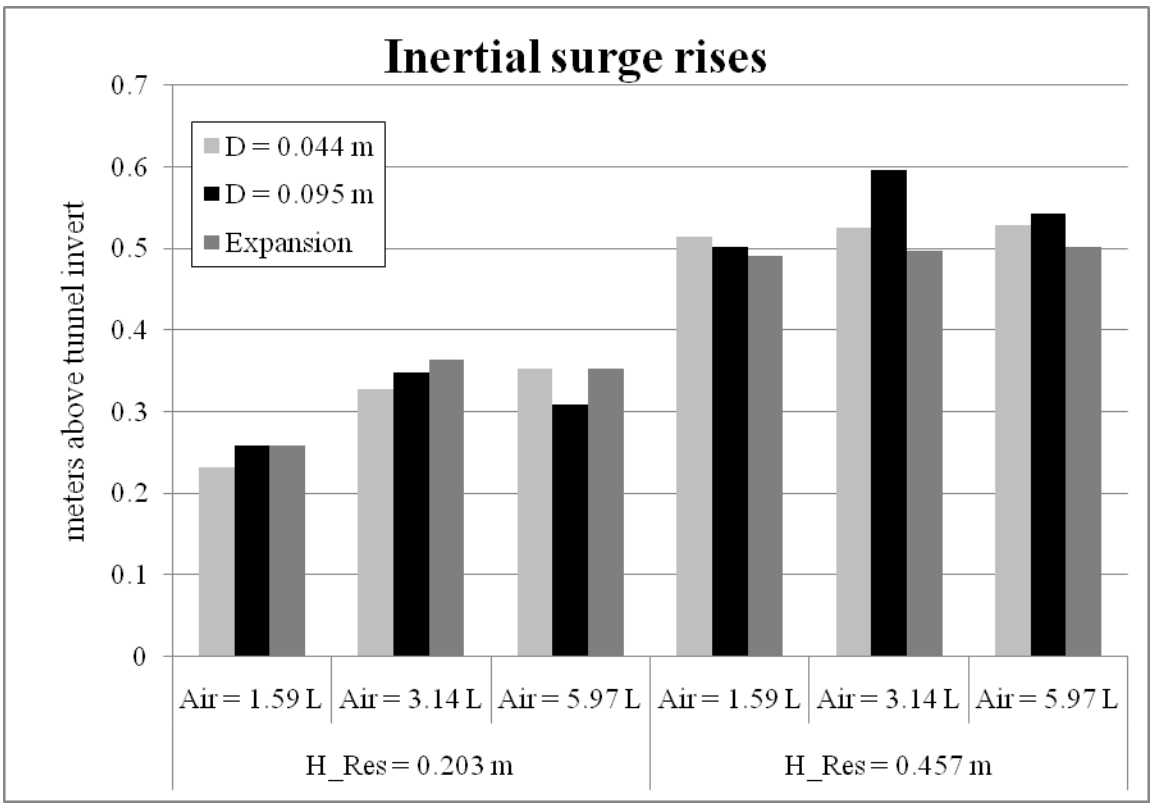

Figure 9.8 Measurements of highest inertial surge levels

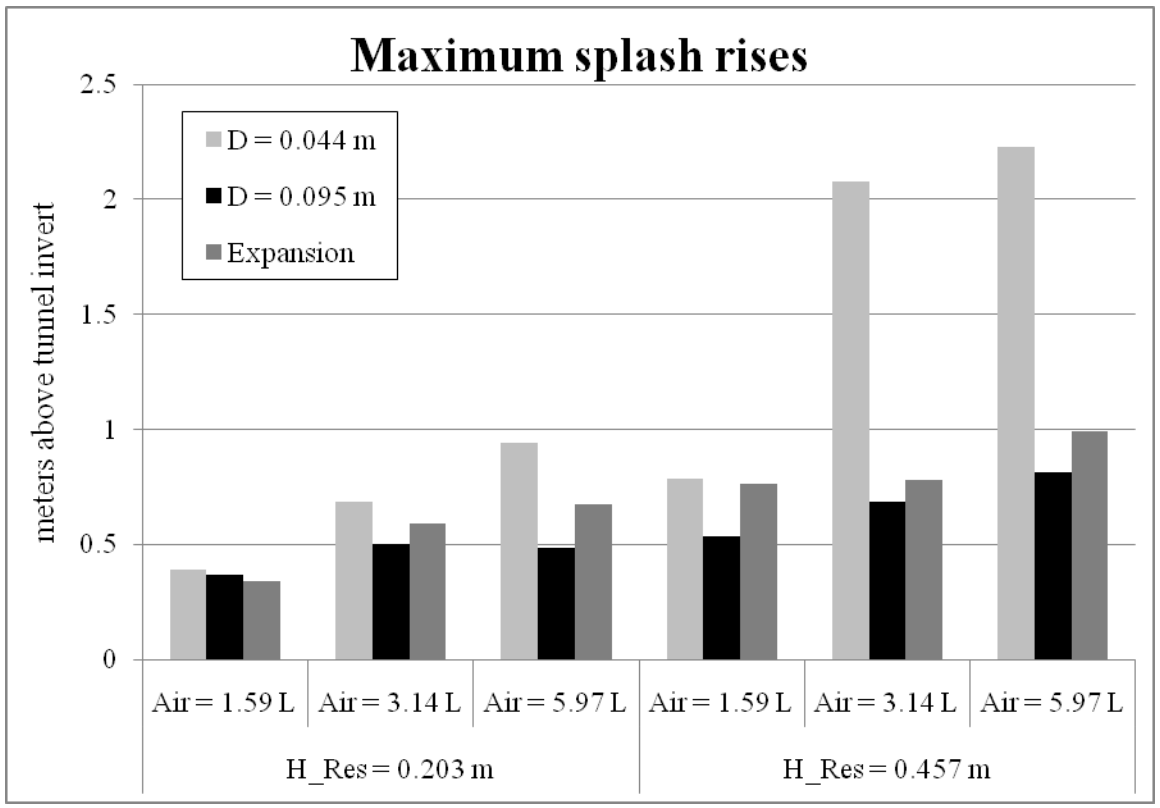

Figure 9.9 Overall maximum splash levels during each experiment

9.5 Numerical Analysis of Inertial Surge through Expansion

Review of the video records for both sets of experimental conditions clearly indicated a longer period (on the order of 10 s) oscillatory response of the water level in the riser although it was punctuated with releases of discrete air pockets through the riser. As discussed in Chapter 6, the oscillations are initiated with the escape of large diameter air pockets through the riser, and therefore could only be predicted with a model framework that considers release of air pockets through vertical shafts. A simplified numerical model that considers the inertia of the liquid in the system was implemented to compare with the observed surges. Three control volumes can be drawn (as shown in Figure 9.10) around the liquid in the main tunnel and in each section of the riser. The

length of the third control volume changes as the water level within the riser changes. Conservation of mass equations can be formulated based on these control volumes to obtain Equations 9.1 through 9.3:

$$\rho v_1 A_1 = \rho v_2 A_2 = \rho v_3 A_3 \qquad [9.1]$$

$$\frac{d}{dt}(\rho A_3 L_3) - \rho v_3 A_3 = 0 \quad \Rightarrow \quad \frac{dL_3}{dt} = v_3 \qquad [9.2]$$

where ρ = constant density of water, v = fluid velocity, and A = cross-sectional area of the control volume perpendicular to the velocity. With the experimental geometry, the velocities are related as:

$$v_1 = v_2 = 4v_3 \qquad [9.3]$$

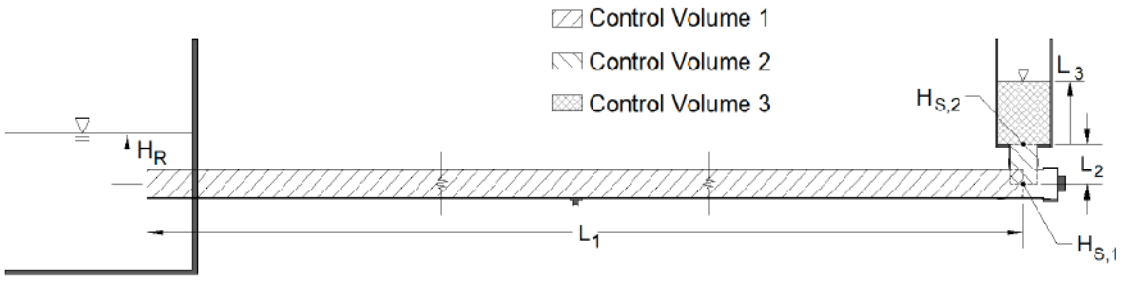

Figure 9.10 Schematic of rigid column implementation.

Equations 9.4 through 9.6 present the momentum equations for each of the control volumes:

$$\rho A_1 L_1 \frac{dv_1}{dt} = \rho A_1 g (H_R - H_{S,1}) \qquad [9.4]$$

$$\rho A_2 L_2 \frac{dv_2}{dt} = \rho A_2 g (H_{S,1} - H_{S,2} - L_2) \qquad [9.5]$$

$$\rho A_3 L_3 \frac{dv_3}{dt} + \rho A_3 v_3 \frac{dL_3}{dt} - \rho A_3 v_3^2 = \rho A_3 g (H_{S,2} - L_3) \qquad [9.6]$$

where H_R = reservoir pressure head at the upstream end of the tunnel, $H_{S,1}$ = pressure head at the base of the shaft, and $H_{S,2}$ = pressure head at the riser expansion. Matching the pressures between the control volumes allows for the reduction of the three momentum equations to Equation 9.7;

$$\frac{dv_1}{dt} = \frac{g}{L_1 + L_2 + \frac{L_3}{4}}\left(H_R - L_3 - L_2\right) \qquad [9.7]$$

It is noted that friction and local losses (due to the riser entrance and the expansion, for example) could be included in the above formulation; these would be relatively minor in terms of their effect with the resulting effect that the surge will be slightly over-predicted with Equation 9.7. An increase in the period of oscillation caused by losses is also expected based on simple U-tube oscillation models. However, a larger issue is that the representation of the mass within the control volume is assumed to be completely water, and the proportion of air is not accounted for here.

A specific example is used to compare the numerical model with experimental measurements. The best observation of surge oscillation was during Experiment 4A because the water level stayed within the viewable range for the longest time without air interruptions. Twice during this experiment the water level dropped to a value of 0.22 m above the tunnel invert while the reservoir level was 0.286 m. Using initial conditions for this water level (L_3 = 0.027) and $v_{1,\ 2,\ and\ 3}$ = 0, the rigid column approach was implemented and the results are shown in Figure 9.11. The observed water levels and associated times from the video are also shown in Figure 9.11.

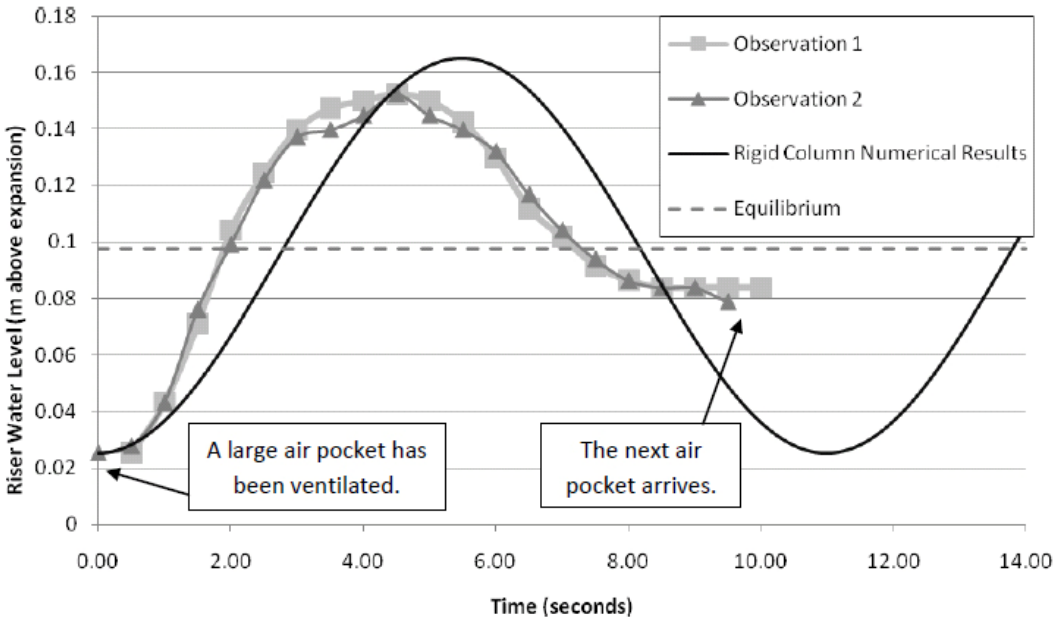

Figure 9.11 Comparison of predicted and observed riser water level elevations.

Although the numerical model does fairly well to predict the behavior of the surge oscillations within the riser, there are some discrepancies within the numerical framework. First, energy losses are neglected which would explain the slightly higher predicted peak surge level. Second, the fundamental period of the surge is slightly over-predicted by the rigid column approach. There are several possible explanations for this discrepancy. One is that the numerical model assumes that the pipe is completely full of water. In reality there is a significant amount of air at the crown of the pipe and this reduction in liquid mass would decrease the fundamental period of the oscillations. The inclusion of energy losses would also slightly adjust the period of oscillation. Another possible explanation is that the numerical model assumes that the velocities everywhere in the system are initially at rest. The continuous movement of the air pockets toward the riser somewhat reduces the validity of this assumption and could explain how the liquid

in the system is able to arrive at the vertical shaft sooner than the numerical model predicts. In general, though, there is sufficient evidence to conclude that inertial surge due to air escape is the physical process responsible for the water level variations in the riser.

9.6 Conclusions

Overall, the geyser mitigation concept of a diameter expansion within the vertical shaft shows considerable potential under certain conditions. Although the optimization of the design concept is incomplete, some general conclusions from the physical investigation can be made.

- The geometric bend strategy was partially effective in relieving the initial bursts of the geyser event. However, the water level eventually reached the higher vertical section of the riser and still resulted in a geyser event.
- The diameter expansion within the riser effectively reduced the increase of upward velocity of the air pocket by causing a radial expansion.
- When compared to a constant diameter riser, equal to the lower diameter, the maximum geyser strength through a diameter expansion ratio of 2 was reduced by an average of 17% in terms of the splash level and 22% in terms of the inertial surge.
- The diameter expansion performed similar to a constant diameter riser equal to the size of the expanded diameter, considering both inertial surge and splash effects.

- The observed velocity of the air rise during one of the strongest geyser events was measured to be 3.0 m/s +/- 0.4 m/s. A rough energy balance shows that the velocity required to lift water beyond the expansion the same distance as the measured splash height is roughly 3.2 m/s; matching the velocity observations.
- A peak velocity is reached as the air rises up through the vertical riser. If the expansion occurs at too high a vertical elevation, it has limited impact on reducing the geyser strength since the upward air rise has already reached a peak velocity. In other words, a diameter expansion just below the ground surface will do very little to solve geyser problems.
- A rigid column model similar to that developed in Chapter 8 can be used to represent the surge oscillations within the vertical shaft between air pocket arrivals by considering the water in the main tunnel as well as any water in the vertical shaft. For the setup demonstrated here, the vertical riser was broken up into two control volumes, above and below the diameter expansion. The numerical results match the peak value and frequency reasonably well. This framework was tested over a very short period, though, since the time gap between air pocket releases was small.
- When scaling the air velocities up to large systems, the shear between the air and water is likely to create flooding instabilities at the interface. This important phenomenon results in an air and water mixture that would probably rise higher than the laboratory observations indicate. Without studying flooding instability, there is no way to make a definitive conclusion regarding the effectiveness of the diameter expansion for reducing the kind of geyser that is described in Chapter 2.

In practice, a mitigation strategy consisting of a diameter expansion seems more effective and feasible than the construction of a horizontal section within the vertical shaft. The diameter expansion is more effective when it is placed at a relatively low location within the vertical shaft to prevent the air from achieving a large upward velocity. Figures 9.7 and 9.8 suggest that the jetting behavior of the Minneapolis geyser events during the air release may be significantly reduced by a diameter expansion, but not so the inertial surge. Two key aspects of the success of the diameter expansion solution are the radial expansion of the air pocket and the increased storage of the water volume around the perimeter. The exact design specifications for the diameter ratio and vertical location of the diameter expansion have not been optimized and the laboratory results may vary from a prototype system. In the case where it seems more feasible to construct the vertical shaft at a diameter equal to the expanded diameter, this may result in the similar benefits as a strategically designed diameter expansion.

Chapter 10

Conclusions

10.1 Summary of objectives

The research presented in this dissertation, primarily performed through physical modeling, aimed to clarify possible mechanisms that can lead to geyser events in collection systems. Since much of the previous literature has ignored the influence of the air phase entirely, interactions between the air and water phases were the primary focus of this study. The present research aimed to identify and understand the basic mechanisms associated with trapped air pockets through a surcharge vertical shaft that might contribute to geysers such as depicted in Figure 2.1. During the course of the study, limited data from a single geyser event in Minneapolis on July 11 was provided; in the same location as shown in Figure 2.1. This gave additional insight as to what might be happening. At the same time, access to numerical modeling results that were performed as part of a preliminary design analysis for the storage tunnel proposed for the DCWASA system were also given. Evidence from both of these real systems pointed toward several different sets of experiments that might shed some light on which parameters and processes might be important in determining the strength of the geysers that form. Experiments were conducted to present an explanation of past geyser occurrences due to the release of large air pockets. Data related to air entrapment,

migration, and vertical flow in risers connected to nearly horizontal conduits was gathered using laboratory scale models. A number of variables were adjusted to determine their relative influence throughout the air entrapment and release processes, including vertical shaft diameter, initial water level, air introduction scenarios, etc. The intended contribution of this work is to highlight the important mechanisms that occur during critical air release scenarios and offer insight regarding the appropriate framework of a numerical model. The release of air which enters the system through entrainment of small bubbles at a drop shaft has different characteristics than the release of a single large air pocket trapped during the rapid filling process; each is examined. Lastly, ventilation design adjustments are recommended to mitigate possible geyser occurrences.

10.2 Case study: Minneapolis geyser

Dangerous geyser events have occurred in large collection systems around the world. Available literature that addresses these events seems to suggest that only the water phase is important. The standard approach is for engineers to use single phase flow models to simulate the transients associated with the filling process. It is important to know whether this is appropriate or whether there are other important physical processes involved in order to properly develop the design of such systems. There was limited field data that was provided for a geyser event that occurred in Minneapolis, Minnesota on July 11, 2004. The data revealed that single-phase water flow mechanisms are unable to produce the observed geyser events. An air/water mixture was observed jetting tens of meters into the air through a large diameter manhole at the 35th Street location. Recorded pressure measurements indicate that the maximum tunnel pressure was 6.0 m which is far

below a value of 28.6 m that would be required to lift the water to grade under hydrostatic conditions. This as well as other evidence presented discussed throughout this dissertation strongly suggest the importance of air during the process. The Minneapolis case study is used as a framework for considering the effects of both air and water which may lead to a geyser event.

10.3 Air pocket formation

The propagation of hydraulic bores during the rapid filling process can lead to air entrapment within a CSO storage tunnel or other collection system. In general, numerical models of the shock-fitting type are only able to accurately predict the behavior of pipe-filling hydraulic bores (although this is a function of the numerical scheme implemented), and more effort would be required to implement a more general approach. It is expected that a real system will more often experience the lower flow rates or more gradually increasing discharge where free surface bores with gradual flow regime transitions will develop, and therefore, improved numerical techniques are required in order to predict the range of behavior of the bore. A shock-capturing model, such as the two-component pressure approach proposed by Vasconcelos, et al. (2006) is capable of predicting the behavior of both pipe-filling bores and gradual flow regime transitions. This laboratory investigation indicates that a free surface bore tends to steepen with propagation distance but even for very long pipelines, gradual flow regime transitions are expected to occur. The data also revealed that free surface bores followed by gradual flow regime transitions are generally more conducive to air entrapment than pipe-filling bores. Air can become entrapped when a free surface bore with a gradual flow regime transition is reflected at a

conduit transition and the reflection fills the pipeline. Laboratory measurements showed that the collision of multiple bores is capable of trapping a large volume of air in multiple smaller pockets. This air subsequently led to a strong geyser event through a vertical shaft near the location of the collision. The hydrologic variability of real systems plus the fact that they typically contain multiple inflow locations prevents the complete avoidance of air entrapment in the system.

There are likely different mechanisms of air release which can lead to geysers. Migration data suggest a fundamental difference between the behavior of a large trapped air pocket and many small pockets, even with the same total air volume. The geyser events observed during the bore collision experiments exhibited some similar characteristics to the Minneapolis geyser event. For instance, quick pressure drops are noticed in both Figures 2.4 and 4.10. The experimental pressure measurements of Figure 4.10 exhibit pressure drops which correspond to sequential air pockets breaking through the free surface water level within the vertical riser. Pressure drops in the field observations of Figure 2.4 correspond with geyser events at the ground surface. These similarities imply that the pressure drops during the Minneapolis geyser event are perhaps caused by the pressure of large air voids being relieved as they break through the free surface level of the liquid in the manhole. Even though there are similarities, a notable difference is that the Minneapolis geyser is presumed to be caused by a single large air pocket where the laboratory geysers resulting from the bore collisions were created by multiple air pockets. Although some of the research of this dissertation suggests that a single large air pocket is more problematic than many small ones, fundamental

differences between the two mechanisms prevent a specific statement without knowing more about the system geometry and the filling process.

10.4 Air pocket migration

The migration direction of an air pocket is an important question when considering the placement of ventilation shafts during the design of CSO storage tunnels. In general, these systems have large diameters and relatively low velocities, which lead to air pockets migrating in the direction of increasing elevation as opposed to being pushed downward with the direction of liquid flow. The volume of the air pocket is a key variable and larger air pockets were capable of intruding into the water with relative velocities approaching the infinite intrusion relations developed by Benjamin (1968). The largest air pocket migrated only 9% slower than the Benjamin relation. Altogether, for a given air intrusion thickness, the observed migration velocities of discrete pockets during the capsule experiments were less than the Montes (1997) relation for an infinite intrusion. A small backflow of water under the advancing air pocket would slightly increase the relative velocity from the observations. In addition, curvature at the interface between the air and water creates uncertainty in measuring the appropriate air intrusion thickness. Experiments showed a fundamental difference in migration behavior for air injected as small bubbles, which effectively moved with the flow of liquid. The air injection experiments essentially represented air entrained at drop-shafts, while the capsule experiments represented the movement of large trapped air pockets. The exact migration velocity of an air pocket is difficult to predict due to the variation of the air pocket's size and shape, the friction with the pipe wall, the shear stress from the flowing

liquid, and the frequent coalescing with other air pockets. The Benjamin relation could be used qualitatively to predict air arrival at a vertical shaft, although engineering judgment is required in light of these experimental results to identify critical scenarios.

10.5 Air release

The initial rise of an air pocket within a surcharged vertical shaft was studied through an experimental investigation. The free surface level and the nose location of the air pocket were tracked carefully while adjusting three variables: the equilibrium water level, the air pocket volume, and the vertical shaft diameter. As the nose of the air pocket rose within the liquid column of the vertical shaft, momentum was transferred to the surrounding liquid, causing it to rise significantly in some cases. The height of liquid rise was increased by a higher equilibrium water level, a larger air pocket volume, or a smaller diameter vertical shaft. The diameter of the vertical shaft was an especially important variable, as smaller sizes produced much larger geyser events at the laboratory scale.

The rise velocities for some of the experiments exceeded the Davies and Taylor (1950) relation by as much as an order of magnitude. The highest vertical accelerations always occurred when the air pocket volume was significantly larger than the liquid surcharge volume within the shaft. Furthermore, the vertical rise of the air seemed to approach the Davies and Taylor velocity in situations where the air flow in the shaft was limited by the air arrival rate. This is a reasonable difference considering that the Davies and Taylor experiments used an emptying cylinder which is quite different than the setups used in the present study. The numerical model of Vasconcelos and Wright

(2011) can be used to predict the rise heights and velocities of the air / liquid interfaces, although it tended to under-predict the rises. A modification is suggested in Chapter 6 which uses the reservoir pressure as the pressure within the air pocket; a case which better represents the configuration of real systems. Predictions from the modified model more closely matched the observed data than the original numerical model framework. Overall, a numerical model used to predict the vertical behavior of an air pocket release needs to incorporate the tunnel dynamics into the analysis.

After the nose of the air pocket reaches the liquid free surface within the vertical shaft, a chaotic movement of the air and water mixture develops. Physical experiments focused on a continued injection which established a continued release of air (but which still formed discrete pockets), measuring the overall maximum height which the water reached over a period of time. Larger air flows, smaller riser diameters, and higher equilibrium water levels each contributed to greater geyser heights. The release of air pockets created a local low pressure at the base of the vertical shaft in between air pocket arrivals which initiated a liquid flow within the main tunnel toward this location. The inertia of this liquid flow caused it to go beyond the equilibrium level within the riser, setting up an inertial oscillation of the liquid. The highest geyser elevations were noticed when the timing between the release of a large air pocket coincided with a peak liquid velocity into the vertical shaft due to the system inertia. The greatest measured geyser strength caused by continuous air injection was 1.52 m, or five times beyond the equilibrium level (0.314 m) within the riser.

10.6 Surge oscillations from air release

The influence of liquid inertia within a system containing a vertical shaft was investigated using a physical model. The introduction of a pipe-filling bore front was used as a simplified representation of the arrival of an air pocket's tail end. As the bore front propagated through the system, a noticeable amount of air became entrained within the flow behind the front. However, the magnitude of the liquid surge did not appear to be influenced by the presence of this entrained air. This implies that numerical models that consider the air and water as distinct phases should be able to predict the surge magnitudes. The main controlling factors of the maximum peak pressures were the nature of the flow regime transition, related in these experiments to reservoir elevation and initial depth in the experiments studied. Less influential factors during these experiments were the riser diameter and the degree of ventilation within the shaft. A rigid-column numerical model is capable of predicting the liquid surge behavior by using a numerical framework of three control volumes: upstream of the riser, downstream of the riser, and within the riser. After calibration of the roughness parameter, the numerical model performed quite well in comparison to the experimental results. The same type of model was used to show the behavior of the inertial oscillations within the riser after an air pocket has been released, as in Figure 9.11. Even though inertial surge is an important physical process during rapid filling, pressure measurements shown in Chapter 2 do not indicate that it was significant during the formation of the Minneapolis geyser events. Also, this geyser may be an anomaly in that the air apparently does not enter the system through an entrapment process that involves bore propagation, since the pressure data does not show significant surge effects. Severe geysers such as the Minneapolis

example are almost certainly associated with the displacement of surcharged water in a vertical shaft by a rising pocket of air, but it would be very beneficial to have more confirmation of this at the field scale.

10.7 Geyser reduction strategies

One strategy tested for the mitigation of geyser events was to adjust the geometry of the vertical shaft. A diameter expansion appears more efficient in reducing the geyser strength than creating a horizontal section within the vertical shaft through the use of two 90° bends. Two key aspects of the success of the diameter expansion solution are the radial expansion of the air pocket and the increased storage of the water volume around the perimeter. A radial expansion occurred within the air pocket as it reached the expanded diameter. The vertical location of the diameter expansion is important because if it is too high, specifically above where the rising air position produces a peak velocity, it has a very limited impact on reducing the geyser strength since the upward velocity of the air/water mixture is already achieved. Therefore the diameter expansion is more effective when placed at a relatively low location within the shaft. For the experiments where the lower riser diameter is equal to the tunnel diameter and then expands to a diameter twice that size the expansion reduced the strength of the geyser by an average of 17% and 22% in terms of splash level and free surface level, respectively, in comparison to a constant diameter riser equal to the tunnel diameter. A general comparison between the diameter expansion and a constant diameter equal to the expanded diameter revealed roughly the same results, as long as the expansion was not placed high within the riser. An observed velocity during one of the strongest geyser events was measured to be 3.0

m/s +/- 0.4 m/s, matching a rough energy check based on the observed height of rise. The exact design specifications for the diameter ratio and vertical location of the diameter expansion have not been optimized and the laboratory results may vary from a prototype system. In the case where it seems more feasible to construct the vertical shaft at a diameter equal to the expanded diameter, this is expected to have similar results to a strategically designed diameter expansion.

An important phenomenon known as flooding instability is difficult to produce at the laboratory scale, at least with the experimental setup used here. The velocity of the escaping air would be greater in the real system due to the scaling between the model and the prototype shaft diameter. Therefore, the fast moving air in a large system could create enough shear at the interface with the water to entrain the water upward. In real systems, the rise velocity of an air pocket through a large vertical shaft is likely to exceed the flooding instability threshold discussed by Guedes de Carvalho, et al. (2000). The rise of this air and water mixture would therefore likely increase the height of the maximum water rise compared to the laboratory observations. It is difficult to determine the potential for this phenomenon, but it is believed to be very important based on visual observations of an air/water mixture during the Minnesota geyser event of Chapter 2. The importance of this phenomenon is assuming the air is arriving at a sufficiently high enough rate at the base of the riser, as assumed in the numerical model of Chapter 6. This requires either a very large air entrainment flux through the system or else a large trapped pocket. The approximate air flux would need to be significantly larger than the Davies and Taylor rise velocity multiplied by the cross-section of the vertical shaft. A single pressurized air pocket is important if it is significantly larger than the volume of

liquid initially within the shaft. Again, flooding limits the conclusions of the effectiveness of the diameter expansion to control that type of geyser, so more field measurements would be helpful as well as laboratory measurements at a larger scale.

10.8 Implications for numerical modeling

Developing appropriate numerical modeling techniques for predicting the behavior of air pockets within a CSO storage tunnel is an ongoing science. A 1-D shock-capturing model has the advantage over a typical shock-fitting model of simulating gradual flow regime transitions which are capable of trapping large amounts of air as they reach tunnel transitions. Applying a shock-fitting model to a real system with complex geometries and multiple inflows, while generalizing for these types of transitions, is difficult. A model such as Vasconcelos, et al. (2006) two-component pressure approach seems capable of predicting the behavior of the liquid during rapid filling and can be used to estimate a potential amount of air trapped for a specific filling scenario. At this point, the migration of the air is difficult to compute in a numerical framework. One reason is that the hydrostatic pressure assumption breaks down near the air pocket's nose and tail regions due to the strong curvature at the interface between these two phases. This invalidates the use of simple one-dimensional models in the vicinity of the air pockets and would require special treatment of them such as an internal boundary condition in such models. This eliminates some of the computational advantages of shock capturing models for example. Another reason is the shear waves between the air and water can cause the air pockets to break apart into smaller pockets. Similarly, smaller air bubbles that might enter through a drop-shaft for example, might coalesce into larger air volumes

where the buoyancy then produces a significant effect on the two phase flow behavior. This study has confirmed that air pockets migrate faster as the volume of air within the pocket increases. It has also shown that as the volume of the air pocket increases it approaches the Benjamin 1968 relation for air intrusion velocities relative to the water velocity. From a numerical modeling perspective, this suggests the use of Benjamin's air intrusion velocity as an upper bound for air pocket migration is appropriate, but it may be inappropriate to describe certain types of air pocket migration. Although generalizing for both gradual flow regime transitions and air pocket migration may be quite complex, nevertheless it may be necessary.

Once the air pocket reaches the location of a vertical shaft, a vertical 1-D rigid column model is appropriate such as used in Vasconcelos and Wright 2011. This numerical model can be used to simulate the rise of the air pocket's nose upward through the liquid within the riser. A difficulty remains in determining the pressure inside of the air pocket, which is fundamentally based on the geometric configuration of the system. For rising air pockets in which a large portion of the volume exists within the horizontal tunnel, the pressure within the air pocket is more appropriately represented by the tunnel conditions as opposed to the pressure head from the liquid within the riser. Once the air pocket's nose reaches the liquid free surface, a chaotic churning process develops as the air continues to escape through the disrupted liquid column. The rise of liquid during this chaotic process is very difficult to approximate with a numerical framework, especially with the possibility of flooding instability for larger systems.

Coincident with the vertical air release, the horizontal behavior of the liquid in the main tunnel also changes. A coupling between the horizontal numerical model and the

vertical numerical model is required. As a pocket of air is released through the vertical shaft, there is a drop in the system pressure at this location. This low pressure initiates a liquid flow into the vertical shaft setting up an inertial oscillation. Experimental results show that strong geyser events are created when the liquid velocity upward is very fast at the same time as a large amount of air is released. The release of air subsequently creates another low pressure which restarts the liquid flow toward the shaft again. Therefore, a tunnel model needs to include important feedback from the riser dynamics when attempting to simulate potential geyser events.

10.9 Recommendations

The experimental investigations of this dissertation and the field data provided on an actual geyser event have revealed important insights to the physical processes involved in geyser formation. Field evidence and laboratory results indicate the roles of air entrapment and air release are very important when studying geyser events. Therefore modeling frameworks which only simulate the behavior of the liquid phase should not be exclusively considered when designing large collection systems such as CSO storage tunnels. It appears that there can be a fundamental difference in the behavior of air entrained at drop-shafts and large entrapped air pockets. Specifically the entrainment, unless it is at a very high rate, may not be able to produce the Minnesota type geysers since the air flux arriving at a ventilation shaft is likely insufficient to permit the type of flow required. Even with trapped air pockets, if the volume is too small, presumably relative to the surcharged liquid volume within the shaft, then the process cannot develop. In general terms, increasing the amount of ventilation to a collection system will reduce

the potential for air entrapment, especially at high elevation points and other slope changes within the main tunnel. The elimination of an air pocket is a surge problem and can be modeled within standard frameworks, provided that you can account for the air interaction in the vertical shaft. The migration of air pockets within large diameter systems is generally in the direction of higher elevation, even when the liquid is flowing in the opposite direction. However, even with adequate ventilation, the entrapment of air pockets within the system is virtually unavoidable due to hydraulic bores which can move through the system during rapid filling. Chapter 4 showed that a collision of such bores can lead to large trapped air pockets which can create geyser events. Numerical models can be used to estimate the surcharged liquid levels within vertical shafts due to the rapid filling process. A simultaneous release of large air pockets with maximum surcharge levels is a critical scenario, and the rise of the liquid can be estimated using a modeling framework similar to Vasconcelos and Wright (2011). If the simulated rise of liquid is capable of creating a geyser event, strategies for reducing the geyser strength are to design a diameter expansion within the shaft or to increase the diameter of the entire shaft, but this requires additional study. Other creative strategies for mitigating geyser events could be investigated with further research. It is critical that experiments at a larger scale be performed to determine the scalability of the laboratory results reported here and, in particular, to quantify the influence of the flooding instability process.

Appendix

Comparison of Experimental and Numerical Results for Initial Air Rise

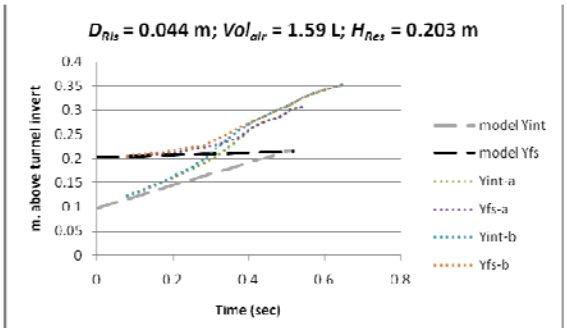

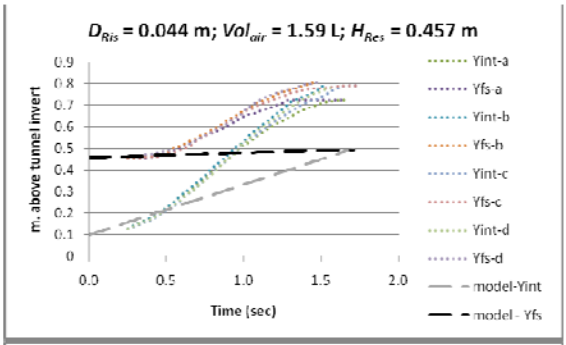

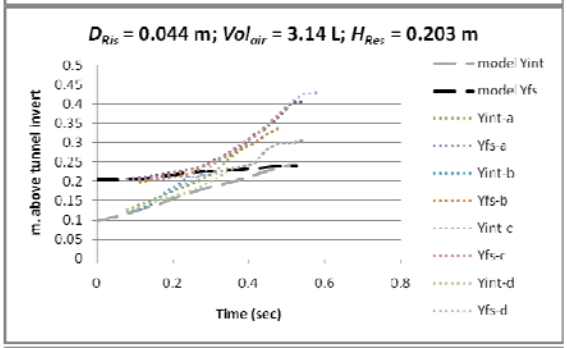

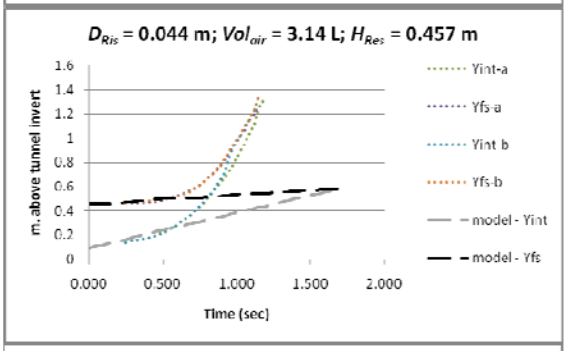

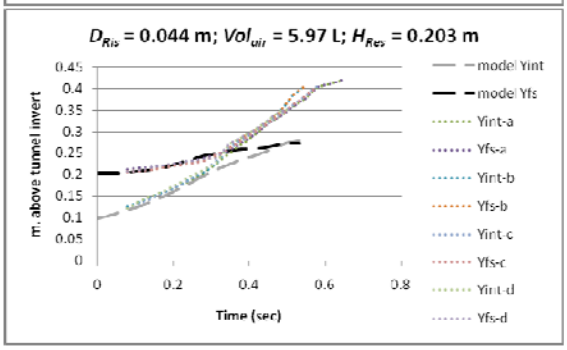

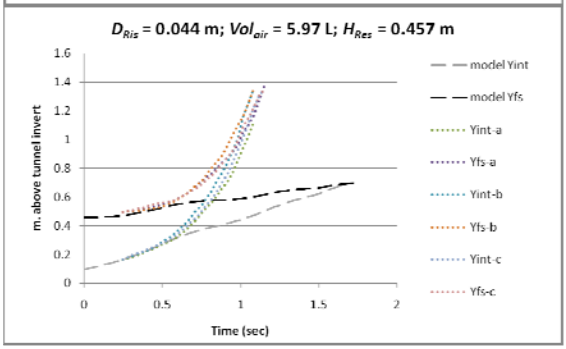

Continued Comparison of Experimental and Numerical Results for Initial Air Rise

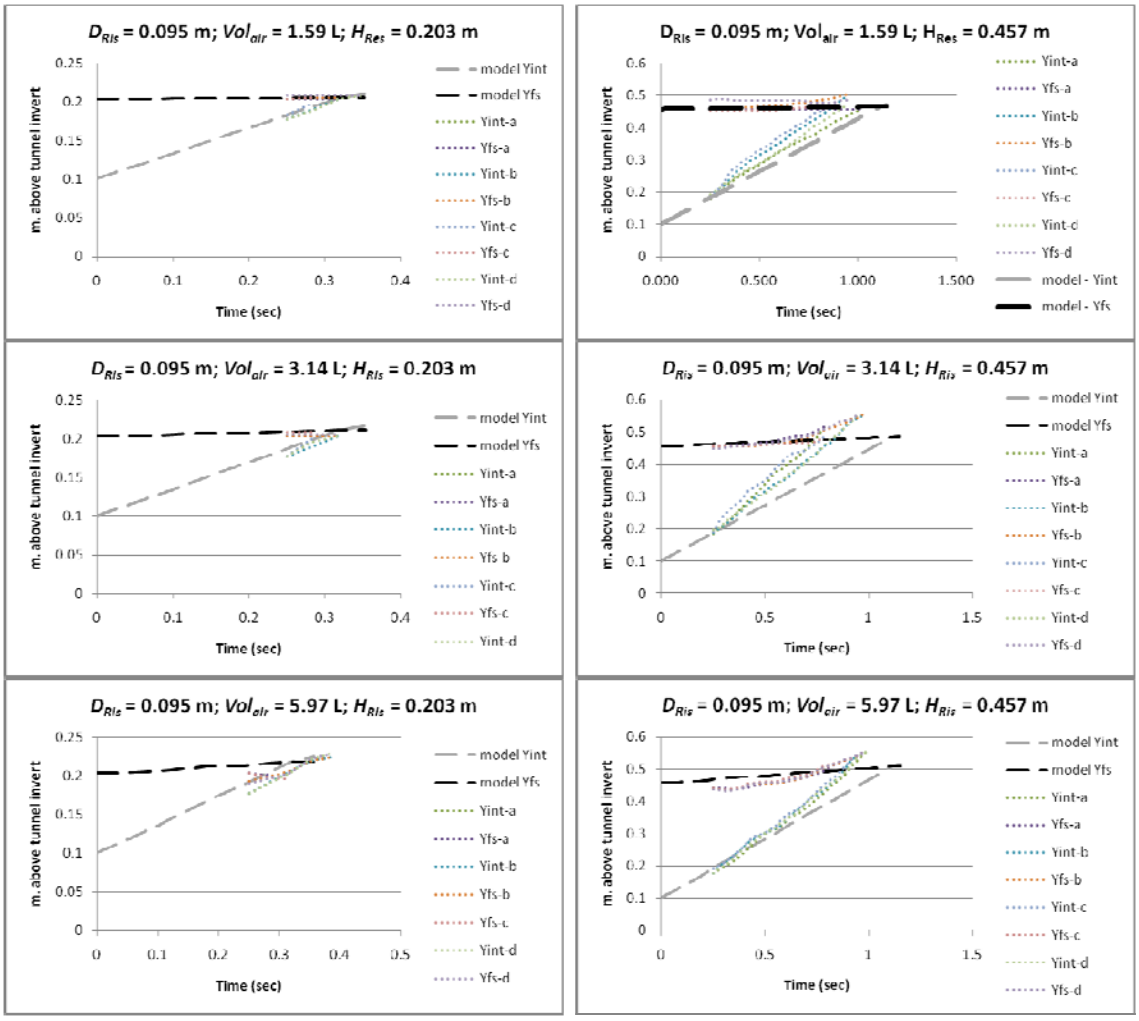

References

Anderson, A.G. and Dahlin (1975) "Dropshafts for the Tunnel and Reservoir Plan." Report 154, St. Anthony Falls Hydraulics Lab, University of Minnesota.

Batchelor,G. K. (1967). *Introduction to Fluid Dynamics*. Cambridge University Press. Cambridge, U. K.

Bellos, C.V. and Sakkas, J.G. (1987) 1-D Dam-break Flood-wave Propagation on Dry Bed, *Journal of Hydraulic Engineering*, 113(12), 1510-1524.

Benjamin, T. B. (1968). Gravity currents and related phenomena. *J. Fluid Mech.*, 31(2), 209–248.

Capart H, Sillen X, and Zech Y (1997) Numerical and experimental water transients in sewer pipes. *J. Hydraulic Res.* 35(5), 659–670

Cardle JA, and Song CSS (1988) Modeling of unsteady flow in storm sewers. *Int. J. Eng. Fluid Mech.* 1(4), 495–518.

Davies, R.M. and Taylor, G.I. (1950). The mechanics of large bubbles rising through extended liquids and through liquids in tubes. *Proceedings of the Royal Society of London. Series A, Mathematical and Physical Sciences*, Vol. 200, No. 1062, pp 375-390.

Ettema, R, Jain, S.C. and Kennedy, J.F. (1982) Hydraulic Design of Drop Structures: A State of the Art Review, IIHR Report No 98, Iowa Institute for Hydraulic Research, University of Iowa, July, 1982.

Guedes de Carvalho, J. R. F., Talaia, M. A. R., and Ferreira, M. J. F. (2000) Flooding instability of high-density gas slugs rising in vertical tubes filled with water. *Chem. Engrg. Sci.*, 55, 3785-3802.

Guo, Q., and Song, C. C. S. (1990). Surging in urban storm drainage systems. *J. Hydr. Engrg.*, ASCE, 116(12), 1523-1537.

Guo, Q., and Song, C. C. S. (1991). Drop shaft hydrodynamics under transient conditions. *J. of Hydr. Engrg.*, ASCE, 117(8), 1042-1055.

Hamam, M. A. and McCorquodale, J. A. (1982). Transient conditions in the transition from gravity to surcharged sewer flow. *Canadian J. of Civ. Eng.*, 9, 189-196.

Henderson, F. M. (1966). *Open Channel Flow*, 522 pp., Macmillan, New York, 1966.

Hewitt, G.F. and Wallis, G.B. (1963). Flooding and associated phenomena in falling film flow in a tube. *Multiphase flow symposium winter annual meeting of ASME*, Philadelphia, (62-74).

Izquierdo,J., Fuertes,V.S., Cabrera,E., Iglesias,P. L. and Garcia-Serra,J. (1999) Pipeline start-up with entrapped air. *J. Hydr. Res.*, 37(5) 579-590

Jain, S.C. and Kennedy, J.F. (1983) Vortex-Flow Drop Structures for the Milwaukee Metropolitan Sewerage District Inline Storage System. IIHR Report No 264, Iowa Institute for Hydraulic Research, University of Iowa, July, 1983.

James, W. (1992). *Stormwater Management Modelling: Conceptual Workbook*. Computational Hydraulics International, 200pp.

Kennedy, J.F., Jain, S.C. and Quinones, R.R. (1988) Helicoidal-Ramp Dropshaft, *Journal of Hydraulic Engineering*, 114(3), 315-325.

Li, J. and McCorquodale, A. (1999). Modeling Mixed Flow in Storm Sewers. *J. Hydr. Eng.*, 125(11), 1170-1180.

Little, M.J., Powell, J.C., Clark, P.B. (2008). Air Movement in Pipelines – some new developments. *10th International Conference on Pressure Surges*. Edinburgh, UK. BHR Group Ltd. pp111-122.

Lyons, T. (2010) Test Results on DCWASA 1:15 Scale Dropshaft Model for Option 12 Geometry: Reduced Shaft Diameter. Technical Memo, May 26, 2010, Iowa Institute for Hydraulic Research, University of Iowa.

Montes, J.S. (1997). Transition to a free-surface flow at end of a horizontal conduit. *J. of Hydr. Research*, 35(2), 225-241.

Nakazatomi, M., Shimizu, H., Miyake, G., and Sekoguchi, K. (1992). Rising characteristics of a single measure of gas slug in stagnant liquid-effect of pressure. *JSME International Journal*, series II, 35, 388-394.

Nielsen, K.D. and Davis, A.L. (2009) Air migration analysis of the Terror Lake tunnel, *Proceedings 33rd IAHR Congress*, Vancouver, Canada., 262-268.

Nicklin, D.J. (1963). The air-lift pump: theory and optimization. *Transactions of the Institution of Chemical Engineers*, Vol. 41a, pp 29-39.

Odgaard, J. and Lyons, T. (2010) Test Results on DCWASA 1:15 Scale Dropshaft Model for Option 11 Geometry: 8.5 ft Tall Baffle. Technical Memo, May 28, 2010, Iowa Institute for Hydraulic Research, University of Iowa.

Politano M, Odgaard AJ, Klecan W (2007) Case study: numerical evaluation of hydraulic transients in a combined sewer overflow tunnel system. *J. Hydraulic Eng.* 133(10), 1103–1110.

Roberts, P.J.W. (2004) Physical Modeling of Drop Shaft Structures and Deaeration Chambers. Report, School of Civil and Environmental Engineering Georgia Institute of Technology, August 4, 2004.

Sekoguchi, K., Mori, K., Kaji, M., Miwa, M., Nakazatomi, M., Shimizu, H. (1996). Characteristics of Interfacial Profiles in Upward and Downward Gas-Liquid Two-Phase Plug Flow. *Heat Transfer – Japanese Research*, 25(8), 568-579.

Townson, J.M. (1991). *Free-surface hydraulics*. Cambridge University Press. Cambridge, U.K.

Trajkovic, B., Ivetic, M., Calomino, F., Dippolito, A. (1999). Investigation of transition from free surface to pressurized flow in a circular pipe. *Water Sci. Technol*. 39(9), 105–112.

Tramba, A., Topalilwu, A., Kastrinakw, E.G., Nychas, S.G., Fmcois, P., Scrivener, O. (1995). Visual Study of an Airlift Pump Operating at Low Submergence Ratios. *The Canadian Journal of Chemical Engineering*, Volume 73, 755-764.

Vasconcelos, J.G. (2005) *Dynamic approach to the description of flow regime transition in stormwater systems.* PhD dissertation, Environmental Engineering, The University of Michigan, Ann Arbor, Michigan.

Vasconcelos, J. G. and Wright, S. J. (2005). Experimental investigation of surges in a stormwater storage tunnel. *J. Hydr. Eng*, 131(10), 853-861.

Vasconcelos J.G. and Wright, S.J. (2006) Mechanisms for air pocket entrapment in stormwater storage tunnels. *Proceedings of World Environmental and Water Resources Congress*, Omaha, Nebraska, Paper 40856-14275.

Vasconcelos JG, Wright SJ, Roe PL (2006) Improved simulation of flow regime transition in sewers: two-component pressure approach. *J. Hydraulic Eng.* 132(6), 553–562.

Vasconcelos, J.G. and Wright, S.J. (2008). Rapid Flow Startup in Filled Horizontal Pipelines. *Journal of Hydraulic Engr.*, ASCE, 134(7), 984-992.

Vasconcelos, J.G. and Wright, S.J. (2009) Investigation of rapid filling of poorly ventilated stormwater storage tunnels, *Journal of Hydraulic Research*, 47(5) 547-558.

Vasconcelos, J.G. and Wright, S.J. (2011). Geysering Generated by Large Air Pockets Release Through Water-Filled Ventilation Shafts. *Journal of Hydraulic Engr.*, ASCE.

Vijayan, M., Jayanti, S., Balakrishnan, A.R., (2001). Effect of tube diameter on flooding. *Int. J. Multiphase Flow,* 27, 797-816.

Wickenhäuser, M. and Kriewitz, C.R. (2009) Air-water flow in downward inclined large pipe. *Proceedings 33rd IAHR Congress*, Vancouver, B.C., 5354-5361.

Wilkinson, D.L. (1982) Motion of Air Cavities in Long Horizontal Ducts, *Journal of Fluid Mechanics*, Vol. 188 109-122.

Wright, S.J., Lewis, J.L. and Vasconcelos, J.G. (2007) Mechanisms for stormwater surges in vertical shafts. *Ch. 5, Monograph 15, Contemporary Modeling of Urban Water Systems*, W. James, K.N. Irvine, E.A. McBean, R.E. Pitt and S.J. Wright Eds., CHI, 109-132.

Wright,S. J., Vasconcelos, J. G., Creech, C.T., Lewis, J.W. (2008) Flow regime transition mechanisms in rapidly filling stormwater storage tunnels. *Environ. Fluid Mech.*, 8, 605-616.

Wylie, E.B., and Streeter, V.L. (1993). *Fluid Transients in Systems*. Prentice-Hall, Inc. Pearson Education Company, Upper Saddle River, New Jersey.

Zhou, F., Hicks, F.E. and Steffler, P.M. (2002) Transient flow in a rapidly filling horizontal pipe containing trapped air. *J. Hydr. Eng.*, 128 (6) 625-634.